# A MATHEMATICAL MODEL FOR OXYGEN MASS BALANCE IN A 7.5 MW FBC POWER PLANT USING COTTON STALK

Thesis submitted in partial fulfillment of the requirements for the award of degree of

**MASTER OF ENGINEERING**

IN

**CAD/CAM & Robotics**

**Thapar University, Patiala**

By:
**GURINDER PAL SINGH MULTANI**
**(Roll No. - 80681006)**

Under the supervision of:
**Dr. S. K. MOHAPATRA**
Professor and Head,
Mechanical Engineering Department

MECHANICAL ENGINEERING DEPARTMENT
THAPAR UNIVERSITY
PATIALA – 147004
JUNE 2008

# CERTIFICATE

I hereby certify that the work which is being presented in the thesis entitled, "*A MATHEMATICAL MODEL FOR OXYGEN MASS BALANCE IN A 7.5 MW FBC POWER PLANT USING COTTON STALK*", in partial fulfillment of the requirements for the award of degree of Master of Engineering in **CAD/CAM & Robotics** submitted in Mechanical Engineering Department of Thapar University, Patiala, is an authentic record of my own work carried out under the supervision of ***Dr. S. K. Mohapatra.***

The matter presented in this thesis has not been submitted for the award of any other degree of this or any other university.

Gurinder

**(Gurinder Pal Singh Multani)**

This is to certify that the above statement made by the candidate is correct and true to the best of my knowledge.

**(Dr. S. K. MOHAPATRA)**
Supervisor and Head
Mechanical Engg. Department
Thapar University,
PATIALA

**Countersigned by**

**(Dr. S. K. MOHAPATRA)**
Professor and Head
Mechanical Engineering Department
Thapar University,
PATIALA

**(Dr. R. K. SHARMA)**
Dean (Academic Affairs)
Thapar University,
PATIALA



i

# ACKNOWLEDGMENT

*Words are often less to revels one's deep regards. With an understanding that work like this can never be the outcome of a single person, I take this opportunity to express my profound sense of gratitude and respect to all those who helped me through the duration of this work.*

*This work would not have been possible without the encouragement and able guidance of my guide & head of the department* **Dr. S. K Mohapatra**. *His enthusiasm and optimism made this experience both rewarding and enjoyable. Most of the novel ideas and solutions in this work are the result of our numerous stimulating discussions. His feedback and editorial comments were also invaluable for the writing of this thesis report.*

*I, hereby would also like to thank Mr. Jaswant Singh, Chief Engineer, Malwa power limited, Muktsar, Punjab for his valuable support in collection of the required material for this thesis report.*

*At last, I would like to thank to all the members and employees of Mechanical Engineering Department, Thapar University, Patiala for their everlasting support.*

**Gurinder Pal Singh Multani**

**ROLL NO. 80681006**

# ABSTRACT

Due to urbanization and industrialization, there is increase in demand for more energy sources. This will increase burden on the natural resources and fossil fuels day by day. These resources are depleting at such a fast rate that, they may finished up very quickly. In order to reduce this burden for increased demand of energy sources, use of biomass is a good alternative. Biomass is an important resource and with the help of fluidized bed combustion process it can be effectively converted into thermal energy and hence for power generation.

India is basically an agri-based nation. So the availability of biomass is not a problem. We can use this biomass for the generation of the power that will meet the required demand in today scenario. In India, fluidized bed combustion technology is gradually emerging as a potential technology. A number of small scale fluidized bed combustion power plants have been commissioned in India in the recent past as a result, a large amount of data is available for modeling and simulation.

In the present work, a three phase mathematical model for oxygen mass balance in a atmospheric bubbling fluidized bed boiler at Malwa power limited, Muktsar, Punjab has been developed. In this model some input parameters taken from the plant have been used in order to find out the physico-chemical parameters like minimum fluidization velocity, bubble diameter etc. Then these physico-chemical parameters are incorporated in the mathematical model to find out the percentage of oxygen, carbon dioxide and nitrogen. It has been assumed that the bubble diameter remains constant along the bed height and the fluidized bed is assumed to consist of number of equivalent stages such that each stage height is equal to the bubble diameter. Then the results have been compared with the plant data and reasonable agreement is obtained.

# CONTENTS

# LIST OF FIGURES AND TABLES

# LIST OF SYMBOLS USED

| | |
|---|---|
| $A$ | Cross-sectional area of the bed ($m^2$) |
| $A_b$ | Cross-sectional area of bed occupied by bubble phase ($m^2$) |
| $A_{cw}$ | Cross-sectional area of bed occupied by cloud-wake phase ($m^2$) |
| $A_{cw_g}$ | Cross-sectional area of bed available for gas flow in the cloud-wake phase ($m^2$) |
| $A_{kt}$ | Attrition rate constant |
| Ar | Archrmedes number |
| $C_o$ | Initial oxygen concentration (kg-mol/$m^3$) |
| $C_{avg_n}$ | Average oxygen concentration leaving stage n (kg-mol/$m^3$) |
| $C_{avg}$ | Average oxygen concentration leaving top of bed (kg-mol/$m^3$) |
| $C_{b_n}$ | Oxygen concentration leaving stage n in bubble phase (kg-mol/$m^3$) |
| $C_{cw_n}$ | Oxygen concentration leaving stage n in cloud-wake phase (kg-mol/$m^3$) |
| $C_{e_n}$ | Oxygen concentration leaving stage n in emulsion phase (kg-mol/$m^3$) |
| $C_p$ | Oxygen concentration in the particulate phase (kg-mol/$m^3$) |
| $C_s$ | Carbon concentration per unit dense phase (kg-mol/$m^3$) |
| $C_s'$ | Oxygen concentration at the carbon surface (kg-mol/$m^3$) |
| $d_p$ | Feed particle diameter (m) |
| $D_b$ | Average equivalent bubble diameter (m) |
| $D_{bm}$ | Fictitious maximum bubble diameter (m) |
| $D_{bo}$ | Initial bubble diameter (m) |
| $D_R$ | Bed diameter (m) |
| $D_e$ | Molecular diffusion coefficient of gas ($m^2$/s) |
| $dd_p/dt$ | Particle shrinkage rate (m/s) |

| | |
|---|---|
| $f_c$ | Ratio of cloud volume to the volume of bubble |
| $f_{cw}$ | Ratio of volume of cloud-wake phase to the volume of bubble |
| $f_w$ | Ratio of wake volume to the volume of bubble |
| $F_{ME}$ | Actual molar feed rate of fluidizing air (kg-mole/s) |
| $F_{MTH}$ | Stoichiometric air feed rate (kg-mole/s) |
| g | Acceleration due to gravity (m/s) |
| H | Expanded bed height (m) |
| $H_{mf}$ | Bed height at minimum fluidization (m) |
| $(K_{bc})_b$ | Gas interchange coefficient between bubble and cloud-wake phases ($s^{-1}$) |
| $(K_{be})_b$ | Gas interchange coefficient between bubble and emulsion phases ($s^{-1}$) |
| $(K_{ce})_b$ | Gas interchange coefficient between cloud-wake and emulsion phases ($s^{-1}$) |
| K | Overall reaction rate constant ($s^{-1}$) |
| $K_{cw}$ | Reaction rate in the cloud-wake phase ($s^{-1}$) |
| $K_s$ | Surface reaction rate constant (m/s) |
| $K_g$ | Mass transfer coefficient (m/s) |
| $M_c$ | Molecular weight of carbon (kg/mol) |
| N | Number of equivalent stages |
| $N_{or}$ | Number of orifice openings in distributor plate |
| $P_{av}$ | Average pressure in the combustor (atm) |
| $R_g$ | Gas constant (atm-$m^3$/ kg-mole) |
| Sh | Sherwood number |
| $T_b$ | Absolute bed temperature (K) |
| $T_p$ | Char surface temperature (K) |
| $u_b$ | Rise velocity of a crowd of bubbles (m/s) |

| | |
|---|---|
| $u_{br}$ | Rise velocity of an isolated single rising bubble (m/s) |
| U | Superficial velocity (m/s) |
| $U_b$ | Superficial gas velocity of the bubble phase (m/s) |
| $U_{cw}$ | Superficial gas velocity of cloud-wake phase (m/s) |
| $U_{mf}$ | Superficial velocity of fluidizing gas under minimum fluidization (m/s) |
| W | Fuel feed rate into the combustor (kg/s) |
| X | Oxygen conversion |
| XC | Carbon content of the fuel |
| XH | Hydrogen content of the fuel |
| XO | Oxygen content of the fuel |
| XS | Sulphur content of the fuel |
| XW | Moisture content of the fuel |
| Z | Bed height above distributor plate (m) |

***Greek symbols***

| | |
|---|---|
| $\rho_g$ | Density of fluidizing gas ($kg/m^3$) |
| $\rho_s$ | Density of feed particle ($kg/m^3$) |
| $\mu_g$ | Viscosity of fluidizing gas (kg/m.s) |
| $\varepsilon_b$ | Volume fraction of bubbles in the bed |
| $\varepsilon_{mf}$ | Voidage at minimum fluidization |

# CHAPTER 1

# INTRODUCTION

Next to the food, the fuel and the power are the most important items on which national standard of life depend. The flourishing power generation is the sign of the wealthy nation, because it makes the best use of the available resources to its maximum effect. Electricity is the only form of energy which is easy to produce, easy to transport, easy to use and easy to control.

Agro-residue has traditionally been the chief source of heat energy in rural areas and a valuable fuel for the urban areas. In spite of rapid increase in the supply or and access to and use of fossil fuels, agro-residue is likely to continue to play an important role in India, as it is in several other countries. The traditional fuel firing have got limitations and are techno-economical unviable to meet the challenges of future. Completely new techniques are being developed for cleaner and more efficient combustion.

Electricity in bulk quantities is produced in power plants, which can be of following types:

a) Thermal
b) Nuclear
c) Hydraulic
d) Gas Turbines
e) Geothermal

Thermal, nuclear and geothermal power plants use the steam for the power production. But gas turbine plants are often used as peaking units. They run for short interval of time to meet the peaking loads. Hydraulic power plants are multi-purpose because they not only used for generating power but also used for irrigation, navigation etc. But the initial set up cost for the hydraulic power plants is very high.

Thermal power plants generate more than 80% of the total electricity produced in the world. Fossil fuels like coal, fuel oil and natural gas are the energy source and steam is the working fluid. In 1947, the total power generation capacity was only 1360MW, and by 1991 it grew to 65,000MW, of which 69% was generated in thermal power plants. But the problem faced with the thermal power generation is that, the fuel is not plenty. In order to compensate this problem, now attention is more towards

utilizing the biomass like rice husk, rice straw, paddy straw, wheat stalks, cotton stalks etc. Biomass holds a special promise owing to its inherent ability to store solar energy and is the only non-conventional and renewable energy sources.

India is basically an agriculture country and the biomass here is plenty and use of these different biomasses will help to compensate the increase in demand of the electricity. Completely new techniques are developed for cleaner and more efficient combustion.

Some of the combustion technologies that are currently used are:

- Pulverized Coal Combustion (PCC)
- Cyclone Furnace Combustion (CFC)
- Integrated Gasification Combined Cycle (IGCC)
- Fluidized Bed Combustion (FBC)

Among the above combustion technologies, FBC is an advanced technique that is reaching the stage of widespread industrial application. FBC helps in achieving high efficiency combustion of low-grade fuels like wood and other biomass of agro-waste.

## 1.1 Fluidized bed combustion system

By suspending a solid fuel on an upward-blowing jet of air a so-called fluidized bed can be obtained. The result is a turbulent mixing of gas and solids, which provide more effective chemical reactions and heat transfer. The behaviour resembles to a bubbling fluid and gives a rapid mixing of particles. Compared to cyclone combustion the temperature is lower.

The boilers are designed to suit the fuel characteristics. The configuration and the size of the boiler furnaces and burners differ considerably depending upon whether the coal is anthracite, bituminous, lignite oil or gas. FBC can on the other hand accept any fuel including low grade coals. The control of $SO_2$ and NOx emissions would be simplified if there was some way to entrap the sulphur during combustion and at the same time, the coal could be burnt effectively and efficiently at a temperature below 1100°C. FBC offers the capability to do this.

FBC is of particular value for low-grade, high ash coals that are difficult to pulverize and might have varying combustion properties. By utilizing FBC-systems it

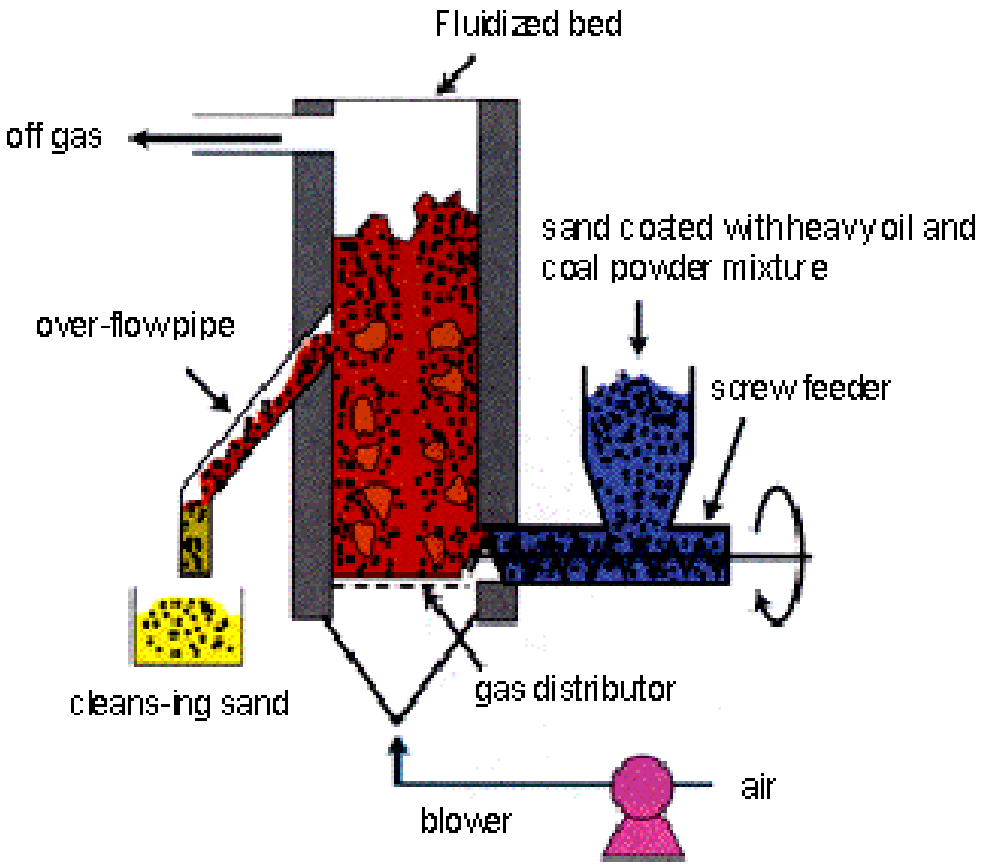


**Figure 1.1 - Fluidized bed system**

has been possible to turn normally unusable waste coal into energy. Limestone or dolomite is used for controlling sulphur emissions, but also allow more efficient heat transfer from the boiler to the steam generator. More than 95% of the sulphur in coal can be absorbed by sorbents inside the boiler, while the combustion temperature is lowered. However the lower temperature also creates increased emissions of carbon dioxide and polycyclic aromatic hydrocarbons. Fluidized-bed combustion evolved from cyclone furnaces and efforts to find a combustion process able to control pollutant emissions without external emission controls. A wide array of fuels is also available as FBC systems can burn everything from high-grade coal to biomass and municipal waste. Combustion takes place in the temperature interval of 700ºC - 1000ºC, far below the threshold where nitrogen oxides form. In general fluidized-bed combustion are considered to be very environmental friendly and has been focus for lots of research and development of cleaner combustion technologies.

## 1.2 Principle of fluidized bed combustion

When a gas is passed through a packed bed of finely divided solid particles, it experiences a pressure drop across the bed. At low gas velocities, this pressure drop is small and does not disturb the particles. But if the gas velocity is increased further a stage is reached when the particles are suspended in the gas stream and the packed bed becomes a fluidized bed as shown in Figure 1.2. With further increase in gas velocity, the bed becomes turbulent and rapid mixing of the particles occurs. This mixture of solid particles and gas is like a fluid.

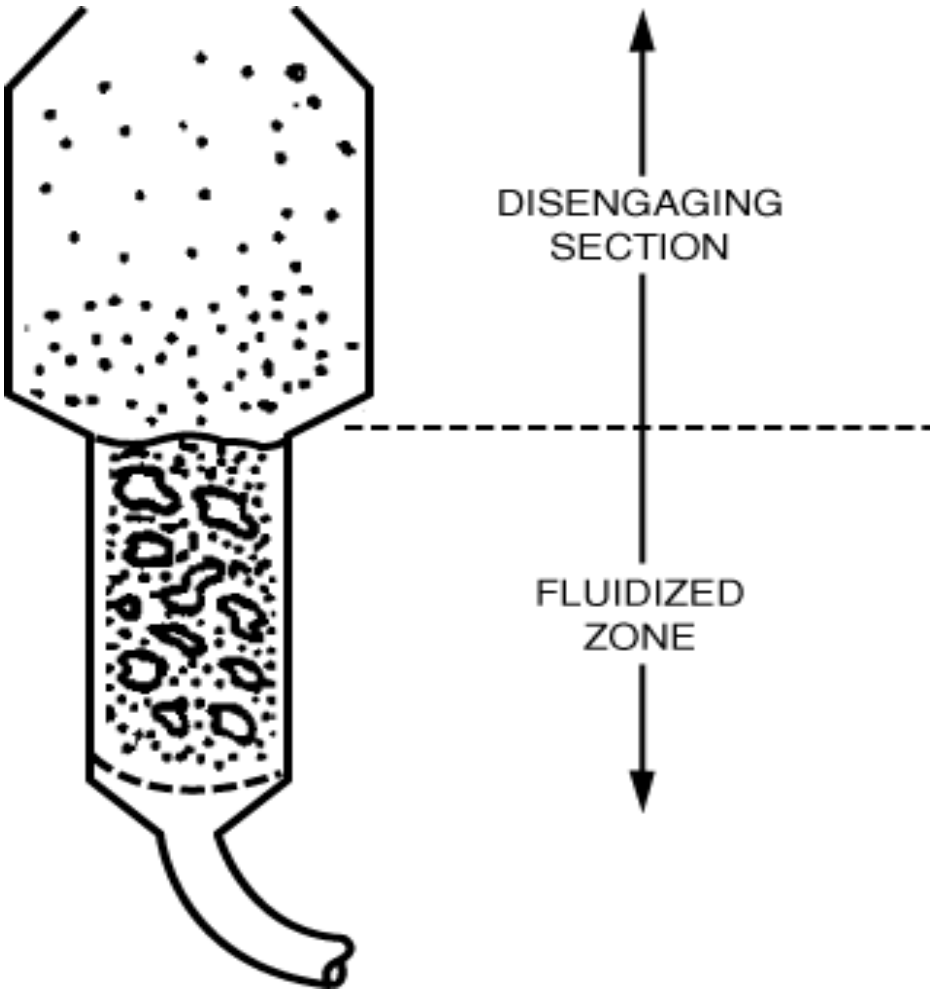


**Figure 1.2 – Diagram showing fluidized zone and disengaging zone**

Fluidized bed furnaces employ an alloy retort filled with sand-like alumina particles. When a controlled stream of air or gas is passed upward through a distributor below the retort, the particles float on a cushion of the air/gas stream and

move around turbulently without elutriation. The now "fluidized" bed looks and behaves remarkably like a boiling liquid bath. When heated (externally or internally) and when the fluidizing gas mixture is also the required heat treatment atmosphere (neutral or reactive), the fluidized bed becomes an excellent heat treatment furnace for components that are immersed into it. When a fluid is pumped upward through a bed of fine solid particles at a very low flow rate the fluid percolates through the void spaces (pores) without disturbing the bed. This is a ***fixed bed*** process.

If the upward flow rate is very large the bed mobilizes pneumatically and may be swept out of the process vessel. At an intermediate flow rate the bed expands and is in what we call an ***expanded*** state. In the fixed bed the particles are in direct contact with each other, supporting each other's weight. In the expanded bed the particles have a mean free distance between particles and the particles are supported by the drag force of the fluid. The expanded bed has some of the properties of a fluid and is also called a ***fluidized*** bed.

As shown in Figure 1.3, the velocity of the fluid through the bed opposite to the direction of gravity determines whether the bed is fixed, expanded, or is swept out. There is a minimum fluidization velocity, ($U_{mf}$) at which the bed just begins to fluidize.

* When $U_o < U_{mf}$, then the bed remains as a ***fixed bed***; see Figure 1.3(a).

* When $U_o \geq U_t$, then *the* bed is called ***mobilized bed***; see Figure 1.3(b).

* When the approach velocity ($U_o$), (otherwise known as the empty tank velocity, given by the fluid volumetric flow rate divided by the cross-sectional area of the vessel), is greater than or equal to the minimum fluidization velocity ($U_{mf}$) *and* it is less than the terminal velocity ($U_t$) of the particles $U_{mf} \leq U_o < U_t$ then the bed forms a ***fluidized bed***; see Figure 1.3(c).

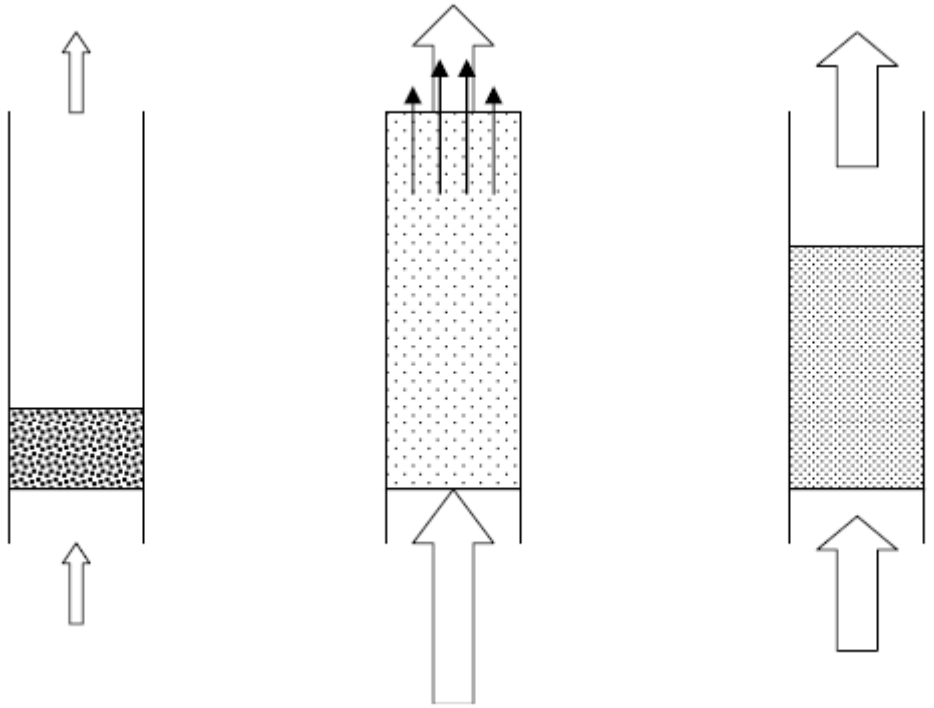

(a) Slow flow rate, Fixed bed, $U_o < U_{mf}$,

(b) High flow rate, Mobilized bed, $U_o \geq U_t$,

(c) Intermediate flow rate, Fluidized bed, $U_{mf} \leq U_o < U_t$,

**Figure 1.3 – Schematic diagram of Fixed bed, Mobilized bed, Fluidized bed**

## 1.3 Types of fluidized beds

In many liquid-solid systems an increase in velocity above $U_{mf}$ results in a smooth progressive expansion of the bed. Large scale instabilities and heterogeneities are not observed. A bed such as this is called a ***homogeneous*** fluidized bed. This is typically observed when the fluid and solids have similar intrinsic densities.

There are seven important parameters that determine the characteristics of the bed:

1) **Bed Temperature** – Normal temperature used are around 750ºC-950ºC depending upon the use and the fuel properties. To control the temperature of the bed, the bed is continuously cooled. This is done by circulating water through the cooling tubes immersed in the bed. The tubes normally contain water for steam or hot water production.

2) **Particle Size** – It is strongly connected to the fluidization velocity. Lower the velocity, lower we have to make the particle size to keep the same fluidization.

3) **Fluidization Velocity** – Depending upon the particle size the fluidization velocity is kept in the interval 0.4-4m/s. the oxygen in the air is necessary for the combustion which means higher velocity in deep beds. Low beds with big cross sectional area use lower fluidization velocity.

4) **Bed Height** – Common values are between 1-4 meters. Increased fluidization velocity gives higher bed level.

5) **Tube Location** – In the case with the immersed cooling tubes, the tube size and the tube placement strongly affect the effectiveness of the bed. Wrong dimensioning of the tube placement will lead to pressure drops and worst heat transfer.

6) **Heat Transfer Coefficient** – Heat transfer from the bed to the cooling tubes is due to convection and radiation. The radiation part is affected by the temperature only. The convection part is affected by the particle size, temperature, distance between tubes and the fluidization velocity. Convective heat transfer increases when the tube temperature increases, smaller particles and the higher distance between the tubes. The fluidization effect the convective heat transfer in such a way that the particle destroys the thin air layer surrounding the tubes. Increased convective heat transfer will be the result.

7) **Pressure Drop** – The pressure drop on the fluidized bed is dependent on the fluidization velocity at low air flows. The pressure drop increases with increasing velocity up to the incipient fluidization. Increasing the velocity from this point does not affect the pressure drop anymore. The pressure drop remains constant pneumatic transportation occurs.

When there is a large difference in the densities of the fluid and solid phases an increase in fluid velocity typically causes large bubbles or other such instabilities. Several types of beds are described in Figure 1.4.

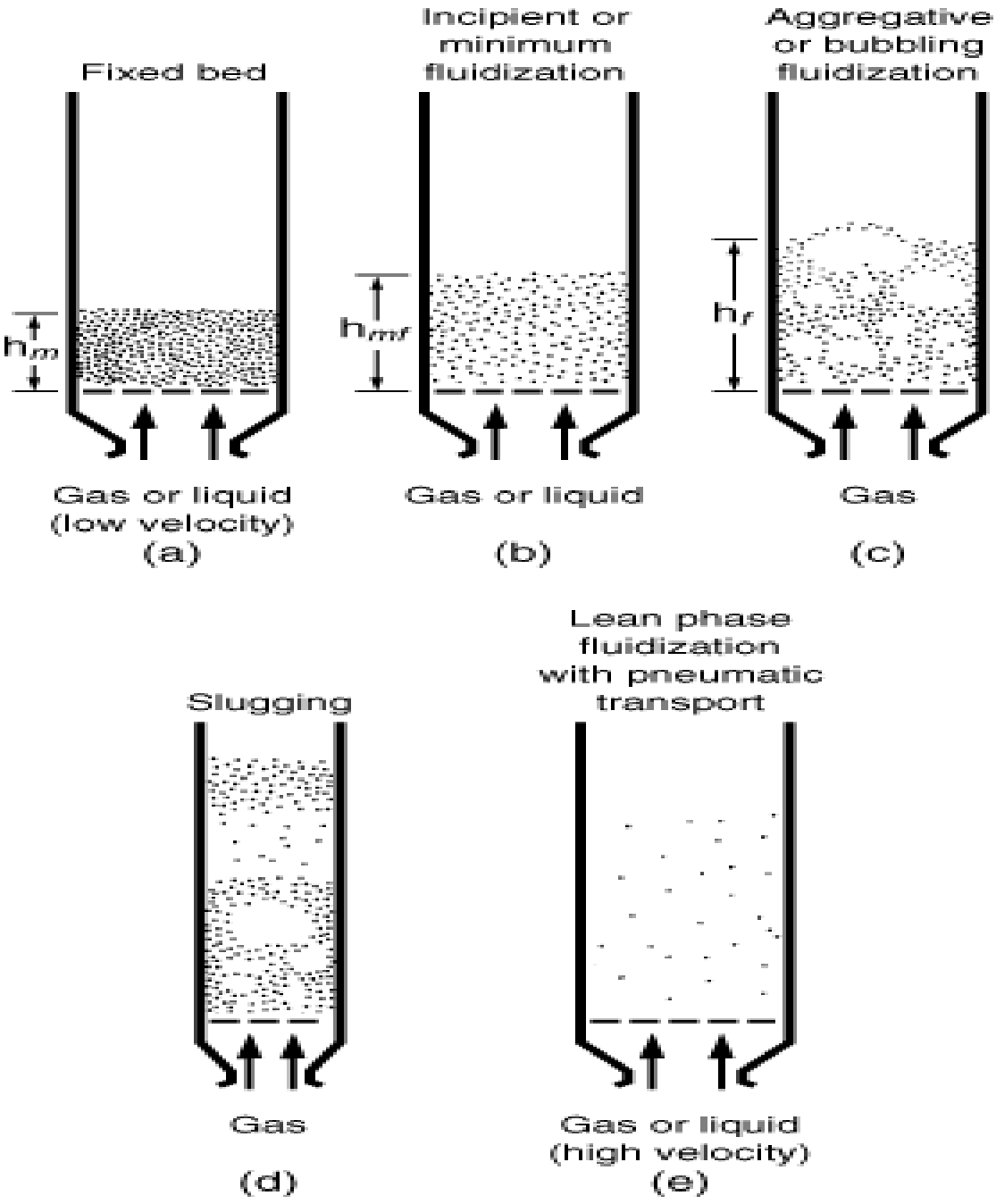


**Figure 1.4 - Various forms of contacting of a batch of solids by fluid**

If a fluid is passed upward through a bed of fine particles, as shown in Figure 1.4(a), at a low rate, the fluid merely percolates through the void spaces between stationary particles. This is a ***Fixed Bed***. With the increase in flow rate, particles move apart and a few vibrate and move in restricted regions. This is called the ***Expanded Bed***.

At a still higher velocity, a point is reached where all the particles are just suspended by the upward flowing gas or liquid. At this point the frictional force between particle and fluid just counter balance the weight of the particles, the vertical component of the compressive force between adjacent particles disappears, and the pressure drop through any section of the bed about equals the weight of the liquid and particles in that section. The bed is considered to be just fluidized and is called as ***incipiently fluidized bed or bed at minimum fluidization***; see Figure 1.4(b).

With an increase in flow rate beyond minimum fluidization, large instabilities with bubbling and channelling of gases are observed. At higher flow rates, agitation become more violent and the movement of the solids becomes more vigorous. In addition, the bed does not expand much beyond its volume at minimum fluidization. Such a bed is called an ***aggregative fluidized bed***, a ***heterogeneous fluidized bed*** or a ***bubbling fluidized bed***; see Figure 1.4(c).

In gas-solid systems, gas bubbles coalesces and grow as they rise, and in a deep enough bed of small diameter they may eventually large enough to spread across the vessel. In the case of the fine particles, they flow smoothly down by the wall around the rising void of gas. This is called ***slugging***; see Figure 1.4(d).

With increase in velocity beyond the turbulent flow, solids are carried out of the bed with the gas. This state is called ***lean-phase fluidized bed***; see Figure 1.4(e).

## 1.4 Types of fluidized bed combustion

There are basically three types of fluidized bed combustion boilers:

1) Atmospheric Bubbling Fluidized Bed Combustion (AFBC)
2) Atmospheric Circulating Fluidized Bed Combustion (CFBC)
3) Pressurized Fluidized Bed Combustion (PFBC)

### 1.4.1 Atmospheric bubbling fluidized bed combustion (AFBC)

A fluid bed boiler consists of a furnace, super-heater, generating bank, economizer and/or air heater, fuel feed and air systems. The furnace bottom is filled with an inert bed material such as sand or limestone. Combustion air is supplied to the bed through air pipes and bubble caps. A bubble cap is a vertical pipe as shown in Figure 1.5.

When air flows through the bed, the inert material expands. The fuel is fed to the bed typically using an air swept spout for uniform distribution. When a solid fuel particle is dropped into the hot fluid bed mass, the moisture evaporates and the fuel quickly ignites due to high conductive heat transfer. Fine fuel particles and volatiles leave the bed un-burnt, and an over-fire air system supplies the balance of air to complete the combustion process. The strength of the BFB is its capability to burn low-grade fuels, such as wood waste and both primary and secondary paper mill sludge. Mill by products are combusted to generate steam, replacing more expensive fuels and greatly reducing the sludge volume to be land-filled.

**Figure 1.5 – Air pipes and bubble caps**

At gas flow rates above the point of minimum fluidization, a fluidized bed appears much like a vigorously boiling liquid; bubbles of gas rise rapidly as shown in Fig. 1.6 and burst on the surface, and the emulsion phase is thoroughly agitated. The bubbles form very near the bottom of the bed, very close to the distributor plate, and as a result the design of the distributor plate has a significant effect on fluidized-bed characteristics.

The bubbles contain very small amounts of solids. They are not spherical; rather, they have an approximately hemispherical top and a pushed-in bottom. Each bubble of gas has a ***wake*** which contains a significant amount of solids. As the bubble rises, it pulls up the wake with its solids behind it. The net flow of the solids in the

emulsion phase must therefore be downward. The gas within a particular bubble remains largely within that bubble, penetrating only a short distance into the surrounding emulsion phase. The region penetrated by gas from a rising bubble is called the ***cloud*** as shown in Figure 1.6.

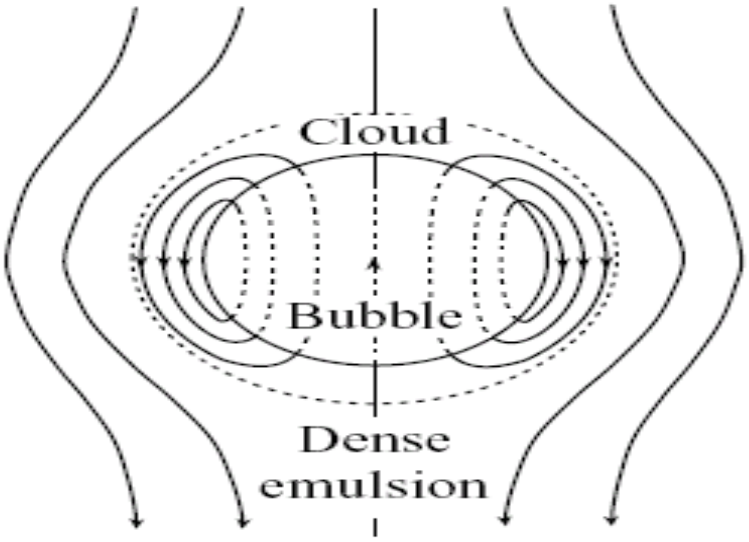


**(a)**

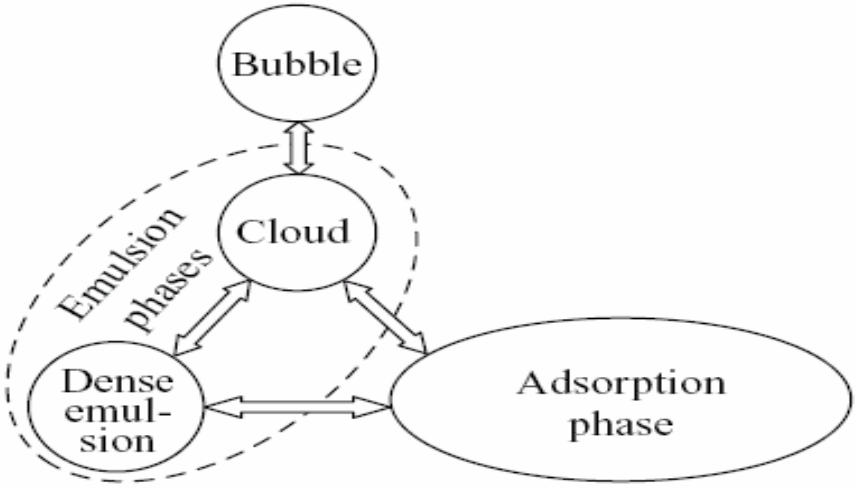


**(b)**

**Figure 1.6 – (a) Gas flow streamlines through and around an idealized spherical bubble, (b) Gas exchange pathways between the gas phases present in the bubbling fluidized bed according to Kunni & Levenspiel**

In recent years, the pulp and paper industry has encountered increasing cost and environmental issues associated with the disposal of by product sludge. Fraser Papers, a recycled fine paper mill located in West Carrollton, Ohio, envisioned an opportunity to capitalize on the utilization of sludge as a waste fuel. Studies were conducted and culminated in the selection of a new bubbling fluidized bed boiler (BFB) as the optimum choice in technology to burn high moisture, low grade fuel, e. g., primary and secondary waste sludge. The principal mode of operation is to burn 100 % of the sludge produced by the mill, in combination with coal to maintain combustion and to augment the mill's steam production needs. The boiler uses flue gas recirculation to control operating temperature in the bed. Some fuels could be burned using different techniques with similar results.

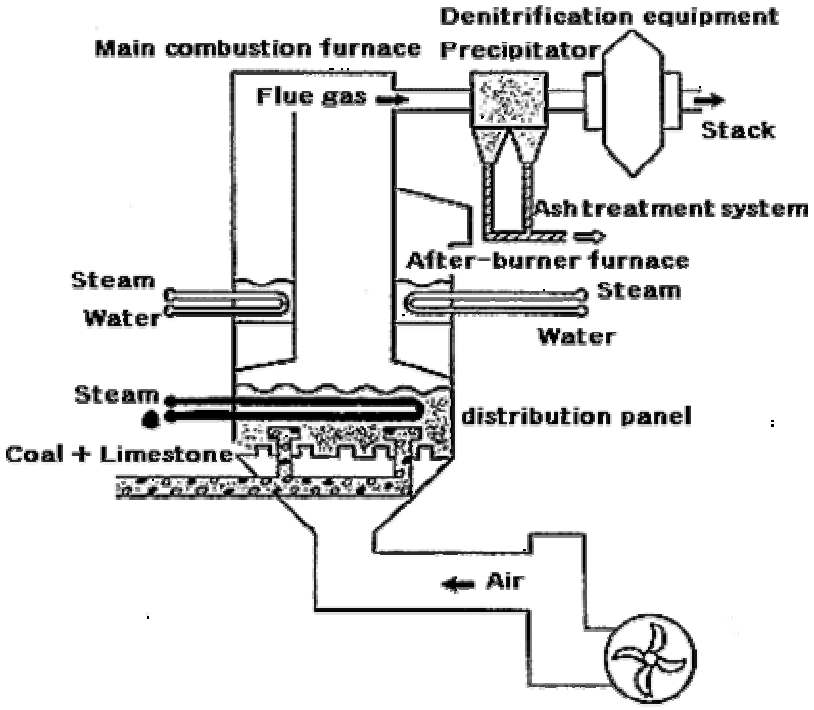


**Figure 1.7 – Schematic diagram of atmospheric bubbling fluidized bed combustion**

Table 1.1 illustrates the sludge and coal analyses for the fuels to be burned at the Fraser Papers mill. The designer evaluated the fuel properties and quantities, the plant steam needs and emissions. Based on this information, the most appropriate technology was bubbling fluid bed (BFB).

**Table 1.1 – Fuel Analysis of coal and sludge**

| Emissions( %) by wt. | Coal | Sludge |
|---|---|---|
| CARBON | 77.00 | 14.70 |
| HYDROGEN | 5.00 | 1.80 |
| NITROGEN | 1.50 | 0.35 |
| OXYGEN | 7.00 | 17.50 |
| SULPHUR | 1.00 | 0.05 |
| ASH | 5.00 | 18.60 |
| MOISTURE | 3.50 | 47.50 |
| HEATING VALUE(Btu/lb) | 13,300 | 2,100 |
| KJ/Kg | 30,936 | 4,885 |

#### 1.4.1.1 Advantages of AFBC

The advantages of bubbling fluidized bed combustion are:-

**1) Open bottom design**

Fluidized-bed boilers must have a system to drain tramp material that collects around the bubble caps affecting fluidization and combustion. The Babcock & Wilcox (B&W) 100% open bottom design mounts the bubble caps on air pipes, which are evenly spaced to allow draining capability from the entire bed area. This design provides a clear vertical path for tramp material to move freely to the drain area.

**2) Air systems**

The purpose of the distributor is to introduce the fluidizing air evenly through the bed cross section thereby keeping the solid particles in constant motion, and preventing the formation of defluidization zones within the bed. The distributor, which forms the furnace floor, is normally constructed from metal plate with a number of perforations in a definite geometric pattern. The perforations may be located in simple nozzles or nozzles with bubble caps, which serve to prevent solid particles from flowing back into the space below the distributor.

The distributor plate is protected from high temperature of the furnace by:

i) Refractory lining

ii) A static layer of the bed material or

iii) Water cooled tubes.

**3) Emissions**

Sulphur dioxide emissions can be reduced by the injection of the sorbent into the bed, and subsequent removal of the ash together with the reacted sorbent. Limestone or dolomite is commonly used for this purpose. Ash carried away by the flue gas is removed in number of stages; firstly in convection section, then from the bottom of air pre-heater/economizer and finally a major portion is removed in dust collectors. The types of dust collectors used are cyclone, bag filters, electrostatic precipitators (ESP's) or some combination of all of these. To increase the combustion efficiency, recycling of fly ash is practiced in some of the units.

**4) Fuel flexibility**

Various types of fuels like bark and wood wastes, paper mill and sewage sludge's, most high moisture fuels, tire derived fuel, oil or natural gas and low grade biomass can easily be burnt in AFBC.

#### 1.4.1.2 Disadvantages of AFBC

The disadvantages of bubbling fluidized bed are:-

**1) High residue disposal cost**

In order to remove sulphur dioxide, a much higher Ca/S ratio is needed than in CFBC. This increases the cost of residue disposal.

**2) High carbon percentage in ash**

The residues consist of the original mineral matter, most of which does not melt at the combustion temperatures used. Where sorbent is added for sulphur dioxide removal, there will be additional CaO/MgO, $CaSO_4$ and $CaCO_3$ present. Carbon-in-ash levels are higher in FBC residues that in those from PCC.

### 1.4.2 Atmospheric circulating fluidized bed combustion (CFBC)

CFBC are used to overcome the drawbacks of the bubbling bed combustion. Circulating beds use high fluidizing velocity, ranging from 3.7m/sec to 9m/sec so the particles are held constantly in the flue gases, and pass through the main combustion chamber and into the cyclone, from which the larger particles are extracted and returned to the combustion chamber. Individual particles may recycle between anything from 10 to 50 times, depending on there size, and how quickly the char

burns away. Combustion conditions are uniform through out the combustor, although the bed is some what denser near the bottom of the combustion chamber.

There is a great deal of mixing and residence time during one pass is very short. CFBC are designed for the particular coal to be used. The method is principally of value for low grade, high ash coals which are difficult to pulverize and which may have variable combustion features. It is also suitable for co-firing coal with low grade fuels, including some waste materials. The direct injection of limestone into the bed offers the possibility of economic $SO_2$ removal without the need of the flue gas desulphurization.

Once the unit is installed, it will operate most efficiently with whatever design fuel is specified. The design must take into account ash quantities, and the ash properties. While combustion temperatures are low enough to allow much of the mineral matter to retain its properties, particle surface temperature can be as much as 200ºC above the nominal bed temperature. Various CFBC designs are used. The fluidizing velocity is high enough to retain a substantial amount of the material, and the solids are separated from the flue gases in a cyclone operating at a temperature near that of the exhaust gas as shown in Fig 1.8. Ash and unburned carbon are re-circulated, probably many times. Even though the solid inventory is distributed through out the unit, a dense bed is required in the lower part of the furnace to mix the fuel during combustion. Because of the recirculation of the bed material, particles residence times are relatively long compared with the gas residence time, and can be measured in tens of the seconds.

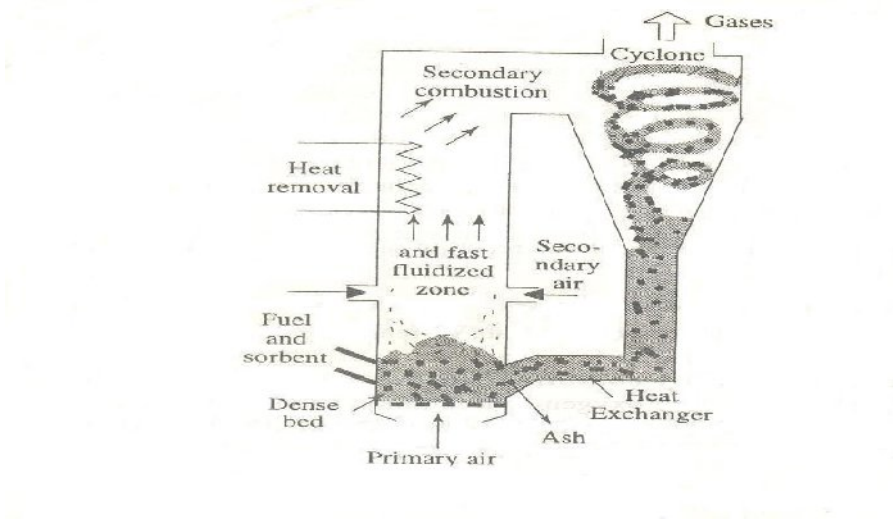


**Fig 1.8 – Atmospheric circulating fluidized bed**

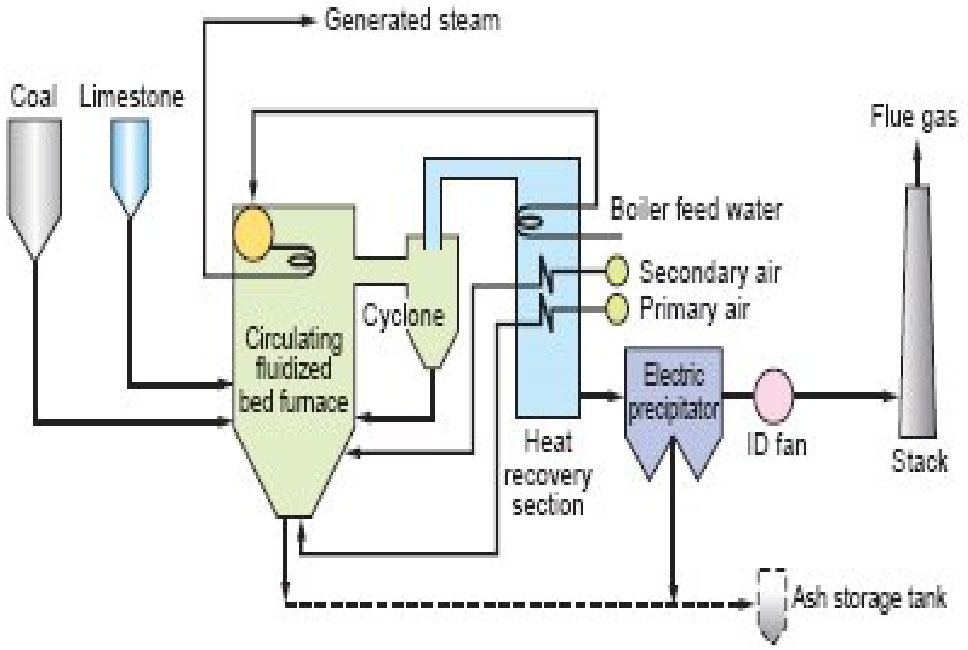


**Figure 1.9 – Process flow of circulating fluidized bed combustion**

The furnace used in CFBC is dividing into three zones:

1) Lower Zone(below the secondary air entry)
2) Upper Zone(above the secondary air entry)
3) Hot Gas and Solid Separator

**1) Lower zone**

The lower zone in the furnace is fluidized by primary combustion air, which constitute about 40-80% of the stiochiometric air required for the coal feed: coal and sorbent as well as the un-burnt char from the hot cyclone. Devolatization and partial combustion of the char occur in this zone, which is oxygen deficient. So to protect the surface from corrosion, this zone is refractory lined. It also serves as an insulated storage of hot solids, providing the CFB boiler with the thermal "flywheel". When the boiler load increases the proportion from primary to secondary air is increased. As a result, a greater amount of hot solids is transported to the upper zone of the furnace and some solid circulation increases. When the boiler loads decreases then the reverse happens and the solid circulation rate decreases.

**2) Upper zone**

Char particles transported to the upper zone are exposed to oxygen rich environment, where the complete combustion takes place. The upper zone is much taller than the lower zone. Unburned char particles that are entrained out of the furnace go around the refractory lined cyclone. The residence time of the char particles within the cyclone is short and the oxygen concentration is the lowest there. So the extent of the combustion inside the cyclone is the small compared to rest of the combustion loop. However, carbon monoxide and the volatiles often burn in the cyclone.

**3) Hot gas and solid separator**

In this zone the hot gases are separated from the un-burnt particles with the help of the cyclone. The cyclone that gives the circulating motion to the particles makes the particles to collect at the bottom of the cyclone, where as the hot gases goes out from the cyclone to the circulating fluidized furnace.

### 1.4.2.1 Advantages of CFBC

The advantages of CFBC are:-

**1) Wide range of fuel adaptability**

Conventional boilers for power generation can use only fossil fuel such as high grade coal, oil, and gas. The CFBC also uses low grade coal, biomass, sludge, waste plastics, and waste tire as fuel.

**2) Low pollution**

Emissions of pollutants such as NOx and SOx are significantly decreased without adding special environment measures. For the case of fluidized bed boiler, the desulphurization is intra-furnace desulphurization using mainly limestone as the fluidizing material. For the denitration, ordinary boilers operate at combustion temperatures from 1,400ºC to 1,500ºC, and the circulating fluidized bed boiler operates at lower temperatures ranging from 850ºC to 900ºC so that the thermal NOx emissions (generated NOx depending on temperature) are suppressed. In addition, the operation of circulating fluidized bed boiler is conducted by two stage combustion: the reducing combustion at the fluidized bed section; and the oxidizing combustion at the freeboard section. Then, the un-burnt carbon is collected by a high temperature cyclone located at exit of the boiler to recycle to the boiler, thus increasing the denitration efficiency.

**3) High combustion efficiency**

High combustion efficiency is attained by excellent combustion mechanism of circulating fluidization mode.

**4) Space saving and high maintenance ability**

Space saving is attained because there is no need of separate desulphurization unit, denitration unit, and fuel finely crashing unit. Accordingly, sections of trouble occurrence become few, and maintenance becomes easy.

#### 1.4.2.2 Disadvantages of CFBC

The disadvantages of CFBC are:-

**1) Lower thermal efficiency**

In the 100-200 MW range, the thermal efficiency of FBC units is commonly a little lower than the same size PCC units by 3-4% points. In CFBC, the heat losses from the cyclones are considerable high. This results in reduced thermal efficiency. The use of the low grade coal also tends to reduce the thermal efficiency of the system.

**2) High heat losses**

Even with the ash heat recovery system, there are high heat losses associated with the removal of both ash and spent sorbent form the system.

### 1.4.3 Pressurized fluidized bed combustion (PFBC)

The research and development of pressurized fluidized bed combined power generation technology was conducted at Wakamatsu Coal Utilization Research Centre (present Wakamatsu Research Institute) of Electric Power Development Co., Ltd. using the 71 MW PFBC Plant, which was the first PFBC plant in Japan. The test plant was the first plant in the world in terms of full-scale adoption of ceramic tube filter (CTF) which is able to collect dust from high temperature and high pressure gas at high performance.

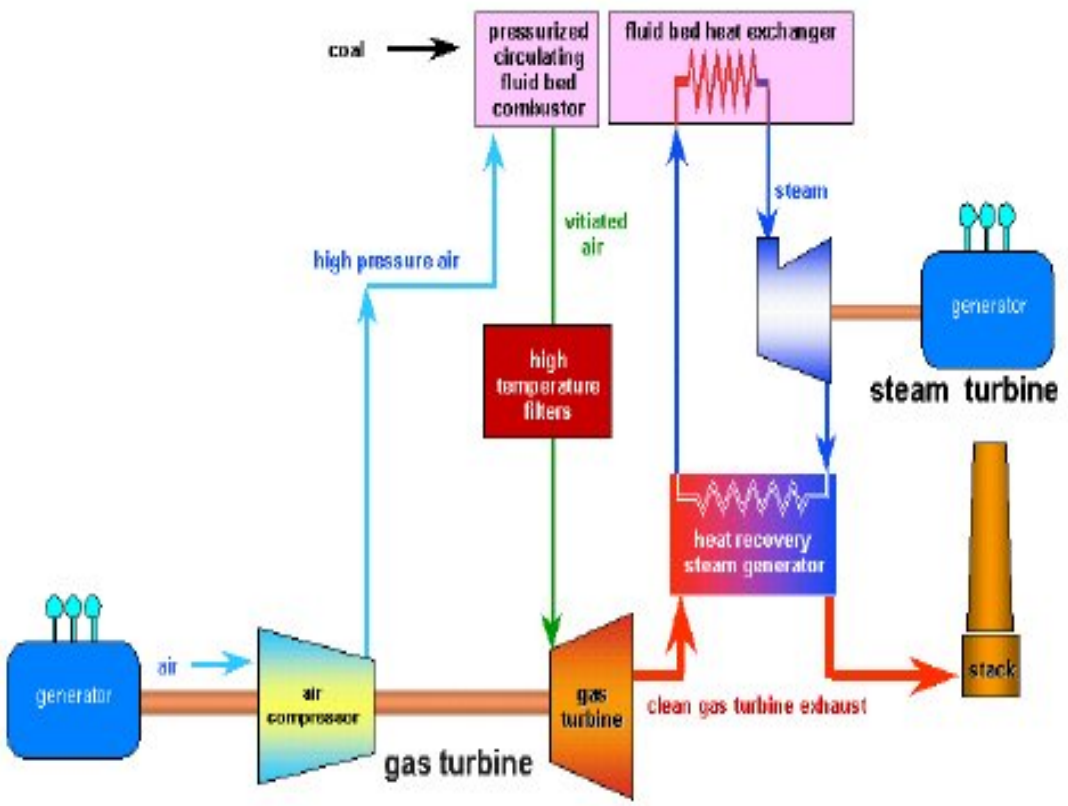


**Figure 1.10 – Pressurized fluidized bed combustion combined cycle**

Pressurized fluidized bed combustion (PFBC) is a variation of the fluid bed technology that is meant for large scale coal burning applications. If the coal-fired fluidized bed combustor is operated at the elevated pressure, the product of the combustion can be expanded through a gas turbine to produce electricity. The product of the combustion has to be sufficiently for a gas turbine to accept without excessive erosion, corrosion and fouling of the turbine. PFBC is under extensive research because of its potential as the coal fired gas turbine and when used in conjunction with a steam plant. A significantly higher efficiency of electricity generation can be obtained from either a gas turbine or steam turbine plant alone.

The first generation PFBC system uses a sorbent such as limestone or dolomite to capture sulphur released by the combustion of coal. Jets of air suspend the mixture of sorbent and burning coal during combustion, converting the mixture into a suspension of red-hot particles that flow like a fluid. Elevated pressures and temperatures produce a high pressure gas stream that can drive a gas turbine and steam generated from the heat in the fluidized bed is sent to a steam turbine, creating the highly efficient combined cycle system.

In more advanced second generation PFBC systems a pressurized carbonizer is incorporated to process the feed coal into fuel gas and char. The PFBC burns the char to produce steam a to heat combustion air for the gas turbine. The fuel gas from the carbonizer burns in a topping combustor linked to the gas turbine, heating the gases to the combustion turbine's rated firing temperature. Heat is recovered from the gas turbine exhaust in order to produce the steam, which is used to drive the conventional steam turbine, resulting in a higher overall efficiency for the combined cycle power plant.

Research being conducted in several FBC subprograms is demonstrating advanced features of the FBC and developing the technology base to lower capital and production costs. Thrusts include simplifications of the FBC systems and components, incorporation of alternative feed and withdrawal systems, and incorporation of advanced subsystems and steam cycles.

**Table 1.2 – Showing the advancements in PFBC power systems.**

| PFBC Power System | First Generation | Second Generation | |
|---|---|---|---|
| | | Initial | Final |
| Net System Efficiency | 40% | 45+% | 50+% |
| Target Date | by 2000 | by 2010 | by 2015 |
| $SO_2$ Emission Relative to NSPS | 1/4th | 1/5th | 1/10th |
| NOx Emissions Relative to NSPS | 1/3rd | 1/5th | 1/10th |
| Air Toxic Emissions Relative to 1990 CAAA | Meet | Meet | Meet |
| Capital Cost, $/kW | 1300 | 1100 | 1000 |
| Cost of Electricity vs. Conventional PC Coal Power Plant | 90% | 80% | 75% |

***Note:***
NSPS - New Source Performance Standards
CAAA - Clean Air Act Amendments

Results from system studies will guide future R&D determine optimum turbine-compressor configuration and lead to the demonstration of first-generation PFBC systems. Optimum configuration of second-generation PFBC for Vision-21

power plants with fuel cells and $CO_2$ sequestration options are also being developed. Gas turbine studies will be performed on gas compositions and heat capacities specific to PFBC, which can lead to higher allowable turbine blade temperature.

#### 1.4.3.1 Advantages of PFBC

Advantages of Pressurized fluidized bed combustion are:-

1) **High thermal efficiency**

   Increase in efficiency through the combined power generation utilizing the pressurized fluidized bed combustion conditions: (gross efficiency of 43%).

2) **Less toxic emissions**

   Providing advanced environmental characteristics including: SOx reduction through the in-bed desulphurization; NOx reduction through the low temperature combustion (about 860°C); Dust reduction by CTF; and $CO_2$ reduction by increased efficiency.

3) **Compact design**

   Space saving of plant through the compact design of boiler adopting pressurized condition and the elimination of desulphurization unit.

## 1.5 Advantages of FBC systems

The advantages of FBC systems are:-

1) **Reduction in boiler size** – High heat transfer rate over a small heat transfer area immersed in the bed result in overall size reduction of the boiler.
2) **Fuel flexibility** – FBC boilers can be operated efficiently with a variety of fuels. Even fuels like washery rejects, agri-wastes can be burnt efficiently. These can be fed either independently or in combination with coal into the same furnace.
3) **Ability to burn low grade fuel** – FBC boilers would give the rated output even with inferior quality fuel. The boilers can fire coals with ash content as high as 62% and having calorific value as low as 2500 kcal/kg. Even carbon content of only 1% by weight can sustain the fluidized bed combustion.
4) **Ability to burn fines** – Coal containing fines below 6mm can be burnt efficiently in FBC boilers, which is very difficult to achieve in conventional firing system.

5) **Pollution control** – Sulphur dioxide formation can be greatly minimized by addition of limestone or dolomite for high sulphur coals. 3% limestone is required for every 1% sulphur in the coal feed. Low combustion temperature eliminates NOx formation.
6) **Low corrosion and erosion** – The erosion and corrosion affects are less due to low combustion temperature, softness of ash and low particle velocity.
7) **Easier ash removal** – Ash removal is easier as the ash flows like liquid from the combustion chamber. Hence less manpower is required for the ash removal.
8) **High Efficiency** – FBC boilers can burn fuel with a combustion efficiency of over 95% irrespective of ash content. FBC boilers can operate with overall efficiency of 84%.

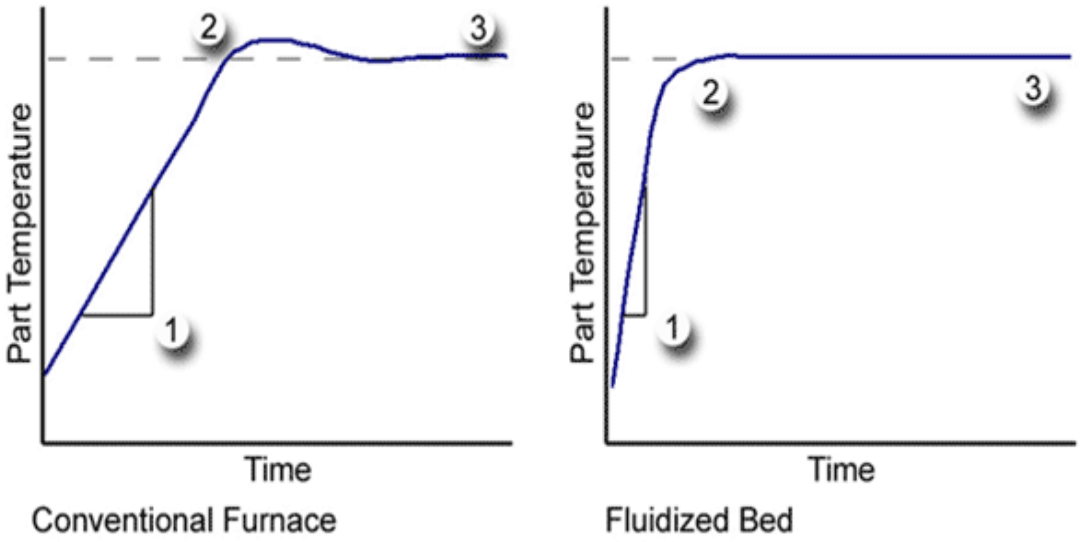


**Figure 1.11 – Graph showing difference in particle temperature vs. time between FBC and conventional furnace**

9) **Less excess air** – The $CO_2$ in the flue gases will be of the order of 14 to 15% at full load. Hence FBC boiler can operate at low excess air, only 20-25%.
10) **Simple operation and quick start up** – High turbulence of the bed facilitates quick start up and shut down. Full automation of start up and operation using reliable equipment is possible.

11) **Fast response to load fluctuations** – Inherent high thermal storage characteristics can easily absorb fluctuations in fuel bed rates. Response to changing load is comparable to that of oil fired boilers.
12) **No slagging in the furnace-no soot blowing –** In FBC boilers, volatilization of alkali components in ash does not take place and the ash is non sticky. This means that there is no slagging or soot blowing.
13) **Provisions of automatic coal and ash handling system** – Automatic systems of coal and ash handling is incorporated, making the plant easy to operate compared to oil or gas fired installation.
14) **Provision of automatic ignition system** – Control systems using micro-processors and automatic ignition equipment give excellent control with minimum manual supervision.
15) **High reliability –** The absence of moving parts in combustion zone results in a high degree of reliability and low maintenance costs.
16) **Reduced maintenance –** Routine overhauls are infrequent and high efficiency in maintained for long periods.
17) **Quick responses to changing demand** – A fluidized bed combustor can respond to changing heat demands more easily than stoker fired systems. This makes it very suitable for applications such as thermal fluid heaters, which require rapid responses.
18) **High efficiency of power generation** – By operating the fluidized bed at elevated pressure, it can be used to generate hot pressurized gases to power a gas turbine. This can be combined with a conventional steam turbine to improve the efficiency of electricity generation and give a potential fuel savings of at least 4%.

## 1.6 Biomass scenario in Punjab

Nowadays the industrial sectors are facing stiff competition from international market and they are unable to compete with the other developing nations due to soaring production cost. The foremost reason for the increasing production cost is due to the high electricity tariff in our country. The major portions of the electricity generated are from rapid depleting fossil fuels like coal, lignite, diesel and natural gas. Usage of

these fossil fuels threatens the life of human being through various environmental impacts like air pollution, global warming and etc.

In this world of cost consciousness and competition one should be able to incorporate any thing that could keep the industry viable. To overcome these problems, we are being forced to switchover to cost effective, Renewable and eco-friendly source of energy. One such energy is biomass, which is available in abundant and also can be cultivated to our energy.

Global production of biomass is an estimated 220 billion dry tones/year, nearly all in the form of natural growth wood and of agricultural and forestry residues. It accounts for about 15% of global energy consumption - 3% in industrialized countries and about 38% in developing countries. In some of the poorest countries, biomass accounts for over 90% of energy consumption (e.g. Nepal, Rwanda, and Tanzania). Agricultural and forestry residues are the fuels most readily available now.

Many of the developing countries produce huge quantities of agro residues but they are used inefficiently causing extensive pollution to the environment. The major residues are rice husk, coffee husk, coir pith, jute sticks, bagasse, groundnut shells, mustard stalks and cotton stalks. Sawdust, a milling residue is also available in huge quantity. Apart from the problems of transportation, storage, and handling, the direct burning of loose biomass in conventional grates is associated with very low thermal efficiency and widespread air pollution. The conversion efficiencies are as low as 40% with particulate emissions in the flue gases in excess of 3000 mg/Nm$^3$ In addition, a large percentage of un-burnt carbonaceous ash has to be disposed of. In the case of rice husk, this amounts to more than 40% of the feed burnt. As a typical example, about 800 tones of rice husk ash are generated every day in Ludhiana (Punjab) as a result of burning 2000 tones of husk. Briquetting of the husk could mitigate these pollution problems while at the same time making use of this important industrial/domestic energy resource.

### 1.6.1 Advantages of using biomass

Advantages of using biomass are:-

1) **Cheap power generation**

The power plant can generate power @ around Rs. 2.0 per unit (kWhr) excluding investment interest**.** The gas produced from around 4 kilogram of biomass can

approximately replace one litre of furnace oil / diesel. One litre of furnace oil will cost Rs. 21/- and four kilogram of biomass will cost Rs. 5/-, i.e. twenty one rupees fuel can be replaced by five rupees fuel. Every litre of furnace oil saved will save us Rs. 16/-. Similarly one litre of diesel @ Rs. 34/- can be replace by 4 kgs of wood @ Rs.5/-, which will result in cost saving of Rs. 29/- for every litre of diesel saving.

Also the plant will generate around 3-4% charcoal as by-product, which can be sold in the market as it is or it can be sold as activated charcoal after value addition, which generates additional revenue. Apart from this we can avail the CDM benefits of around Rs. 0.15 per unit through carbon trading.

**2) Rural electrification and employment**

Rural areas produce enough biomass and agricultural residues so that all its electricity demands can be met by using biomass based power plants. Apart from providing the rural energy self-sufficiency it can also generate enough employment opportunity to the rural people. Distributed generation through locally and abundantly available fuel which can be cultivated to the demand, so completely it is grid independence and self-reliance. Rural employment and waste land development is possible through this sustainable and renewable source of energy.

**3) More eco-friendly**

The plant will also encourage the concept of energy plantation thus resulting in greener environment resulting in more rainfall and reduction in ambient temperature. Hence it provides a sustainable, affordable and eco-friendly alternative to fossil fuel based power plants at low power levels.

**4) Less pollutants emission**

Due to FBC, the combustion of biomass generates very little sulphur dioxide, carbon dioxide and nitrogen oxides compared to fossil fuel based power plants. The process produces very low emissions of un-burnt primary fuel and no fly ash, since the solid fuel is subjected to multistage thermo-chemical conversion process.

**5) Energy conservation**

Energy conservation by consuming lesser energy resources for achieving the same output of electricity owing to higher cycle efficiencies. It improves the country's energy self-reliance and reduces the crippling oil import bill and saves enormous foreign exchange.

### 1.6.2 Power generation through biomass

In the significant development which could enable the Punjab Government to overcome the acute shortage of electricity, the Punjab Energy Developing Agency (PEDA) has allocated six projects to the private companies to produce 66MW of power from bio-mass. Not only this, the PEDA has also decided to set up 10 projects on its own to produce 120MW of electricity to enable the PSEB to overcome the shortage of power. For this PEDA has taken up its case with the World Bank demanding Rs.700 crores for funding the projects. Table 1.3 shows us the rate at which the biomass and power is generated in Punjab.

**Table 1.3 – Details of the amount of biomass and power generation in Punjab during 2004-2005.**

| Crop | Residue | Area (kha) | Crop Production (kT/Yr) | Biomass Generation (kT/Yr) | Biomass Surplus (kT/Yr) | Power Potential (MWe) |
|---|---|---|---|---|---|---|
| Paddy | Straw | 2492.9 | 8835.7 | 13252.9 | 10602.3 | 1272.3 |
| Paddy | Stalks | 2492.9 | 8835.7 | 9203.3 | 7362.6 | 809.9 |
| Wheat | Stalks | 3433.5 | 15561.3 | 31118.1 | 6223.6 | 781.2 |
| Wheat | Pod | 3433.5 | 15561.3 | 6512.6 | 3256.3 | 425.1 |
| Cotton | Stalks | 561.6 | 100.5 | 2122.8 | 1910.6 | 267.5 |
| Paddy | Husk | 2492.9 | 8835.7 | 2079.4 | 1663.5 | 183.0 |
| Maize | Stalks | 168.3 | 458.7 | 820.4 | 164.1 | 21.3 |
| Cotton | Husk | 561.6 | 100.5 | 109.2 | 98.3 | 13.8 |
| Sugarcane | Tops & leaves | 103.2 | 6140.4 | 314.1 | 78.5 | 10.7 |
| Maize | Cobs | 168.3 | 458.7 | 169.1 | 50.7 | 7.1 |
| Mustard | Stalks | 40.2 | 49.0 | 79.8 | 39.9 | 5.2 |
| Cotton | Boll shell | 561.6 | 100.5 | 30.2 | 27.2 | 3.8 |
| Total | | 6799.7 | 31145.5 | 65812.1 | 31477.7 | 3800.9 |

Sugar, pulp and paper industries traditionally used grate-fired boilers for power and steam generation. The major driving force that led to the development of FBC was the need for more efficient technologies for the utilization of the low-grade fuel. In pulp and paper industry, BFB is the preferred technology for the combustion of wood wastes and bark in smaller co-generation plants. Higher environmental awareness, larger plants and multi-fuel capabilities have favoured the CFB boilers for the power and steam generation from biomass fuels.

# CHAPTER – 2

# LITERATURE REVIEW

## 2.1 Significance of mathematical modelling

Active efforts are put to devise appropriate and economic power generation systems from agri-waste all over the world. Although most of the work in the frontal areas of the problem has been done in USA, UK and China, but some pioneering work has been done in a couple of enterprising, developing countries too, resulting in identification of various constraints and problems related to utilization of agri-waste, agro-industrial waste and forest residue for generating electric power. Literature surveyed unfolds the following scenario at the world level. Whereas technology related developmental efforts have been made chiefly in USA, UK and China, the countries like Mexico, Hawaii, Vietnam, Nepal, India and Pakistan have focused mainly on applied and operational aspects. Diverse aspects of the problem have been examined and the results of studies reported at national and international level.

Developing various mathematical models will help us in understanding the various aspects of fluidization and its related phenomenon. Mathematical models have solved the problems in a systematic way and provides the actual picture of the whole process. The mathematical modeling helps in deciding the optimum values of the operating parameters, which results in an efficient operation of the fluidized bed systems. It helps in easy analysis of the system and its related parameters. Through mathematical modeling the best results can be achieved.

## 2.2 Description of some famous models

From the last 30 years lot of work have been done on FBC systems and its related processes. Various scientists have used different fuel using different FBC systems. The results of there work have been thoroughly studied and various mathematical models are developed. Some of the mathematical models are presented below to give the overview of the research that has been done so far.

**Khan A. A. et al.[20]** have developed a model of 1MW atmospheric bubbling fluidized combustor burning waste wood fuel. The model incorporates both the solid and gas phases. The bed is assumed to consist of two phases, of which the emulsion phase takes both gas and solids into account, while the bubble phase consists only of gas. A wide size distribution of biomass feed, representative of the actual boiler feed, has been assumed. The model calculates the gas composition, velocities, and other important hydrodynamic parameters in both the emulsion and bubble phase. A particle size distribution model is included to calculate elutriation losses of fine char particles. This approach is novel in the sense that a population balance for fine particle class is derived, using the well-known mass balance principles, and a coupled discretized population balance equation, valid for the whole particle size range, is presented. The model takes into account devolatilization, fragmentation, and attrition of the solid phase along with gaseous profiles. It includes nine components for which differential equations have been derived and solved to calculate species concentration at any point along the bed height. In total, 20 particle size classes have been considered, 10 of which are considered as feed and the rest as fine classes. The model aims to assess the effect of different parameters on boiler performance and gaseous emissions. A sensitivity analysis of the gaseous emission profiles with respect to different variables and parameters defining different sub-models has been carried out. A homogeneous NOx model has been included with individual kinetic parameters for relevant species. It has been found that gas hydrodynamics play a significant role, and the system can be optimized using these parameters.

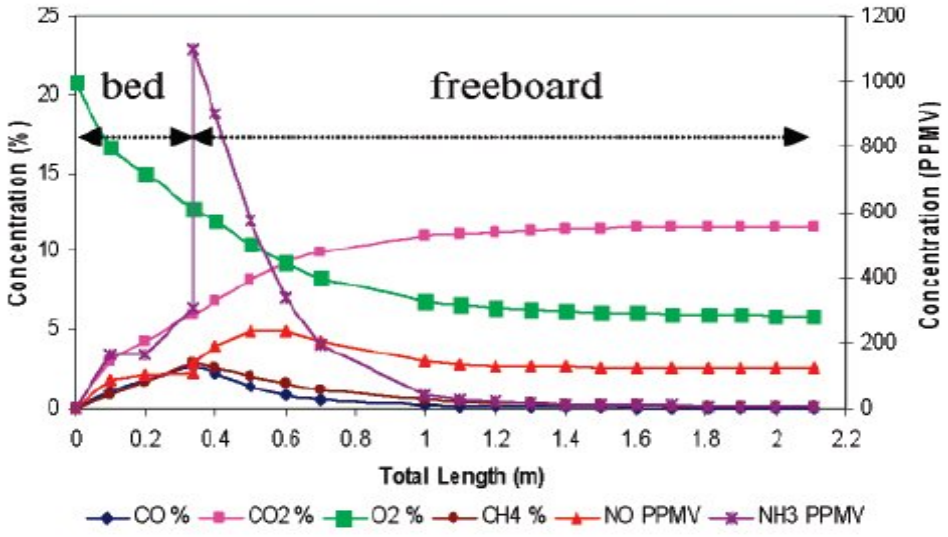


**Figure 2.1 – Predicted species concentration along the boiler length**

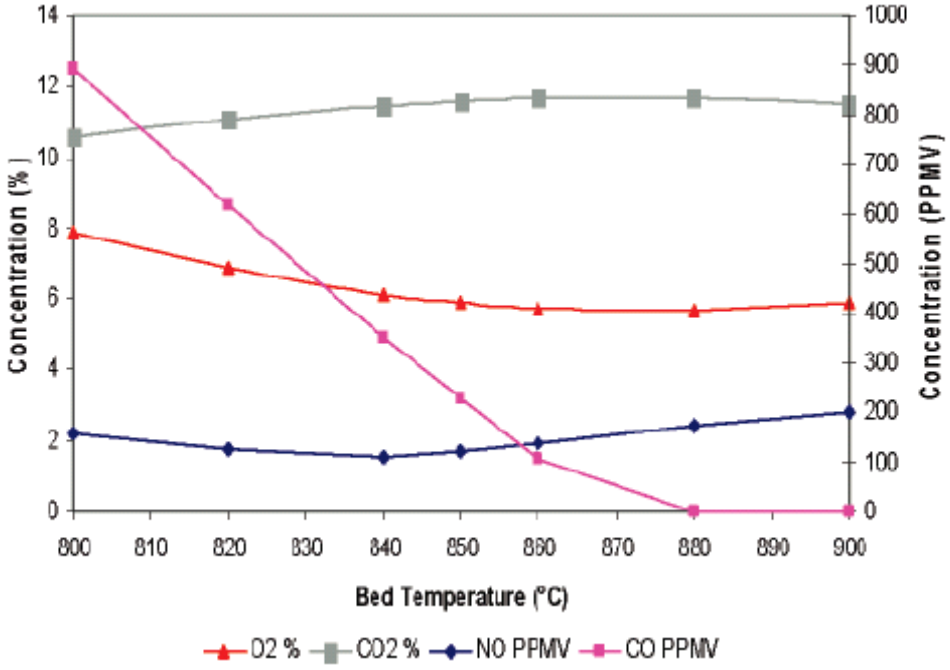


**Figure 2.2 – Effect of temperature on gaseous emissions**

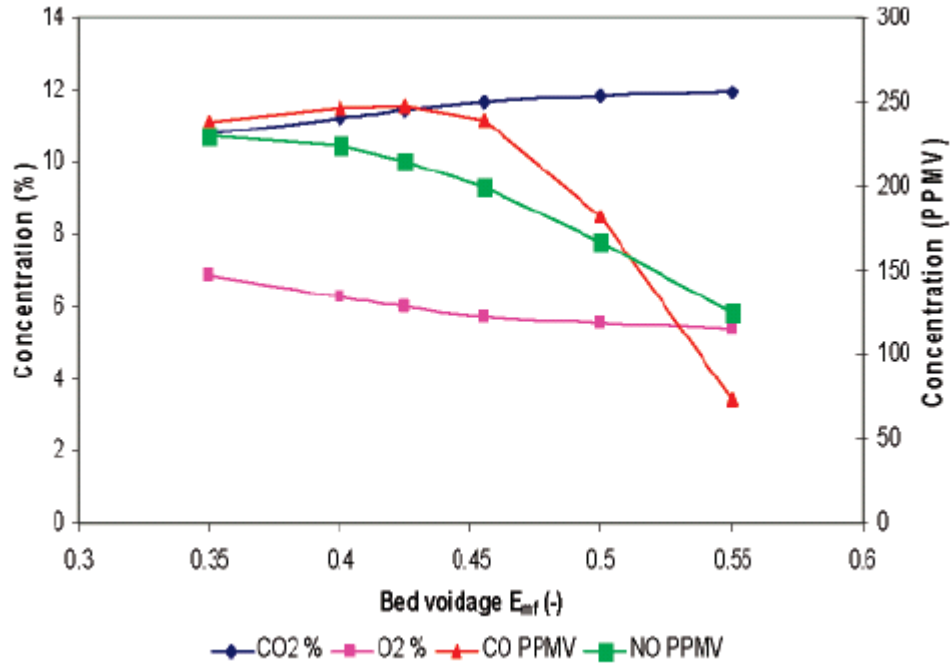


**Figure 2.3 – Effect of bed voidage on gaseous emissions**

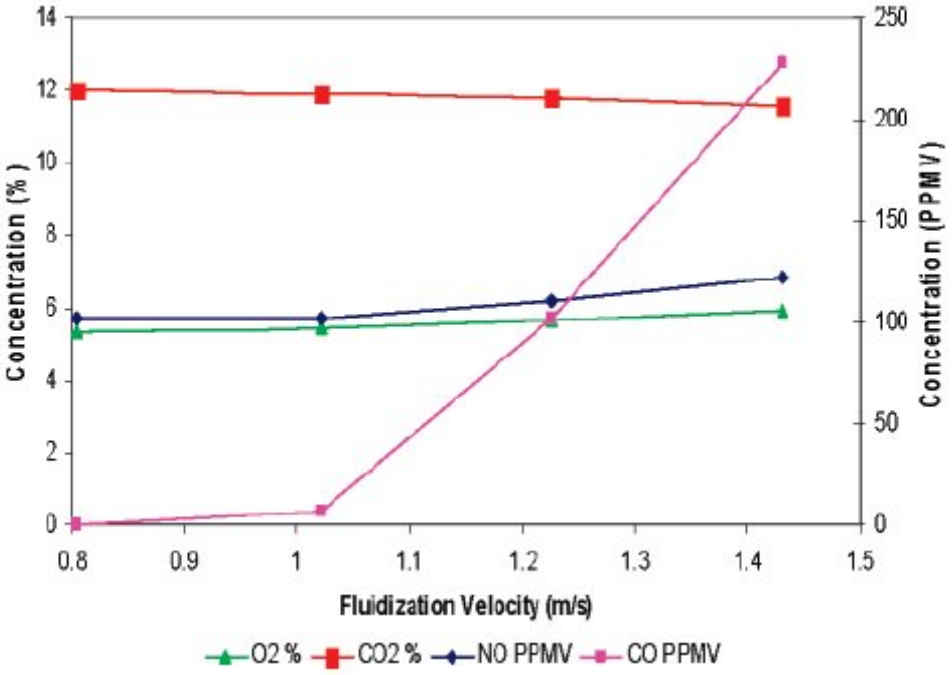


**Figure 2.4 – Effect of fluidization velocity on gaseous emissions**

**Chavarie C. et al.[4]** have done work on the hydrodynamic parameters. When chemical reactions are carried out in fluidized beds, the reactor performance may be strongly influenced by the hydrodynamics of the two phases. In the present study, bubble sizes, bubble frequencies, and visible bubble flow rates have been measured in a large two-dimensional fluidized bed. The operating conditions were chosen to be identical with those used in the reaction studies described in the companion papers. Coherent expressions for the bubble properties are presented and allow hydrodynamic parameters to be specified in the testing of fluidized bed chemical reactor models against measured concentration profiles and overall conversions.

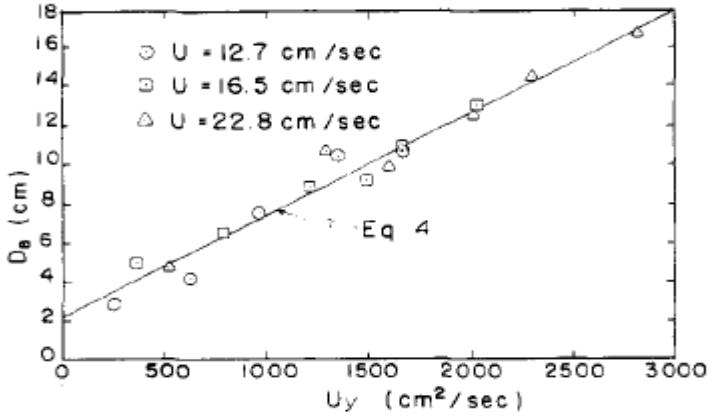


**Figure 2.5 – Bubble diameter as the function of height and superficial velocity**

**Okasha F. [28]** has done a staged combustion of rice straw in a fluidized bed. Staged combustion of rice straw has been investigated using an atmospheric bubbling fluidized bed combustor. The combustor has a 300 mm ID and a 3300 mm height. Secondary air was introduced in the freeboard at 1500 mm above the primary air distributor. Rice straw was fed as cylindrical pellets of a 12 mm diameter and 10–15 mm lengths.

The obtained results indicate that staged combustion appears an effective technique to reduce NOx emissions, in particular, at higher operating temperatures. Typically, at 850$^{o}$C bed temperature, NOx concentration is reduced by about 50% when 30% of fed air is introduced as secondary air. Staged operation has a slight, non-monotonic effect on $SO_2$ emission. Combustion efficiency improves with increasing secondary air ratio reaching a maximum value that is mainly attributed to a reduction in fixed carbon loss. With further increase in secondary air ratio, combustion efficiency; however, decreases again since entrained fixed carbon and exhausted carbon monoxide tend to increase. The range of secondary air ratio, over which combustion efficiency improves, expands at higher operating temperatures.

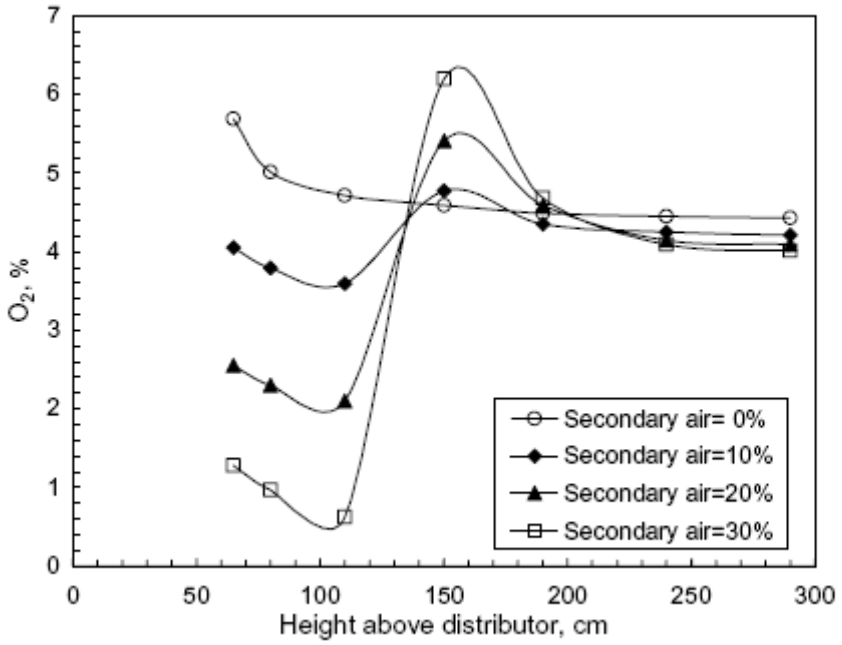


**Figure 2.6 - Effect of secondary air ratio on axial profile of $O_2$**

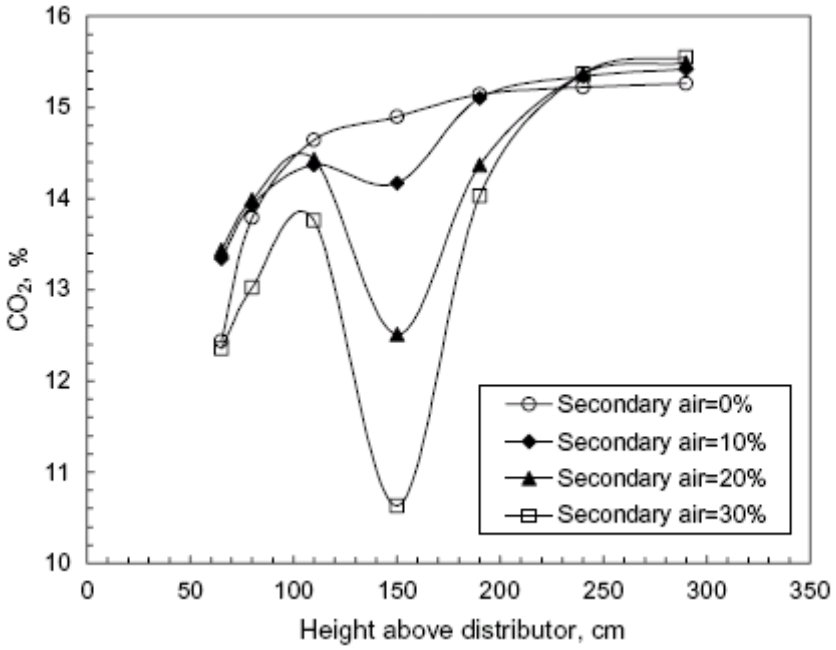


**Figure 2.7 - Effect of secondary air ratio on axial profile of $CO_2$**

**Hayhurst A. N. et al. [17]** have worked on a freely moving, machined sphere of graphite (or a rounded particle of a coal char) attached to a very thin, flexible thermocouple. It has been burnt in a bed of silica sand fluidized by air. Simultaneous measurements were made of [CO] and [$CO_2$] in the off-gases, as well as of the temperature of the burning particle. Each sphere of carbon was large enough (>2 mm) for its burning to be controlled by external mass transfer. These measurements, together with the relative rates of formation of CO and $CO_2$ obtained previously, enabled mass transfer coefficients and Sherwood numbers to be derived. Such measurements were made for different temperatures in the bed, sizes of sand, superficial velocities, and initial diameters of a graphite sphere. Only a slight decrease in Sh was found when the bed's temperature was raised; this was accounted for by changes in the following physical properties: the density of the fluidizing gas, the diffusivity of $O_2$, the viscosity, and minimum fluidizing velocity of the air. There was no clear trend of Sh with the actual superficial velocity of the fluidizing air. On the other hand, Sherwood number was increased significantly by using larger sand particles, mainly as a consequence of increasing the gas velocity in the interstices between the sand particles.

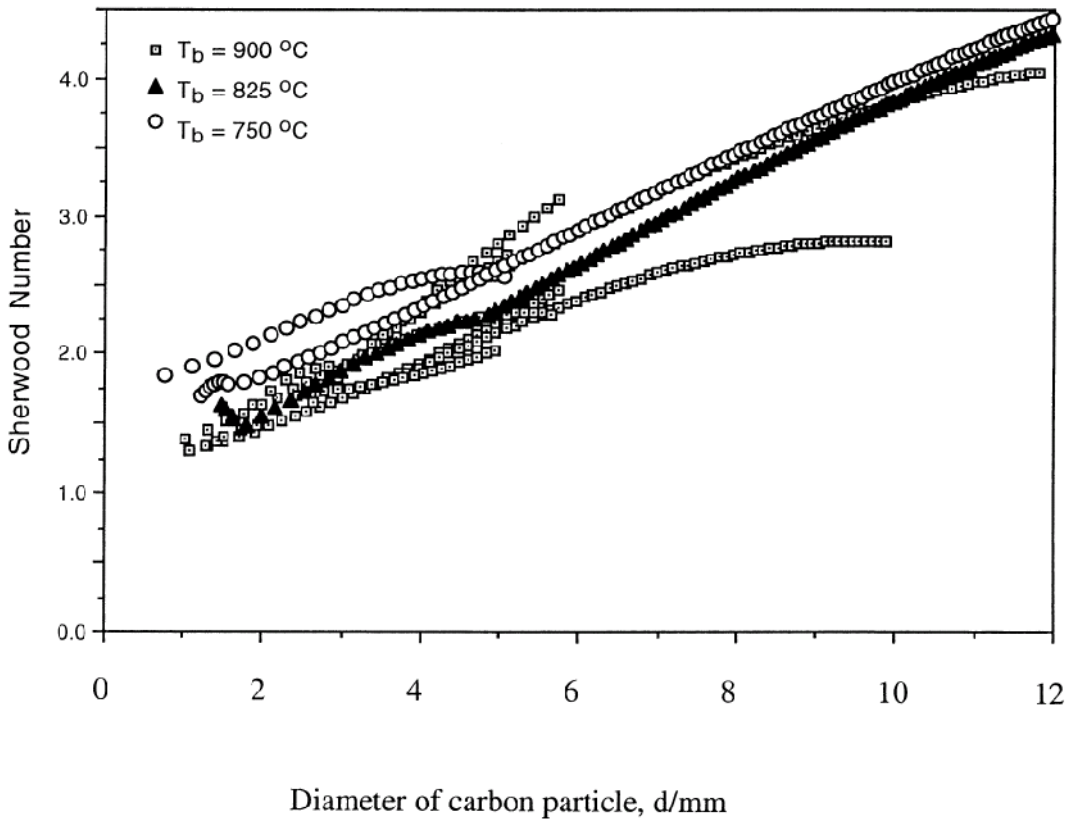


**Figure 2.8 - Plots of Sherwood number against *d*, the diameter of a burning carbon particle for graphite spheres of different initial sizes in beds at 900°C, 825°C, and 750°C for 417 to 571 $\mu$m silica sand with *U*/*Umf* = 3.5.**

**Janvijitsakul K. et al. [18]** have done the co-firing of rice-husk and bagasse in a conical fluidized bed combustor. In this work, "as-received" rice husk and sugar cane bagasse were co-fired in the cone-shaped fluidized-bed combustor with the aim of effective and environmentally friendly utilization of these biomass fuels. Temperatures and volume gas concentrations ($O_2$, CO and NO) were measured at different location points along the combustor height and in the stack flue gas when co-firing the two biomass fuels at different mass/energy fractions as well as when using rice husk only. Axial temperature and gas concentration profiles in this combustor operated at 82.5–82.8 kg/hr fuel feed rates and various values (40–100%) of excess air, *EA*, for the 100%, 75% and 45% rice husk mass fractions in the fuel blend, are discussed. The axial temperature profiles were found to be almost independent of excess air and strongly affected by the rice husk energy fraction ($EF_{rh}$), i.e. contribution by rice husk to the heat input when rice husk and bagasse co-firing. The CO emissions, or CO concentrations in the flue gas leaving the combustor, were

found to reduce for higher values of $EF_{rh}$ and $EA$. Meanwhile, the NO concentrations at all the point over the combustor volume as well as in the stack flue gas were increased for higher $EF_{rh}$ and $EA$ values. Co-firing of rice husk and bagasse led to higher combustion efficiency at reduced environmental impacts compared with those in the case of firing rice husk only. Through the co- combustion with rice husk, an effective use of "as-received" sugar cane bagasse becomes feasible for energy production in fluidized-bed combustion systems.

**Table 2.1 - Proximate and ultimate analysis of rice husk and bagasse**

| Analysis | Rice husk | Bagasse |
|---|---|---|
| Ultimate analysis (wt.%, "dry and ash-free" basis): | | |
| Carbon | 44.99 | 42.64 |
| Hydrogen | 6.39 | 6.62 |
| Oxygen | 48.15 | 50.48 |
| Nitrogen | 0.42 | 0.19 |
| Sulfur | 0.05 | 0.07 |
| Proximate analysis (wt.%): | | |
| Moisture ("as-received" basis) | 11.0 | 48.8 |
| Ash ("dry" basis) | 14.16 | 2.15 |
| *LHV* (MJ/kg) | 12.34 | 6.68 |

**Table 2.2 - Fuel feed rate, moisture content and rice husk energy fraction for the fuels used in the experimental tests**

| Rice husk mass percentage in the fuel blend | Fuel feed rate (kg/h) | Moisture content (%) | Rice husk energy fraction |
|---|---|---|---|
| 100 | 82.8 | 11.0 | 1.00 |
| 75 | 82.5 | 17.4 | 0.85 |
| 45 | 82.7 | 36.9 | 0.60 |

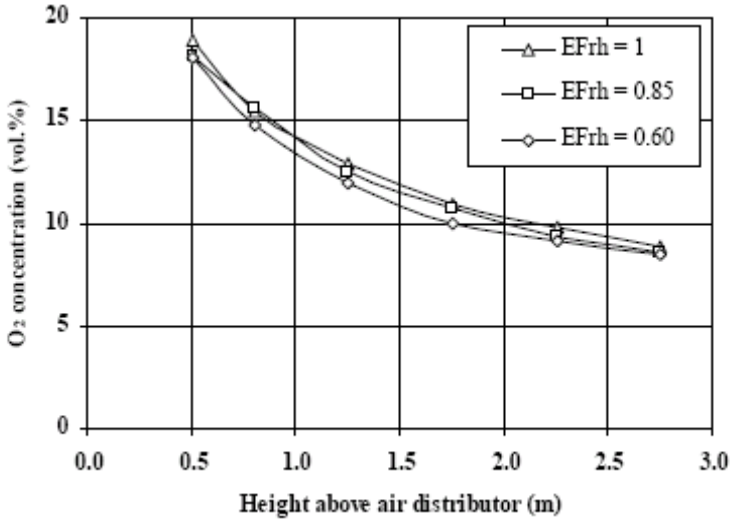


**(a)**

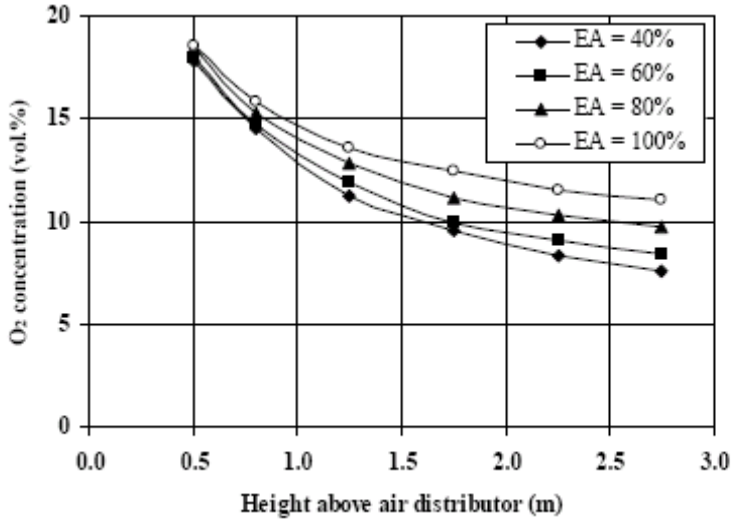


**(b)**

**Figure 2.9 -Effects of the rice husk energy fraction (a) and excess air (b) on the axial O2 concentration profiles in the conical FBC for biomass (co)-firing at the fuel feed rate of 82.5–82.8 kg/h: *EA* = 60% for (a) and $EF_{rh}$ = 0.6 for (b)**

**Wang A. L. T. et al. [32]** presented a mathematical model to simulate the hydrodynamics of a novel design of Pressurized Fluidized Bed Combustor. They make a bench-scale fluidized bed combustor with a novel fluidizing gas injection manifold was successfully built for characterization of Australian black coals under PFBC conditions. Instead of the usual horizontal distributor plate to support the bed

and distribute the fluidizing gas, the fluidizing gas was injected horizontally through 8 radial ports in the cylindrical wall of the combustor. To verify satisfactory hydrodynamic performance with the novel gas injection manifold, the fluidization was directly investigated by measuring differential pressure fluctuations under both ambient and PFBC conditions. In addition, a Perspex cold model was built to simulate the hydrodynamics of the hot bed in the PFBC facility. Under PFBC conditions, the bed operated in a stable bubbling regime and the solids were well mixed. The bubbles in the bed were effectively cloudless and no gas back mixing or slugging occurred; so the gas flow in the bed could be modelled by assuming two phases with plug flow through each phase. The ratio of ($U_{mf}$) for the simulated bed to ($U_{mf}$) for the hot PFBC bed matched the conditions proposed by Glicksman's scaling laws. The bubbles rose along the bed with axial and lateral movements, and erupted from the bed surface evenly and randomly at different locations. Two patterns of particle movement were observed in the cold model bed: a circular pattern near the top section and a rising and falling pattern dominating in the lower section.

The bench-scale model was operated at ambient conditions. The bubbles erupted and randomly from different locations at the bed surface. Occasionally some bubbles could be seen from the side of the bed through the wall of the cold model (Figure 2.10(a) and 2.10(b)) but sometimes those bubbles were found to disappear from sight (moved towards the centre of the bed) as they rose towards the top of the model, when viewed from the side (Figure 2.10(c) and 2.10(d)).

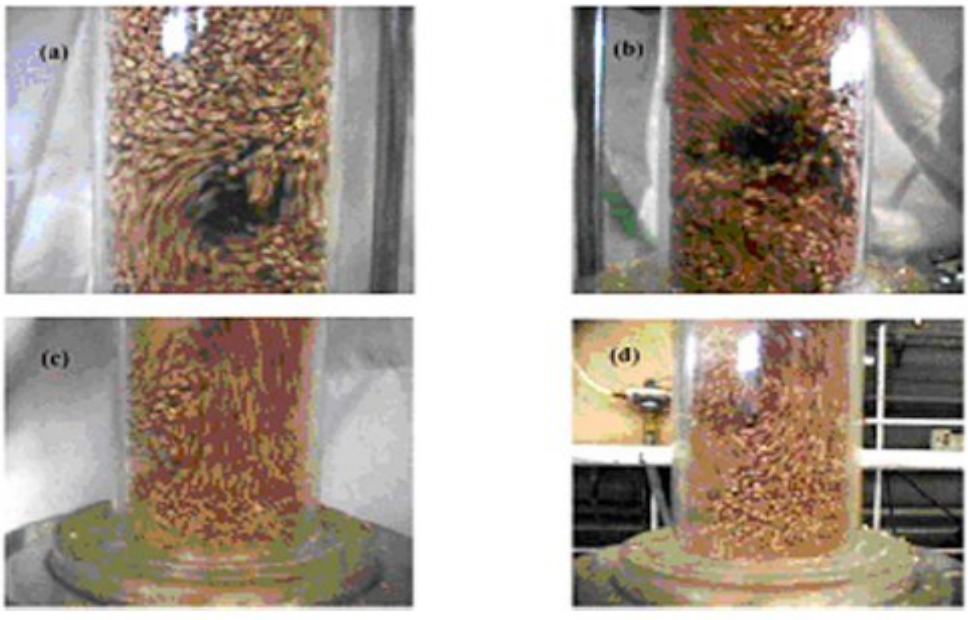


**Figure 2.10 - Bubbles and particle movements in the simulating cold bed**

Two patterns of particle movements were observed as shown in Figure 2.11. The circular pattern as shown in Figure 2.11(a) was found mostly to dominate the hydrodynamics of the top section of the fluidized bed but sometimes irregular turbulence was also observed in this region instead of the pattern mentioned. The rising falling pattern Figure 2.11(b) dominated the hydrodynamics of the lower section of the fluidized bed.

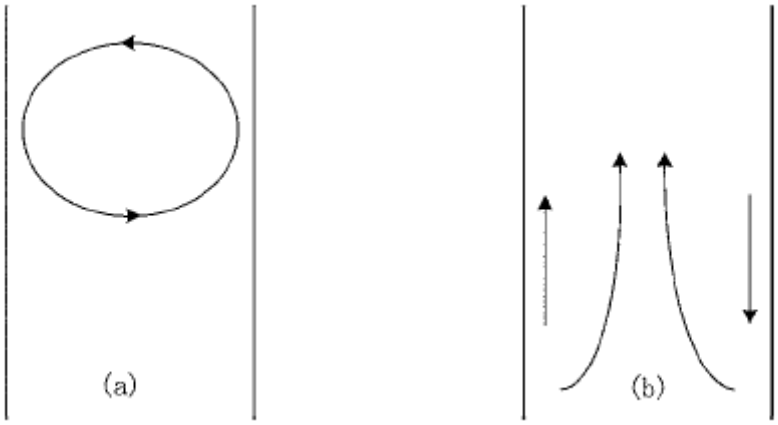


**Figure 2.11 – Particle movement patterns in the bed**

**Mohapatra S. K. et al. [24]** developed a mathematical model for oxygen mass balance for a 10 MW fluidized bed coal combustion power plant operated at Jamadoba (TISCO, India) using coal washery rejects. Assuming tree-phase theory of fluidization, the fluid bed is considered to consist of a number of equivalent stages in series. Within each stage, an exchange of gas takes place between the bubbles, cloud wake and emulsion phases. The model has been used to predict the consumption of oxygen in the fluidized bed combustor, the outlet gas composition, variation of average oxygen concentration along the bed height. Model prediction was compared with plant data and reasonable accuracy was obtained.

They had reported a decrease in the average concentration of the oxygen, as the bed height is increased, as shown in the Fig 2.14 and this is true for different amount of excess air values. Variations of the oxygen concentrations in different phases along the bed height are as shown in Fig 2.15. the oxygen concentration in the bubble phase decreases gradually but, it is steep in the cloud-wake and the emulsion phase at the lower bed levels. The oxygen concentration in the bubble phase is highest, followed by the cloud-wake and the emulsion phases, because the main

combustion reaction occurs in the emulsion phase, as a result of which oxygen consumption in this phase is highest and hence the oxygen concentration lowest.

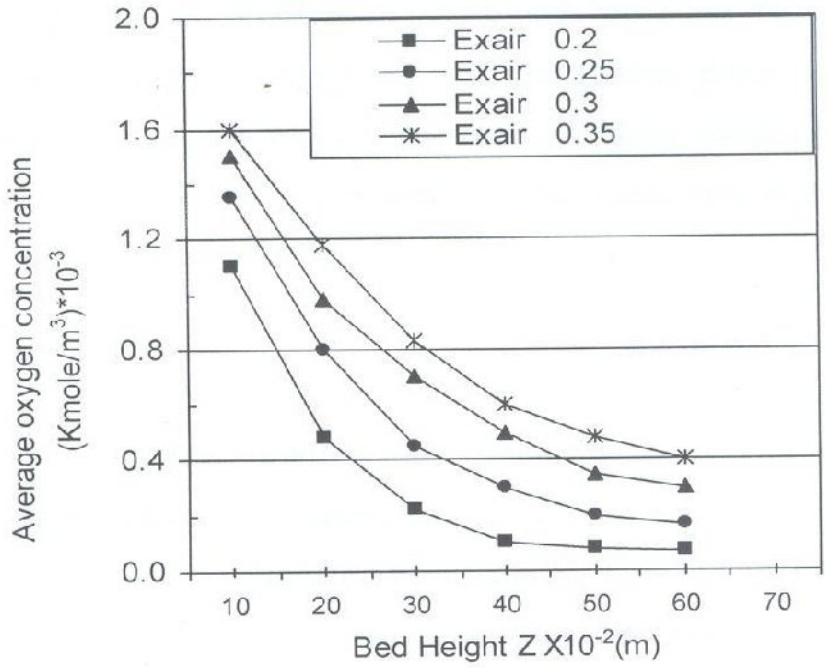


**Figure 2.12 – Variation of average oxygen concentration with bed height using different quantity of air**

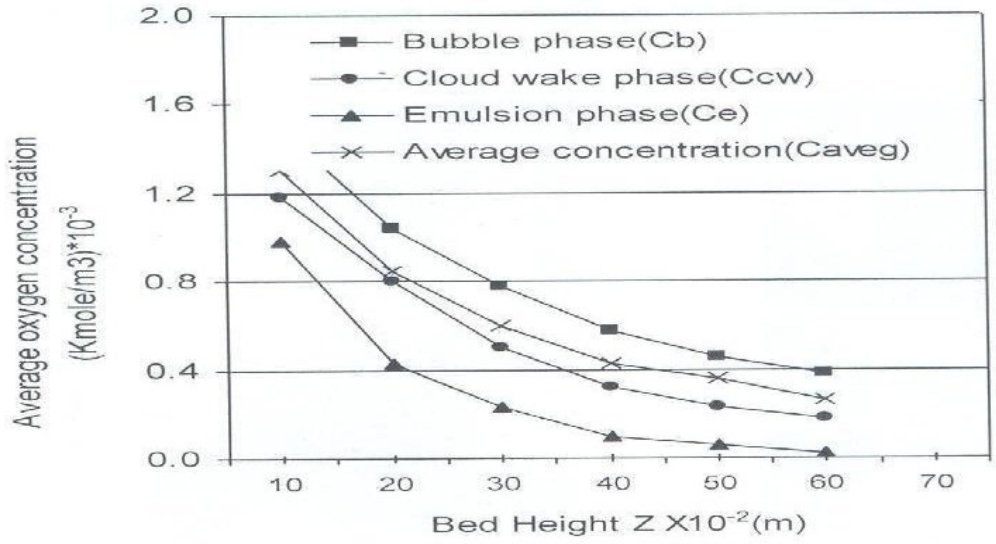


**Figure 2.13 – Variation of average oxygen concentration with bed height using different phases**

**Avedesian M. M. and Davidson J. F. [1]** in **1973** attempted the first application of the two phase theory of fluidization to the batch combustion of char and coke particles in a hot bed of inert material fluidized by air. This was the first realistic approach which formed the basis of subsequent development. Assuming two phase theory of fluidization and perfectly mixed emulsion phase, they derived the bubble diameter which remains constant along the height of the bed. They further assumed that the combustion rate is controlled by the rate of the diffusion of oxygen to the burning particle and chemical reactions are so fast at the prevailing bed temperature that they have no influence on the overall kinetics. Considering the first order reaction kinetics, they derived oxygen molar flow rate to a char surface.

**Davidson J. F. and Harrison D. [7]** proposed the two phase theory of fluidization in **1963**, according to which the gas flowing through the bed via an air distributor plate is divided into two parts, viz. a bubble phase and a dense phase. The word 'phase' refers to a region which may include both gas and solid particles. The phases are distinguished from one another in terms of the volume fraction of solids, by physical appearance and their flow characteristics. The gas flow rate through the dense phase corresponds to minimum fluidization velocity ($U_{mf}$) with constant voidage ($\varepsilon_{mf}$). All gas in excess of that needed to just fluidize the bed phases through it as bubbles (the bubble phase). They proposed that bubbles are regarded as being of uniform diameter $D_b$, which may be determined from bed expansion data employing the following relation:

$$\frac{0.711(g.D_b)^{1/2}}{(U_o - U_{mf})} = \frac{H_{mf}}{(H - H_{mf})} \qquad (2.1)$$

By assuming the bubble to be spherical shaped, Davidson and Harrison derived the following expression for mass transfer coefficient or gas interchange coefficients between bubble and emulsion phases as:

$$(K_{be})_b = 4.5\frac{(U_{mf})}{D_b} + 5.85\frac{(D_e^{1/2}.\, g^{1/4})}{(D_b^{5/4})} \qquad (2.2)$$

**Delebarre A. et al. [9]** worked on the phenomenon that the minimum fluidization does exist or not. This work proposes an equation giving the pressure drop of a gas flowing through a porous medium or a granular bed. The consequences for the onset

of the fluidization are then discussed. It appears that the notion of minimum gas mass-flow rate would improve the description of the transition between fixed and fluidized bed regimes. An equation is then proposed to calculate the minimum fluidization gas mass-flow rate. It is then proved that the minimum fluidization is not only a function of the medium and fluid characteristics but also that it increases with bed inventory. It is then shown that a batch of particles has a minimum fluidization depending on its arrangement in a column and that in some cases, this minimum does not exist at all. As a consequence, the minimum of fluidization, whether it is a velocity or a mass flow rate, cannot be considered as a criterion to characterize a powder.

**Faravelli T. et al. [13]** modelled homogeneous combustion in bubbling beds burning liquid fuels. They introduces a model for the description of the homogeneous combustion of various fuels in fluidized bed combustors (FBC) at temperatures lower than the classical value for solid fuels, i.e., 850°C. The model construction is based on a key bubbling fluidized bed feature: A fuel-rich (endogenous) bubble is generated at the fuel injection point, travels inside the bed at constant pressure, and undergoes chemical conversion in the presence of mass transfer with the emulsion phase and of coalescence with air (exogenous) bubbles formed at the distributor and, possibly, with other endogenous bubbles. The model couples a fluid-dynamic submodel based on two-phase fluidization theory with a sub model of gas phase oxidation. To this end, the model development takes full advantage of a detailed chemical kinetic scheme, which includes both the low and high temperature mechanisms of hydrocarbon oxidation, and accounts for about 200 molecular and radical species involved in more than 5000 reactions. Simple hypotheses are made to set up and close mass balances for the various species as well as enthalpy balances in the bed. First, the conversion and oxidation of gaseous fuels (e.g., methane) were calculated as a test case for the model; then, n-dodecane was taken into consideration to give a simple representation of diesel fuel using a pure hydrocarbon. The model predictions qualitatively agree with some of the evidence from the experimental data reported in the literature. The fate of hydrocarbon species is extremely sensitive to temperature change and oxygen availability in the rising bubble. A preliminary model validation was attempted with results of experiments carried out on a prepilot, bubbling combustor fired by under bed injection of a diesel fuel. Specifically, the model results confirm that heat release both in the bed and in the freeboard is a function of bed temperature. At lower emulsion phase temperatures many combustible species leave the bed unburned,

while post-combustion occurs after the bed and freeboard temperature considerably increases. This is a well-recognized undesirable feature from the viewpoint of practical application and emission control.

**Galgano A. et al. [16]** presented a dynamic model of an atmospheric bubbling fluidized bed combustor using biomass. The model was used to access how the dynamic behaviour of the combustor varies with some of the operating parameters. To this end a bifurfication analysis was first used to study the influence of the selected parameters on the number and quality of steady state solution. Dynamic simulation showed that the bed temperature changes slowly when a step wise change is imposed on the selected parameters. Either a new steady state or extinction eventually results, depending upon the step wise change. The relaxation time of the bed was determined by the heat capacity of the fluidized solids and by the fraction of the heat released recycled to the bed as thermal feed back.

**Kunni D. and Levenspiel O. [22]** in **1968** proposed a three phase model for a bubbling fluidized bed, which considers the cloud-wake region as a separate phase, in addition to the emulsion and bubble phases. Bulk flow of gas through the emulsion and cloud-wake phases is assumed to be small.

**Natrajan E. et al. [27]** in their paper provided an overview of previous works on combustion and gasification of rice husk in atmospheric bubbling fluidized bed reactor and summarized the state of the art knowledge. As the high ash content, low bulk density, poor flow characteristics and low ash melting point makes the other types of reactors either insufficient or unsuitable for rice husk conversion to energy; the fluidized bed seems to be the promising choice. The major conclusion is that the results reported in the are limited and vary widely, emphasizing the need for further research to establish suitable and optimum operating conditions for commercial implementation.

**Premchart W. et al. [29]** have in their paper, summarized the results of an experimental study on combustion of three distinct biomass fuels (saw dust, rice husk, pre dried sugar cane, bagasse etc.) in a single fluidized bed combustor with a conical bed using silica sand as the inert bed material. Temperature, CO, $NO_2$, and $O_2$ concentrations along the combustor as well as in flue gas were measured in the experimental tests. The effects of fuel properties and operating conditions on these variables were investigated. Based on the CO emissions and unburned carbon

contents in fly ash, the combustion efficiency of the conical FBC was quantified for the selected biomass fuels fired under different operating conditions.

**Yagi and Kunii D. [33]** made the first attempt to model a fluid-bed combustor in **1955.** They derived equations for the combustion of single carbon particles of a fixed size, as well as for a particle which is shrinking due to reaction, taking into account the intermediate diffusion and the chemical reaction. Assuming single phase theory, they formulated an expression for solids population balance and carbon load in the bed. The proposed theory was tested and compared with combustion of coke particles in laboratory scale combustor with reasonable accuracy. Though the model received widespread consideration in fluidized bed combustor models, it had its limitations such as:

- Only an isolated bed is considered.
- No consideration was given to the existence of a dilute phase.
- Single carbon particle of fixed size was considered.
- Only the simplest kinetic behaviour, namely, the direct formulation of the carbon dioxide from carbon and oxygen was considered.
- No validation with data from industrial fluidized bed coal combustors was made.

After this attempt some models on two-phase theory of fluidization were proposed.

# CHAPTER – 3

# PLANT DETAILS

Malwa power limited, Muktsar, a 7.5 MW FBC based power plant has been selected for the present study. It was set up in 2005 with the purpose of using the waste cotton stalk. The area of Muktsar is very conducive for the cotton growth and the fuel there is in abundant, as compared to the other plants like Jalkheri, Patiala, where the supply of fuel (rice husk) is less. A large amount of cotton waste is left in the fields after the cotton has been harvested from the plants. This cotton waste is called 'cotton stalk' and has a height varying from 3 feet to 5 feet. Cotton stalk is quite rich in carbon content. Traditionally, this was used for domestic cooking and water heating purposes which caused a lot of pollution. The salient features of the boiler have been discussed in this chapter.

## 3.1 Salient features of the plant

### 3.1.1 Air and flue gases flow pattern

The combustion air is provided by a forced draught (FD) fan. This air, before being passed on to the combustion chamber, is first heated up, by passing it through an air pre-heater. Some portion of forced draught fan outlet air is further pressurized by secondary air fan. This air is used to carry the fuel particles into combustion chamber. The flue gas produced due to the combustion of fuel in water cooled combustion chamber is at 650°C. The flue gas gets cooled to 150°C while passing through water wall tubes, super-heater tubes, bank tubes, and economizer. The flue gas is then passed through dust collecting system and then it is sucked by induced draught (ID) fan. The flue gas is then finally passed out to the atmosphere through chimney.

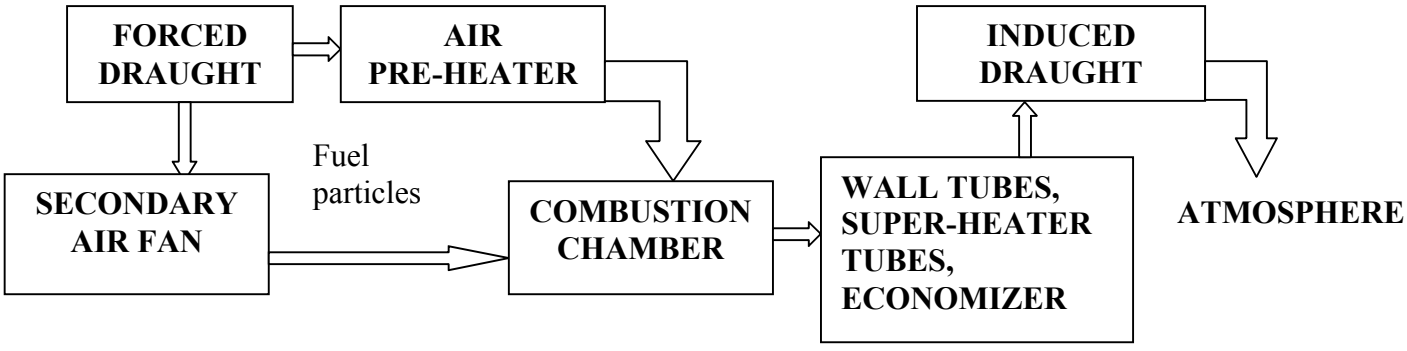


**Figure 3.1 – Process flow of air and flue gases**

### 3.1.2 Fuel and ash handling

The fuel is collected and then dried in the sun. The dried fuel is then cut into smaller pieces with chippers as shown in Figure 3.3 and then again dried in the sun because the percentage of moisture is higher in the cotton stalk. An automatic belt conveyer system shown in figure 3.4 is used for conveying cotton stalk to the boiler. The belt conveyer conveys chipped fuel to the main bunker. As, the unit is having two compartments, from this main bunker, fuel gets distributed to separate feeders for each of the two compartments. Fuel is then fed to each compartment by screw feeders. The amount of fuel can be varied from the control desk by using the regulators connected to the conveyor. The ash produced due to combustion of fuel is trapped & collected with the help of electro-precipitator unit as shown in figure 3.5.

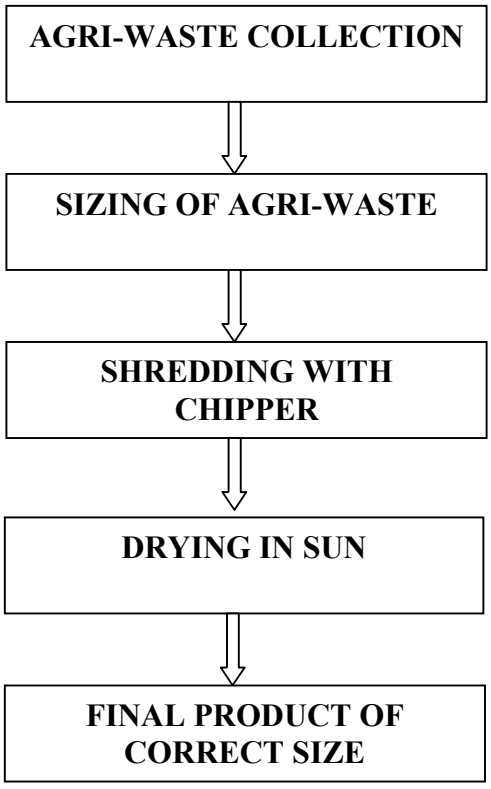


**Figure 3.2 – Process flow for the preparation of correct size of fuel**

**Figure 3.3 - Chipper used for cutting of cotton stalks**

**Figure 3.4 – Belt conveyor carrying fuel**

**Figure 3.5 – Electrostatic precipitator(ESP)**

**Figure 3.6 – Bottom ash under ESP**

### 3.1.3 Water and steam handling

Feed water is filtered of dissolved salts and oxygen in the water treatment plant and pushed into the steam drum by feed pumps, after it has been heated in the economizer. Then, water passes into mud drum through bank tubes. While passing through the bank tubes, water gets heated up by the flue gas passing over the tubes. Then, this hot water enters into bed coils through down corner tubes and gets heated up again.

Then the steam water mixture rises through the water wall panel enters into the upper drum through riser tubes. From steam drum, the saturated steam finally enters into the convection super heater tubes and gets superheated. Then the superheated steam is taken to the process turbine by main steam stop valve.

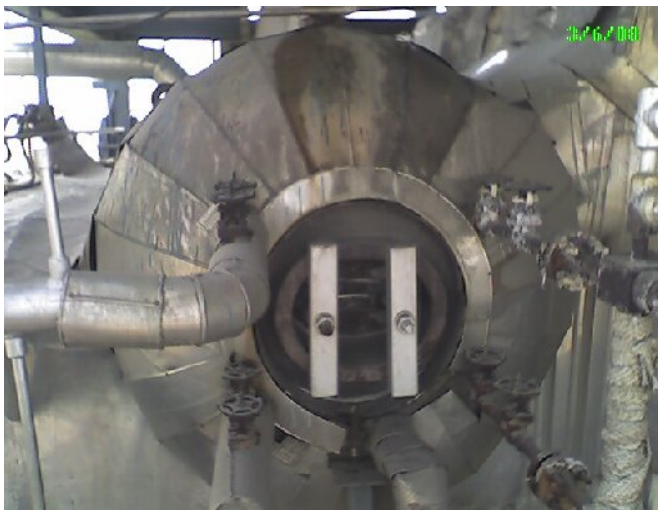

**Figure 3.7 – Steam drum**

$m^2$

**Figure 3.8 – Turbine ventilators**

### 3.1.4 Distribution plate

The distribution plate is the main part of the FBC system. It provides fluidizing air at very high speed which help the fuel particles to distribute uniformly over the whole bed. It is made up of carbon steel base plate with cast iron air nozzles. The air nozzles distribute the fluidizing air from FD fan.

## 3.2 Boiler operation

First of all the collected and stored cotton stalk is passed through a chipper for breaking the stalk into appropriate size for the combustor. The usual size, to which the stalk is chipped, is around 2.5 cm to 4 cm. Then the chipped material is carried with help of semi-automatic trucks and its heaps are prepared. The chipped fuel is manually loaded onto a belt conveyor. The belt conveyor drops the material into two compartments fitted with screw feeders, which then supply the fuel to the fluidized bed combustor. Before running the combustor on cotton stalk, it is fired with the help oil and coal. When the combustor reaches a temperature of around 700°C, then the cotton stalk is continuously supplied.

The boiler is supplied with the filtered and treated water from water treatment plant. Superheated steam at temperature of 475°C and around 67 bar pressure is produced in the boiler and is stored in the steam drum before passing on to the turbine. The turbine is coupled with the generator, which produces power. The generated power is stepped up, synchronized and is transmitted to the nearest 32KV sub-station of the electricity board.

## 3.3 Important parameters of the plant

Some of the important parameters that have been taken are given in a Table 3.1. These parameters are used to develop the mathematical model.

**Table 3.1 – Important Parameters of the plant**

| Parameters | Value | Units |
|---|---|---|
| Capacity | 7.5 | kW |
| Bed type | AFBC | - |
| Bed temperature | 973-1073 | K |
| Bed cross-sectional area | 19.43 | $m^2$ |
| Distribution plate | Nozzle type | - |
| Type of fuel used | Cotton stalk | - |
| Fuel feed rate | 2.778 | kg/sec |
| Steam temperature | 748 | K |
| Feed water temperature | 423 | K |
| Exit temperature | 373 | K |
| Auxiliary consumption | 11.5 % | - |
| Fly ash collector | ESP | - |

# CHAPTER – 4

# EXPERIMENTAL ANALYSIS

Fuel sample (Cotton stalk) that is collected from the Malwa Power Pvt. Ltd., Muktsar, Punjab, were subjected to proximate and ultimate analysis. The data from this experimental analysis is used further for the mathematical modeling.

## 4.1 Proximate analysis of cotton stalk sample

In this type of analysis the percentage of moisture content, volatile matter, ash and fixed carbon is determined. The instruments required for this analysis are muffle furnace, weighing machine, and silica crucible and air oven.

### 4.1.1 Determination of moisture

Moisture is defined as the difference in weight of sample (Cotton stalk) when the same is heated at 110 °C for one hour under specified conditions.

#### 4.1.1.1 Apparatus required

**1) Air oven**

Ventilated drying oven in which constant and uniform temperature of 110°C can be maintained.

**2) Silica crucible**

One silica crucible is required.

**3) Weighing machine**

Weighing machine is required for weighing sample.

#### 4.1.1.2 Procedure

Silica crucible was taken, cleaned and dried in an oven at 110°C for one hour. It was cooled for 15 minutes and then weighed accurately. Approximately one gram of sample (Cotton stalk) was weighed and put into the silica crucible. Then crucible was kept in an air-dried oven, which was maintained at 110°C for one hour. After one

hour crucible was removed from the oven, cooled in a desicator and then weighed accurately.

#### 4.1.1.3 Calculations

| | | |
|---|---|---|
| Weight of dried and empty crucible with lid | = | x gm |
| Weight of sample and crucible with lid | = | y gm |
| Weight of sample and crucible after heating | = | z gm |
| Therefore, weight of sample before heating | = | (y-x) gm |
| Weight of Moisture loss due to heating | = | (y-z) gm |
| Percentage of Moisture | = | $\{(y\text{-}z) \div (y\text{-}x)\} \times 100$ |

### 4.1.2 Determination of volatile matter

Volatile matter is defined as the loss of weight of sample when the same is heated under specified conditions in the absence of air at 900°C for 9 minutes.

#### 4.1.2.1 Apparatus required

**1) Muffle furnace**

A muffle furnace capable of giving uniform temperature of 900°C with the necessary thermocouples and pyrometers.

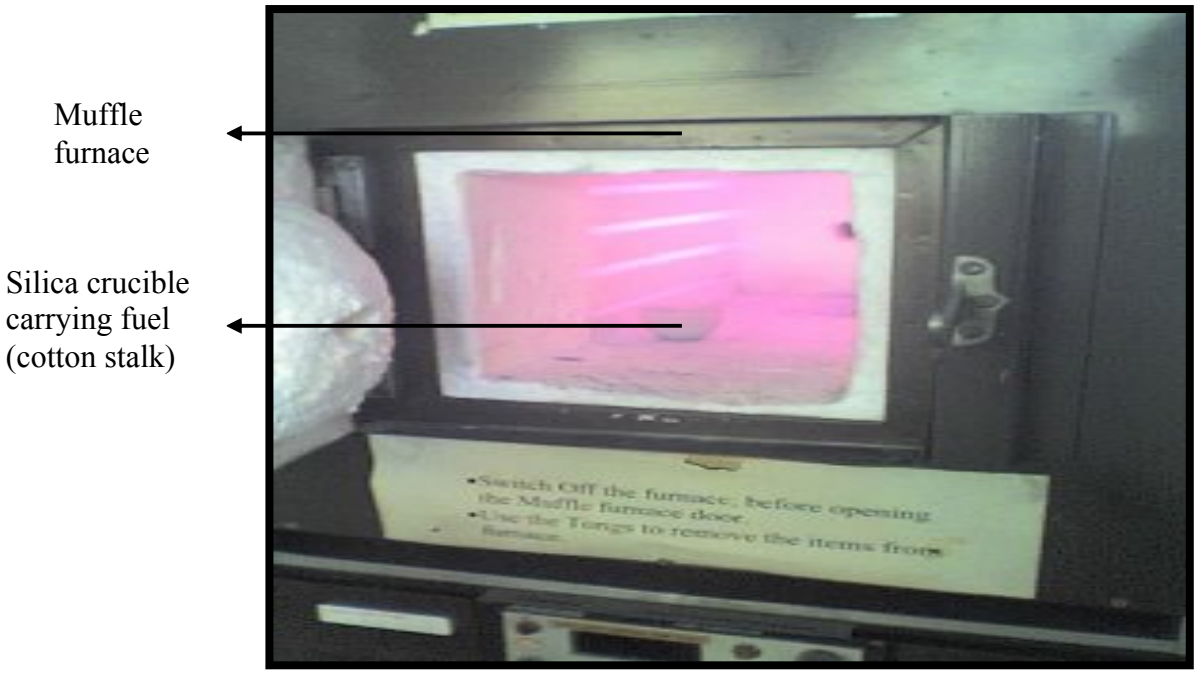


**Figure 4.1 – Silica crucible carrying fuel (cotton stalk) inside the muffle furnace**

**2) Silica crucible**

A translucent silica crucible with lid having external diameter of 25 mm should be used. The total height of crucible should not exceed 38 mm and internal diameter should not be less than 22 mm.

#### 4.1.2.2 Procedure

For the determination of volatile matter, a crucible with lid was taken and then weighed accurately. Now one gram of sample (cotton stalk) was weighed accurately into the crucible and spread evenly in the crucible by gentle tapping the crucible with the lid was transferred in the furnace at 900°C for nine minutes. After nine minutes, the crucible was removed from the furnace and placed on a cooled iron plate to ensure rapid cooling. Then the crucible was placed in a desicator for 15 minutes for further cooling and then weighed accurately.

#### 4.1.2.3 Calculations

| | | |
|---|---|---|
| Weight of dried and empty crucible with lid | = | x gm |
| Weight of sample and crucible with lid | = | y gm |
| Weight of sample and crucible after heating | = | z gm |
| Therefore, weight of sample before loss of weight | = | (y-x) gm |
| Loss of weight | = | (y-z) gm |
| Percentage of volatile matter | = | $\{(y-z) \div (y-x)\} \times 100$ |

### 4.1.3 Determination of ash

Ash is defined as the weight of residue left when a known weight of sample is burnt at 800°C for one hour under specified conditions.

#### 4.1.3.1 Apparatus required

**1) Muffle furnace**

A muffle furnace capable of giving uniform temperature of 900°C with the necessary thermocouples and pyrometers.

**2) Silica crucible**

A translucent silica crucible with lid having external diameter of 25 mm should be used. The total height of crucible should not exceed 38 mm and internal diameter should not be less than 22 mm.

#### 4.1.3.2 Procedure

For the determination of ash, a silica dish was taken, heated at 800°C for one hour. Then the dish was cooled for 20 minutes and then weight of empty dish was taken. Now one gram of sample was weighed accurately into the crucible and spread evenly in the crucible by gentle tapping the crucible with the lid. The silica dish was transferred in the furnace at 450°C for half an hour. Then the temperature of the furnace was raised to 800°C. The dish was kept at this temperature for another one hour. The crucible was removed from the furnace, cooled and then weighed accurately.

#### 4.1.3.3 Calculations

| | | |
|---|---|---|
| Weight of dried and empty crucible | = | x gm |
| Weight of sample and crucible | = | y gm |
| Weight of sample and crucible after heating | = | z gm |
| Therefore, weight of sample before heating | = | (y-x) gm |
| Weight of ash | = | (z-x) gm |
| Percentage of ash | = | $\{(z\text{-}x) \div (y\text{-}x)\} \times 100$ |

### 4.1.4 Determination of fixed carbon

The percentage of the fixed carbon can be found by subtracting the percentage of moisture content, volatile matter and ash content from 100.

#### 4.1.4.1 Calculations

$$\text{Percentage of fixed carbon} = 100 \times \{1\text{-}(XW + XVM + XA)\} \quad (4.1)$$

XW = Moisture content of fuel

XVM = Volatile matter content of fuel

XA = Ash content of fuel

### 4.1.5 Result of proximate analysis

The result of proximate analysis is shown in Table - 4.1.

**Table 4.1 – Result of proximate analysis of cotton stalk**

| Components | Percentage |
|---|---|
| Moisture | 13.89 % |
| Ash | 4.0% |
| Volatile matter | 60.5% |
| Fixed carbon | 21.61% |

## 4.2 Specific gravity test

It is defined as the ratio of mass per unit volume of particle to mass per unit volume of water at $4^{o}C$

### 4.2.1 Procedure

For the determination of specific gravity, first of all the specific gravity bottle was cleaned. Dried, and weighed with tip. Water was filled up to the marked level of the bottle, and weighed. After removing the water, the bottle was dried and about 2 gm of fuel sample was kept and weighed. Then water was filled up to certain level in the specific gravity bottle, and placed in hot water bath at $50^{o}C$ for 30 minutes to remove air bubble, then water was further filled up to the marked level and weighed with the tip.

### 4.2.2 Calculation

Weight of specific gravity bottle with tip = w gm

Weight of specific gravity bottle with tip + water = x gm

Weight of specific gravity bottle with tip + fuel = y gm

Weight of specific gravity bottle with tip + fuel +water = z gm

Weight of fuel = (y-w) gm

Weight of water = (x-w) gm

Weight of water of the volume replaced by fuel = (x-w)-(z-y) gm

Specific gravity of fuel $= \frac{(y-w)}{(x-w)-(z-y)}$

## 4.3 Ultimate analysis of the cotton stalk sample

The ultimate analysis of the cotton stalk was carried out at the Centre with Potential for Excellence in Biomedical Sciences at Punjab University, Chandigarh. The results obtained are given in Table - 4.2. The value of ultimate analysis is then directly used in the model.

**Table 4.2 – Result of ultimate analysis of cotton stalk**

| Components | Percentage |
|---|---|
| C | 42.37 % |
| H | 5.66 % |
| S | 0.00 % |
| 0 | 36.58 % |
| N | 1.50 % |

## 4.4 Sieve analysis in sand testing laboratory

First of all, the fuel sample that is collected from the plant is passed through a sieve's of various sizes in a sand testing laboratory, thereby, getting the fraction of weight lying in particular size intervals. The distribution obtained is given in a Table 4.3.

**Table 4.3 – Size distribution of cotton stalk particles**

| dp(mm) | dp(mm) | dpi(mm) | Weight in interval,(gm) | %age weight fraction |
|---|---|---|---|---|
| -80 | +40 | 60 | 29 | 25.56 |
| -40 | +20 | 30 | 38.5 | 33.92 |
| -20 | +10 | 15 | 24.5 | 21.58 |
| -10 | +4.75 | 7.375 | 14.5 | 12.77 |
| -4.75 | +2.36 | 3.555 | 3 | 2.643 |

| | | | | |
|---|---|---|---|---|
| -2.36 | +1.18 | 1.77 | 2 | 1.762 |
| -1.18 | +0.6 | 0.89 | 2 | 1.762 |

Kunni & Levenspiel develop some relations for those particles whose size varies. For this, they defined the size distribution functions P and p as follows. Let P be the volume fraction of particles smaller than size dp and let $pd(d_p)$ be the volume fraction of particles of size between $d_p$ and $d_p + d(d_p)$.

The relationship between p and P can be found by considering particles of any particular size, dp1, for which we have

$$p_1 = \left(\frac{dp}{d(dp)}\right)_1 \qquad \text{or} \qquad P_1 = \int_0^{d_{p1}} pd\left(d_p\right) \tag{4.2}$$

For discrete distribution of particles with equal or unequal size intervals, we have the following relation between p and P at any given dpi.

$$p_i = \left(\frac{\Delta P}{\Delta d_p}\right)_i \qquad \text{or} \qquad P_i = \sum_1^i \left(p\Delta d_p\right)_i = \sum_1^i x_i \tag{4.3}$$

From this, we get to know that p gives volume (or weight or numbers) distribution of particles directly and has units of reciprocal length, whereas P gives the cumulative distribution of sizes and is dimensionless.

Kunni & Levenspiel also gave this relation for average diameter of particle:

$$\bar{d}_p = \frac{1}{\sum_{all..i}\left[\left(p\Delta d_p\right)_i / d_{pi}\right]} = \frac{1}{\sum_{all...i}\left(x/d_p\right)_i} \tag{4.4}$$

We use equation 4.4 to find out the average particle diameter of cotton stalk sample. Table 4.4 illustrate the that how we find out the average particle diameter of the fuel sample(cotton stalk).

**Table 4.4 – Determination of the average particle diameter**

| $d_p$(mm) | $d_p$(mm) | $d_{pi}$(mm) | Weight fraction in interval ($x_i$) | $(x/d_p)_i$ |
|---|---|---|---|---|
| 0.6 | 1.18 | 0.89 | 0.01762 | 0.019799 |
| 1.18 | 2.36 | 1.77 | 0.01762 | 0.009955 |
| 2.36 | 4.75 | 3.555 | 0.02643 | 0.007435 |
| 4.75 | 10 | 7.375 | 0.12775 | 0.017322 |
| 10 | 20 | 15 | 0.21586 | 0.014391 |
| 20 | 40 | 30 | 0.33921 | 0.011307 |
| 40 | 80 | 60 | 0.25551 | 0.004258 |

$$\bar{d}_p = \frac{1}{\sum_{all...i} \left(x / d_p\right)_i} = 11.8388 \text{ mm}$$

## 4.5 Thermo-Gravimetric Analysis (TGA)

For this analysis first of all the cotton stalk sample is converted into a powdered form. Then the sample is placed inside the crucible of the furnace of TGA. Then the tapping of the crucible is done in order to distribute the cotton stalk sample uniformly. Appropriate amount of nitrogen and oxygen is then passed through the reaction tube containing cotton stalk sample. Then the temperature mechanism is actuated such that the heating rate is maintained from the room temperature to the completion of combustion. Then the percentage weight loss is determined throughout the combustion process.

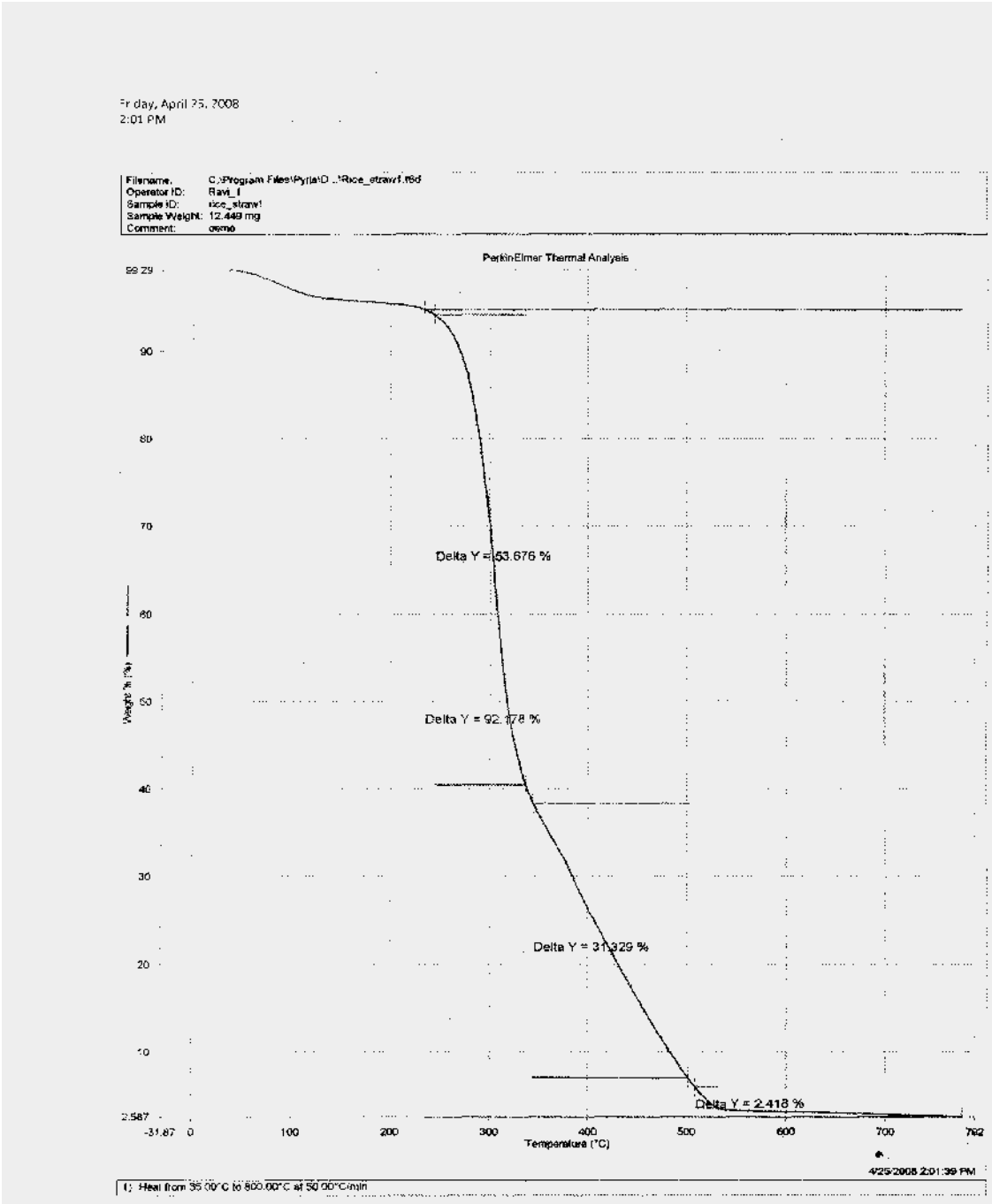


**Figure 4.2 – Thermo-gravimetric analysis of cotton stalk (power form)**

# CHAPTER – 5

# MATHEMATICAL MODELING

A mathematical model has been developed in the present work, for an atmospheric bubbling fluidized bed combustor using cotton stalk as fuel for the fluidization that incorporates the following:

- Physico-chemical parameters in the bed i.e., minimum fluidizing velocity, bubble properties like bubble diameter, bubble rise velocity, superficial velocity of gas etc.
- Oxygen mass balance with constant bubble diameter to find out exit gas composition like percentage of oxygen, carbon dioxide, nitrogen.

## 5.1 Model Assumptions

The mathematical model developed in the present study is based on the following assumptions:-

1) The bed is assumed to consist of a number of equivalent stages. The height of each stage is equal to the average equivalent bubble diameter of bed.
2) Each stage consists of three phase's i.e bubble phase, cloud-wake phase, emulsion phase.
3) All the bubbles are of constant diameter.
4) It is assumed that the bubbles do not contain any solid (carbon) particle and is equally distributed through out the bed. The gas flow rate is considered to be the plug flow.
5) The absolute velocity of the bubble and its cloud and wake rise is same.
6) The voidage in the cloud and wake phase is assumed to be same as that of the emulsion phase.
7) The gas flowing through the emulsion phase is considered to be completely mixed within each stage. The voidage in the emulsion phase is constant and equal to the voidage at incipient fluidization and it remains the same as that under minimum fluidization condition.

8) The gas flowing through the cloud-wake phase is considered to be completely mixed within each stage.

9) The velocity of the gas flowing through the emulsion phase is considered to be equal to the velocity at minimum fluidization.

## 5.2 Physico-chemical parameters in a fluidised bed combustor

In the following text, mathematical relations for some of Physico-chemical parameters in fluidized bed combustors have been given. These relations form the base for developing models for fluidized bed combustors and the values of these parameters directly affect the performance of the combustors.

### 5.2.1 Operating gas velocity

Superficial velocity or the operating velocity is calculated as below:

$$U_o = \frac{F_{ME}\ R_g\ T_b}{P_{av} A} \quad m/s \tag{5.1}$$

Where,

($U_O$) = Operating velocity of fluidizing gas (m/s)

($R_g$) = Gas constant = 0.08206 atm-$m^3$/ (kg-mole) (K)

($P_{av}$) = Average pressure in the combustor (atm)

($T_b$) = Absolute bed temperature (K)

(A) = Cross-sectional area of the bed ($m^2$)

($F_{ME}$)= The actual molar feed rate of fluidizing air and is calculated as below:

$$F_{ME} = F_{MTH}(1.0 + Ex_{air}) \text{ (kg-mole/s)} \tag{5.2}$$

Where,

($Ex_{air}$) = Fractional excess air

$F_{MTH}$ is the stoichiometric air feed rate, which is determined from the fuel composition and fuel feed rate using the simple stochiometrical relationship given below.

$$F_{MTH} = W\,(1.0 - XW)\left\{\frac{\left[\frac{XC}{12} + \frac{XH}{4} + \frac{XS}{32} - \frac{X0}{32}\right]}{0.21}\right\} \qquad (5.3)$$

Where,

W = fuel feed rate into the combustor (kg/sec)

XW = Moisture content of the fuel

XC = Ultimate carbon content of the fuel

XH = Ultimate hydrogen content of the fuel

XS = Ultimate sulphur content of the fuel

XO = Ultimate oxygen content of the fuel

### 5.2.2 Minimum fluidization velocity

A number of correlations are available in literature (Table 5.1) to define minimum fluidization velocity, the application of which varies to a great extent depending upon the particle size in the bed. According to Kunni & Levenspiel, the equation (5.4) recommended by Chitester et. al.(1984) gives the best results for coarse particles.

$$U_{mf} = \left(\frac{\mu}{d_p \rho_g}\right)\left[\left\{(28.7)^2 + \frac{0.0494 d_p^{\,3} \rho_g (\rho_p - \rho_g)(g)}{\mu^2}\right\}^{1/2} - 28.7\right] \qquad (5.4)$$

Chitester et. al.'s (1984) correlation was used to calculate the minimum fluidization velocity in the present model because the particle size is greater than 100µm. The result of this relation is more closely matched with the larger particle size.

**Table 5.1 Expressions for minimum fluidization velocity**

| Sr. No. | Empirical correlation | Authors |
|---|---|---|
| 1. | $U_{mf} = \left(\frac{\mu}{d_p \rho_g}\right)\left[\left\{(33.7)^2 + \frac{0.0408 d_p^3 \rho_g (\rho_p - \rho_g)(g)}{\mu^2}\right\}^{1/2} - 33.7\right]$ | Wen and Yu (1966) |
| 2. | $U_{mf} = \left(\frac{\mu}{d_p \rho_g}\right)\left[\left\{(25.46)^2 + 0.0382 Ar\right\}^{1/2} - 25.46\right]$ | Bourgeoi & Grenier(1968) |
| 3. | $U_{mf} = \left(\frac{\mu}{d_p \rho_g}\right)\left[\left\{(25.25)^2 + 0.0651 Ar\right\}^{1/2} - 25.25\right]$ | Babu et al. (1978) |
| 4. | $U_{mf} = \left(\frac{\mu}{d_p \rho_g}\right)\left[\left\{(18.75)^2 + 0.03125 Ar\right\}^{1/2} - 18.75\right]$ | Zheng et.al. (1985) |
| 5. | $U_{mf} = \left(\frac{\mu}{d_p \rho_g}\right)\left[\left\{(25.28)^2 + 0.0571 Ar\right\}^{1/2} - 25.28\right]$ | Saxena & Vogel(1977) |
| 6. | $U_{mf} = \left(\frac{\mu}{d_p \rho_g}\right)\left[0.00138\, A_r / \left(A_r + 19\right)^{0.11}\right]$ | Ilavsky & Bena(1967) |
| 7. | $U_{mf} = \left(\frac{\mu}{d_p \rho_g}\right)\left[\left\{(30.1)^2 + 0.0417 Ar\right\}^{1/2} - 30.1\right]$ | Sathyanaryana &Rao(1989) |

Where $Ar = \frac{d_p^3 \rho_g (\rho_p - \rho_g)(g)}{\mu^2}$

## 5.2.3 Viscosity of fluidizing gas

Subramani et. al.(2007) gave an equation for estimating the viscosity of fluidizing air, which is a function of bed temperature only and is presented below:

$$\mu_g = \left[ 1.46\,(10^{-6})\,\left(\frac{T_b^{1.504}}{T_b + 120}\right) \right] \tag{5.5}$$

### 5.2.4 Density of fluidizing gas

The density of fluidizing gas can be found from the work of Bird et al. (1960). The final expression for density of fluidizing gas, which is a function of bed temperature only, is presented below:

$$\rho_g = \frac{353.2}{\sqrt{T_b}} \tag{5.6}$$

### 5.2.5 Terminal velocity

To avoid the particles from getting blown out of the bed, the superficial velocity must be limited under the maximum fluidization velocity, which is called terminal velocity of the particles.

The terminal velocity of the particles as given by Geldart et. al. (1984) is:

$$U_t = \sqrt{\frac{4gd_p}{3C_D}\frac{(\rho_s - \rho_g)}{\rho_g}} \tag{5.7}$$

Where $C_D$ is the drag coefficient for a spherical particle.

The relationships between drag coefficient ($C_D$) and Reynolds number (Re) was given by Kunni & Levenspiel (1969) as:

$$C_D = \frac{24}{\mathrm{Re}} \qquad \text{if } \mathrm{Re} < 0.4 \tag{5.8}$$

$$C_D = \frac{10}{\sqrt{\mathrm{Re}}} \qquad \text{if } 0.4 < \mathrm{Re} < 500 \tag{5.9}$$

$$C_D = 0.43 \qquad \text{if } 500 < \mathrm{Re} < 200000 \tag{5.10}$$

The given equations 5.8, 5.9, 5.10 are substituted into equation 5.7 to obtain 3 terminal velocities $U_t$ of particles. These values of $U_t$ are used to find out the Reynolds number (Re). In our case the value of Reynolds number is higher, so we use equation 5.10 for finding the value for $C_D$.

Cheremisinoff et. al. also gave few similar empirical correlation for terminal velocity, given as under:

$$U_t = \left[ \left( \frac{4}{225} \right) \frac{\left( \rho_s - \rho_g \right)^2 g^2}{\rho_g \ \mu} \right]^{1/3} \times d_p \qquad \text{if } 0.4 < \text{Re} < 500 \qquad (5.11)$$

$$U_t = \left[ \frac{3.1 d_p \left( \rho_s - \rho_g \right) g}{\rho_g} \right]^{1/2} \qquad \text{if } 500 < \text{Re} < 200000 \qquad (5.12)$$

### 5.2.6 Voidage at minimum fluidization

Observing that parameters like the bed porosity at minimum fluidization ($\varepsilon_{mf}$), $Re_{mf}$ and $A_r$ change with temperature, Subramani et. al. attempted to develop an empirical correlation to predict $\varepsilon_{mf}$ as a function of $Re_{mf}$ and $A_r$ , using least square method.

$$\varepsilon_{mf} = 0.3507 A_r^{0.0387} \ \text{Re}_{mf}^{-0.0704} \qquad (5.13)$$

For fine particles the following relation is used.

$$\varepsilon_{mf} = 0.586(\phi)^{-0.7} \left( \frac{\mu^2}{\rho_g \eta d_p^{\ 3}} \right)^{0.029} \left( \frac{\rho_g}{\rho_s} \right)^{0.021} \qquad (5.14)$$

Where, $\eta = g(\rho_s - \rho_g)$

$\phi =$ Sphericity

Another relation proposed by Wen and Yu

$$\varepsilon_{mf} = \left( \frac{0.071}{\phi} \right)^{\frac{1}{3}} \qquad (5.15)$$

And/or

$$\varepsilon_{mf}^{\ 3} = \frac{0.091(1-\varepsilon_{mf})}{\phi^2} \qquad (5.16)$$

### 5.2.7 Average equivalent bubble diameter

Various correlations can be found in literature for the estimation of bubble diameter in a fluidised bed. One of the widely used correlation was proposed by Mori and Wen in 1975 taking into account the effect of bed diameter and distributor type on bubble diameter as follows:

$$d_b = d_{bm} - (d_{bm} - d_{bo}) \exp\left(-\frac{0.3z}{d_t}\right) \tag{5.17}$$

Where, $d_{bm} = 1.6377\,[A\,(U_o - U_{mf})]^{0.4}$ (5.18)

and $d_{bo} = 0.8716\left[\frac{A\,(U_o - U_{mf})}{N_{or}}\right]^{0.4}$ (5.19)

$N_{or}$ = Number of orifice openings for perforated distributor plates per unit area

$$N_{or} = \left(\frac{2}{\sqrt{3} \times l_{or}^{\,2}}\right) \tag{5.20}$$

and

For porous distributor plates.

$$d_{bo} = 0.376\,(U_o - U_{mf})^2 \tag{5.21}$$

Rowe (1976) also presented an expression to estimate bubble diameter for fluidized bed combustors, which is given below:

$$d_b = (U - U_{mf}) Z^{0.75} g^{-0.25} \tag{5.22}$$

Stubington et al.(1984) modified the above expression for tuyer cap type distributors as follows:

$$d_b = 0.43(U - U_{mf})^{0.4} (Z + 4\sqrt{A})^{0.8} g^{-0.2} \tag{5.23}$$

Kunni & Levenspiel (1990) presented some expressions for low and high gas flow which took into account the number of orifices, spacing between orifices etc.

$$U_o - U_{mf} = N_{or} v_{or} \tag{5.24}$$

Where

$v_{or}$ = volumetric flow rate through an orifice ($m^3/s$);

$$d_{b0} = 1.30 \frac{v_{or}^{0.4}}{g^{0.2}} \tag{5.25}$$

Hence the bubble diameter just above the distributor becomes

For low gas flow rate:

$$d_{b0} = \frac{1.30}{g^{0.2}} \left[ \frac{U - U_{mf}}{N_{or}} \right]^{0.4} ; \qquad \text{if } d_{b0} \le l_{or} \tag{5.26}$$

Where $l_{or}$ = spacing between adjacent holes.

For high gas flow rate:

$$d_{b0} = \frac{2.78}{g} \left( U - U_{mf} \right) ; \qquad \text{if } d_{b0} > l_{or} \tag{5.27}$$

In another approach, Werther gave the following expression for bubble size at any height 'z' in a bed of Geldart B group solids supported by a porous plate distributor:

$$d_b = 0.853 \left[ 1 + 0.272 \left( U - U_{mf} \right) \right]^{1/3} \left( 1 + 0.0684 z \right)^{1.21} \tag{5.28}$$

It was found in the present study that best results were obtained using the Khan et. al. expression for bubble diameter.

### 5.2.8 Bubble velocity

The absolute rise velocity of an isolated single rising bubble, $u_{br,}$ was first suggested by Davidson and Harrison (1963) to be given by:

$$u_{br} = 0.711 \sqrt{g.d_b} ; \qquad \text{When } d_b/d_t < 0.125 \tag{5.29}$$

According to Wallis, the wall effects retard the rise of bubbles when $d_b/d_t$ > 0.125, hence he suggested,

$$u_{br} = \left[ 0.711 \left( g d_b \right)^{1/2} \right] 1.2 \exp\left( -1.49 \frac{d_b}{d_t} \right) ; \text{ When } 0.125 < d_b/d_t < 0.6 \tag{5.30}$$

He further recommended that for $d_b/d_t$ >0.6, the bed should not be considered as bubbling, rather the flow should be the slug flow.

Kunni & Levenspiel (1991), Geldart (1973) & Werther (1973) also recommended the following relation:

$$u_b = 1.6\left[\left(U - U_{mf}\right) + 1.13 d_b^{0.5}\right] d_t^{1.35} + u_{br} \qquad (5.31)$$

Davidson and Harrison (1963) also proposed on theoretical grounds that the average absolute velocity of a crowd of bubbles in a fluidized bed may be expressed as:

$$u_b = U_0 - U_{mf} + u_{br} \qquad (5.32)$$

### 5.2.9 Bubble properties

According to Rowe and Partridge (1965), the ratio between the volumes of wake dragged upward behind a rising bubble to the volume of bubble, $f_{w,}$ may be taken to be roughly as 0.2.

For estimating the size of cloud, ratio of cloud volume to bubble volume ( $f_c$ ), the Davidson and Harrison (1963) correlation was tried.

$$f_c = \frac{3U_{mf}}{(\varepsilon_{mf}.u_{br} - U_{mf})} \qquad (5.33)$$

The ratio of volume of cloud-wake phase to the volume of bubble $f_{cw}$ is obtained as follows:

$$f_{cw} = f_w + f_c \qquad (5.34)$$

But, it was found that equation (5.33) gave absurd values of $f_c$, for the present case. We have therefore taken $f_c$ as an adjustable parameter, the value of which lies in between 0.025 and 0.15. This in turn implies that $f_{cw}$ is now an adjustable parameter, with its value varying from 0.2 to 0.4.

### 5.2.10 Distribution of gas flow among the three phases

Since the volumetric flow rate of fluidising gas, $Q$, is distributed among the three phases, thus we have;

$$Q = Q_{mf} + Q_{cw} + Q_b \qquad (5.35)$$

Where $Q_{mf}$ = Volumetric flow rate via emulsion phase

$Q_{cw}$ = Volumetric flow rate via cloud-wake phase

$Q_b$ = Volumetric flow rate via bubble phase

Dividing equation (5.35) by the cross-sectional area of the bed, we can get the superficial velocity of fluidising gas;

$$U=U_{mf}+U_{cw}+U_b \tag{5.36}$$

Here $U_b$ is the superficial gas velocity of the bubble phase and it is different from the average absolute rise velocity of a crowd of bubbles.

$U_{cw}$ is the velocity of cloud-wake phase.

The cross-sectional area of the bed occupied by bubbles is;

$$A_b=\varepsilon_b.A \tag{5.37}$$

Where $\varepsilon_b$ is the volume fraction of bubbles in the bed or the fraction of the bed consisting of bubbles.

The cross-sectional area of bed occupied by cloud-wake phase is given below:

$$A_{cw}=f_{cw}.\varepsilon_b.A \tag{5.38}$$

In the model, the void fraction in the cloud-wake phase is assumed to be $\varepsilon_{mf}$. Hence the cross-sectional area of bed available for gas flow in the cloud-wake phase is expressed by;

$$A_{cw_g}=f_{cw}.\varepsilon_b.\varepsilon_{mf}.A \tag{5.39}$$

The bubble and its associated cloud and wake is assumed to rise at the same absolute rise velocity of crowd of bubbles, $u_b$. So the volumetric flow rate of gas flowing through the cloud-wake phase is expressed as:

$$Q_{cw}=u_b\ A_{cw_g}=U_{cw}\ A \tag{5.40}$$

Substituting the value of $A_{cw_g}$ from equation (5.39) into equation (5.40), we get

$$u_b=\frac{U_{cw}}{(f_{cw}.\varepsilon_b.\varepsilon_{mf})} \tag{5.41}$$

The volumetric flow rate of gas through the bubble phase;

$$Q_b = u_b A_b = U_b \ (A) \tag{5.42}$$

Now substituting the value of $A_b$, from equation (5.37) into equation (5.42), we get

$$u_b = \frac{U_b}{\varepsilon_b} \tag{5.43}$$

Equating equations (5.41) & (5.43), we have

$$U_{cw} = f_{cw} . \varepsilon_{mf} . U_b \tag{5.44}$$

After substituting equation (5.44) into equation (5.36), we get

$$U_b = \frac{U_o - U_{mf}}{(1.0 + f_{cw} . \varepsilon_{mf})} \tag{5.45}$$

From equations (5.44) & (5.45) the cloud-wake phase velocity may be calculated as;

$$U_{cw} = f_{cw} . \varepsilon_{mf} \frac{(U_o - U_{mf})}{(1.0 + f_{cw} . \varepsilon_{mf})} \tag{5.46}$$

Also,

$$\frac{(A_b + A_{cw})}{A} \langle 1.0 \tag{5.47}$$

$$\varepsilon_b (1.0 + f_{cw}) \langle 1.0 \tag{5.48}$$

It is because the cross-sectional area occupied by bubble, cloud and wakes should always be less than the total cross-sectional area of the bed as pointed out by Bukur et al. (1978). This condition is of special significance in AFBC because the same is operated relatively at higher operating velocity.

### 5.2.11 Volume fraction of bubbles in the bed, $\varepsilon_b$

Now substituting the value of $A_b$ from equation (5.33) into equation (5.38), we get

$$\varepsilon_b = \frac{U_b}{u_b} \tag{5.50}$$

### 5.2.12 Expanded bed height, H

The bed expansion above the height at minimum fluidisation is assumed to be entirely due to the presence of bubbles and hence it is related to expanded bed height;

$$H=\frac{H_{mf}}{(1.0-\varepsilon_b)} \tag{5.51}$$

### 5.2.13 Number of equivalent stages, N

As, height of each stage is taken to be equal to the average equivalent bubble diameter so, the number of equivalent stages can be calculated as below;

$$N=\frac{H}{d_b} \tag{5.52}$$

### 5.2.14 Interphase gas exchange coefficients

It is of particular importance because it is one of the determining factors in predicting the performance of fluidised bed combustors. The interphase gas exchange coefficient between any two phases can be looked upon as the flow of gas from one phase to the other and vice – versa. The interphase coefficient between bubble and emulsion phases can be defined as;

$$(K_{be})_b=\frac{\left[\begin{array}{c}\text{volume of gas going from bubbles to emulsion}\\ \text{or from emulsion to bubbles}\end{array}\right]}{(\text{volume of bubbles in the bed})(\text{time})} \tag{5.53}$$

The overall coefficient of gas interchange between bubble and emulsion phase, therefore, has been investigated by several authors.

Davidson and Harrison (1963) assumed that there were both convective and diffusional flows contributing to the gas interchange and the correlation is given by;

$$(K_{be})_b=4.5\frac{U_{mf}}{d_b}+5.85\frac{D_e^{1/2}\,g^{1/4}}{d_b^{5/4}} \tag{5.54}$$

In the above equation the second term represents the mass transfer which is given by analogy with the liquid-film controlled diffusion process from a rising bubble.

Kunii and Levenspiel (1969) then proposed a new theory for estimating the interchange coefficients. They assumed that there were two transfer steps, namely the

transfer between the bubble and cloud phase and that between the cloud and emulsion phases.

They further assumed that the coefficient for the former step is given by Davidson and Harrison (1963) equation and the coefficient for the latter step is given by Higbie's penetration model. Their correlation is as follows;

$$\frac{1}{(K_{be})_b}=\frac{1}{(K_{bc})_b}+\frac{1}{(K_{ce})_b} \tag{5.55}$$

$$(K_{bc})_b=4.5\frac{U_{mf}}{D_b}+5.85\frac{D_e^{1/2}g^{1/4}}{D_b^{5/4}} \tag{5.56}$$

$$(K_{ce})_b=6.78\left(\frac{\varepsilon_{mf}D_e u_b}{D_b^3}\right)^{1/2} \tag{5.57}$$

$D_e$, the oxygen diffusivity is expressed in terms of surrounding temperature using Bird et al. (1960) correlation as;

$$D_e=5.14\times10^{-9}\times(T_b)^{1.5} \tag{5.58}$$

### 5.2.15 Reaction rate constant

Chemical reaction rate in fluidised bed combustion plays an important role in the formulation of oxygen mass balance model. The reactions which govern the combustion of fuel are:

$$C + O_2 \rightarrow CO_2 \tag{5.59}$$

$$2C + O_2 \rightarrow 2CO \tag{5.60}$$

$$CO_2 + C \rightarrow 2CO \tag{5.61}$$

$$2CO + O_2 \rightarrow 2CO_2 \tag{5.62}$$

The first three are heterogeneous reactions and are generally assumed to take place either at the external or internal surface area of the char particles. The fourth one is a homogeneous reaction and takes place in or outside of the boundary layer of the char particles. In this context, two basic mechanisms have been postulated for char combustion:

- The single film model proposed by Burke and Schumann.

- The double film model proposed by Burke and Schumann.

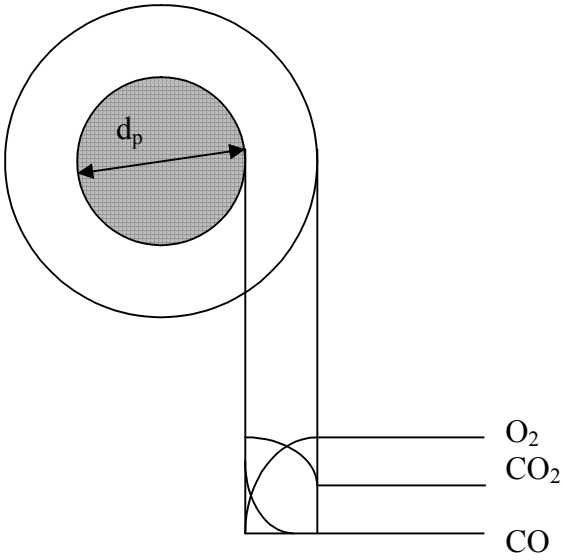


**Figure 5.1 – Single film theory**

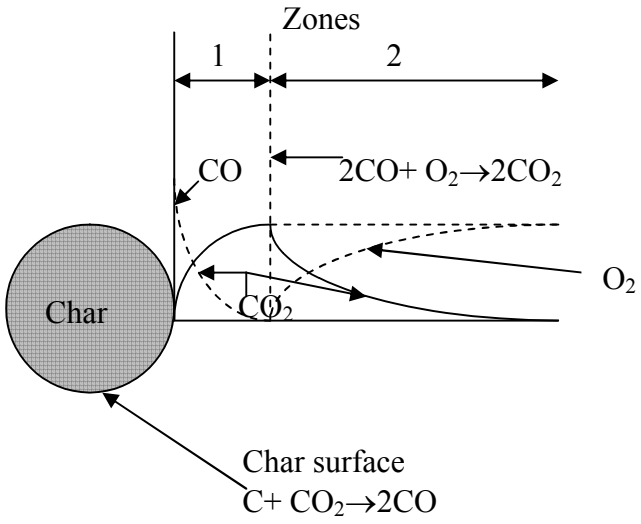


**Figure 5.2 – Double film theory**

The first postulate assumes the direct oxidation of the char particles by diffusion of oxygen through a stationary film to the surface of the carbon particles where it reacts to produce varying amounts of CO and $CO_2$ by reaction (5.59) and (5.60) respectively. The CO formed is then oxidised to $CO_2$ by a homogeneous reaction (5.62), which takes place in the boundary layer around the particle or in the

remaining gaseous phase of the bed. When the combustion of CO occurs close to the particle, the reaction at the surface may effectively be described by reaction (5.59). Figure 5.1 shows the concentration profile of various species as per single film model.

In the second postulate as proposed by Burke and Schumann, oxygen diffusing towards a burning particle is consumed before it reaches the particle by reaction (5.62) and carbon reacts at the surface with $CO_2$ only by reaction (5.61). The CO formed diffuses away from the particle and burned in a thin flame front in the boundary layer with incoming oxygen. This reaction produces more $CO_2$ of which from the stochiometry, one half diffuses away and other half diffuses back to the surface to complete the cycle. Hence no oxygen will reach the external edge of the boundary layer. The schematic representation of the double film model is shown in Figure 5.2.

The two models have received support from a number of researchers and useful reviews of the subject are to be found in the works of Spalding (1955), Field (1969), Caram and Amundson (1977), Yates and Walker (1978), Bukur and Davidson (1981), Ross and davidson (1981), Turnbull et al. (1984), and Park (1989).

Park (1989) has shown from extensive experiments that the temperature difference between burning char particles and bulk of the bed can be maximum upto 200K. However Campbell and Davidson (1975) have pointed out that the combustion mechanism on which the double film theory is based requires particle temperature in excess of 1373K. As, the present FBC unit is operating at a temperature of about 923 K so, the single film theory of char combustion has been considered where carbon reacts with oxygen to produce $CO_2$.

The rate of mass transfer is defined as the flow material normal to a unit surface as;

$$Q_{transfer} = \frac{1}{S} \times \frac{dN}{dt} \text{ kg.mol oxygen/m}^2\text{-sec} \qquad (5.63)$$

Hence the reaction step must similarly be defined as;

$$Q_{reaction} = \frac{1}{S} \times \frac{dN}{dt} \text{ kg.mol oxygen/m}^2\text{-sec} \qquad (5.64)$$

Oxygen diffuses through a film of thickness (ΔX) onto a plane surface of carbon particle where it reacts with carbon to yield gaseous product $CO_2$ which diffuses back through the film into main gas stream. The intrinsic rate of chemical reaction will be proportional to oxygen concentration at the carbon surface $C_s'$.

Considering the carbon oxygen reaction to be first order;

$$\frac{1}{S}\times\frac{dN}{dt}=K_s\times C_s' \tag{5.65}$$

Now at steady state the intrinsic rate must be equal to the rate at which oxygen is supplied to the surface via gas film. Hence

$$K_g(C_p - C_s')=K_s\times C_s' \tag{5.66}$$

i.e. mass transported = surface reaction rate

The surface oxygen concentration $C_s'$ is derived from equation (5.66) as follows;

$$C_s'=\frac{K_g\times C_p}{(K_g+K_s)} \tag{5.67}$$

Substituting equation (5.48) in equation (5.46), we get

$$\frac{1}{S}\times\frac{dN}{dt}=\frac{C_p}{(1/K_s+1/K_g)} \tag{5.68}$$

The chemical reaction rate constant $K$ at any instant which is controlled by surface reaction and gas diffusion coefficients and is obtained from the above equation as:

$$\frac{1}{K}=\frac{1}{K_s}+\frac{1}{K_g} \tag{5.69}$$

Where, $K_s$ the surface reaction rate constant for carbon particles is adopted from the expression given by Parker and Hotel (1936).

$$K_s = 4.32\times10^{11}\ T_p^{-0.5}\ \exp(-44000/8314.72\times T_p) \tag{5.70}$$

The mass transfer coefficient $K_g$ is expressed by dimensionless Sherwood number ( Sh ) as:

$$K_g = \frac{Sh \times D_e}{d_p} \tag{5.71}$$

Sherwood number can be defined as a dimensionless concentration gradient at the surface, and it provides a measure of the convection mass transfer occurring at the surface.

Many a correlation were available for estimating the Sherwood number but in this model, La Nauze et al. (1984) correlation has been adopted and the correlation is given as:

$$Sh=2\varepsilon_{mf}+[4.0\varepsilon_{mf}d_p(U_{mf}/\varepsilon_{mf}+U_b)/\pi D_e]^{1/2} \text{ for } d_p/d_{pbed} \geq 4.0 \tag{5.72}$$

$$\text{and } Sh=2.0\varepsilon_{mf}+[4.0d_p U_{mf}/\pi D_e]^{1/2} \text{ for } d_p/d_{pbed} < 4.0 \tag{5.73}$$

Khan et. al. (2007) gave a correlation for estimating Sherwood number using Schmidt number, Reynold's number and voidage at minimum fluidization, and is given as:

$$Sh = 2\varepsilon_{mf} + 0.69S_c^{0.33}\,\mathrm{Re}^{0.5} \tag{5.74}$$

Where Schmidt number 'Sc' is given as;

$$Sc = \frac{\mu_g}{\rho_g D_e} \tag{5.75}$$

## 5.2.16 Particle shrinkage rate

According to shrinking core model, as soon as the fuel enters into the FBC, it decomposes into volatiles and combustible matter. During a short ignition period, pores start to form, while the fuel softens and re-solidifies to become char, where combustion reaction takes place till final burnout of char is achieved.

Wen (1968) and Ishida et al. (1971) on the basis of studies of numerous systems, conclude that the shrinking core model is the best simple representation for the majority of reacting gas solid systems.

$$\left(\frac{dd_p}{dt}\right)_{\text{over all}} = \left(\frac{dd_p}{dt}\right)_{\text{attrition}} + \left(\frac{dd_p}{dt}\right)_{\text{combustion}} \tag{5.76}$$

The shrinkage rate by attrition was determined by Merick and Highly (1974) correlation as follows;

$$(\frac{dd_p}{dt})_{attrition} = \frac{1}{3} A_{kt} (U - U_{mf}) \tag{5.77}$$

where: $A_{kt}$ is a dimension less attrition rate constant.

According to Turnbull et al. (1984);

$$(\frac{dd_p}{dt})_{combustion} = \frac{2M_c}{\rho_p} (\frac{1}{K_s} + \frac{d_p}{Sh\, D_e})^{-1} C_p \tag{5.78}$$

Where, $M_c$ is the molecular weight of carbon

$$\frac{dd_p}{dt} = \frac{1}{3} A_{kt} (U_0 - U_{mf}) + \frac{2M_c}{\rho_p} (\frac{1}{K_s} + \frac{d_p}{ShD_g})^{-1} .C_p \tag{5.79}$$

## 5.2.17 Inlet oxygen concentration

The inlet oxygen molar concentration is evaluated at the bed temperature, at 1 atm. pressure as;

$$C_0 = \left[ (\frac{0.21}{22400})(\frac{273.0}{T_b}) \right] \times 1000 \ \text{kg-mole/m}^3 \tag{5.80}$$

## 5.3 Development of model for oxygen mass balance

For the oxygen mass balance, the FBC is assumed to consist of a number of equivalent stages in series, similar to the approach suggested by El-Halwagi and El-Rifai in 1988 for a fluid bed catalytic reactor. The height of each stage is equal to the average equivalent bubble diameter in the bed. Each stage consists of a bubble, cloud-wake, and emulsion phase. Oxygen which is present in the bubble cannot take part in combustion, the bubble phase oxygen is transported across the bubble cloud interface into the more carbon rich cloud-wake phase, where the combustion reaction takes place. Un-reacted oxygen in the cloud-wake is further transported to the very carbon rich emulsion phase. Most of the oxygen is consumed in the emulsion phase.

### Oxygen balance around stage 'n' for bubble phase

$$\left|\begin{matrix}\text{Oxygen in from stage}\\(n-1)\text{ by convection}\end{matrix}\right| - \left|\begin{matrix}\text{Oxygen out to stage}\\(n+1)\text{ by convection}\end{matrix}\right| - \left|\begin{matrix}\text{Oxygen transfer to}\\\text{cloud - wake phase}\end{matrix}\right| = 0 \qquad (5.81)$$

It is represented symbolically as;

$$U_b C_{b_{n-1}} - U_b C_{b_n} - (K_{bc})_b \varepsilon_b \int_{Z_{-1}}^{Z_n} (C_b - C_{cw_n}) dZ = 0 \qquad (5.82)$$

### Oxygen balance around stage 'n' for cloud-wake phase

$$\left|\begin{matrix}\text{Oxygen in from stage}\\(n-1)\text{ by convection}\end{matrix}\right| + \left|\begin{matrix}\text{Oxygen coming from}\\\text{bubble phase by transfer}\end{matrix}\right| - \left|\begin{matrix}\text{Oxygen going out from cloud -}\\\text{wake to emulsion by transfer}\end{matrix}\right| -$$

$$\left|\begin{matrix}\text{Oxygen out to stage}\\(n+1)\text{ by convection}\end{matrix}\right| - \left|\begin{matrix}\text{Oxygen consumed in}\\\text{cloud - wake phase}\end{matrix}\right| = 0 \qquad (5.83)$$

Symbolically it can be represented as;

$$U_{cw} C_{cw_{n-1}} + (K_{bc})_b \varepsilon_b \int_{Z_{n-1}}^{Z_n} (C_b - C_{cw_n}) dZ - K_{ce}(C_{cw_n} - C_{e_n}) - U_{cw} C_{cw_n} - K_{cw} C_{cw_n} = 0$$

Rearranging the above equation, we get

$$U_{cw} C_{cw_{n-1}} - U_{cw} C_{cw_n} + (K_{bc})_b \varepsilon_b \int_{Z_{n-1}}^{Z_n} (C_b - C_{cw_n}) dZ - K_{cw} C_{cw} - K_{ce} C_{cw_n} + K_{ce} C_{e_n} = 0$$

$$U_{cw}C_{cw_{n-1}}+(K_{bc})_b\varepsilon_b\int_{Z_{n-1}}^{Z_n}(C_b-C_{cw_n})dZ+K_{ce}C_{e_n}-(U_{cw}+K_{cw}+K_{ce})C_{cw_n}=0 \quad (5.84)$$

where $K_{ce}=(K_{ce})_b\varepsilon_b\Delta Z$ (5.85)

$K_{cw}=(K)(f_{cw})(\varepsilon_b)(\Delta Z)$ (5.86)

$\Delta Z=Z_n-Z_{n-1}=D_b$ (5.87)

## Oxygen Balance Around Stage 'n' For Emulsion Phase

$$\left|\begin{matrix}\text{Oxygen in from stage}\\(n-1)\text{ by convection}\end{matrix}\right|-\left|\begin{matrix}\text{Oxygen out to stage}\\(n+1)\text{ by convection}\end{matrix}\right|+\left|\begin{matrix}\text{Oxygen coming from}\\\text{cloud- wake phase.}\end{matrix}\right|-\left|\begin{matrix}\text{Oxygen consumed in}\\\text{emulsion phase}\end{matrix}\right|=0 \quad (5.88)$$

Which can be represented symbolically as;

$$U_{mf}C_{e_{n-1}}-U_{mf}C_{e_n}+K_{ce}(C_{cw_n}-C_{e_n})-K_eC_{e_n}=0$$

Expanding, we get

$$U_{mf}C_{e_{n-1}}-U_{mf}C_{e_n}+K_{ce}C_{cw_n}-K_{ce}C_{e_n}-K_eC_{e_n}=0$$

$$U_{mf}C_{e_{n-1}}+K_{ce}C_{cw_n}-(U_{mf}+K_e+K_{ce})C_{e_n}=0 \quad (5.89)$$

Where $K_e=K[1-\varepsilon_b(1+f_{cw})]\Delta Z$ (5.90)

$K_{ce}=(K_{ce})_b\varepsilon_b\Delta Z$ (5.91)

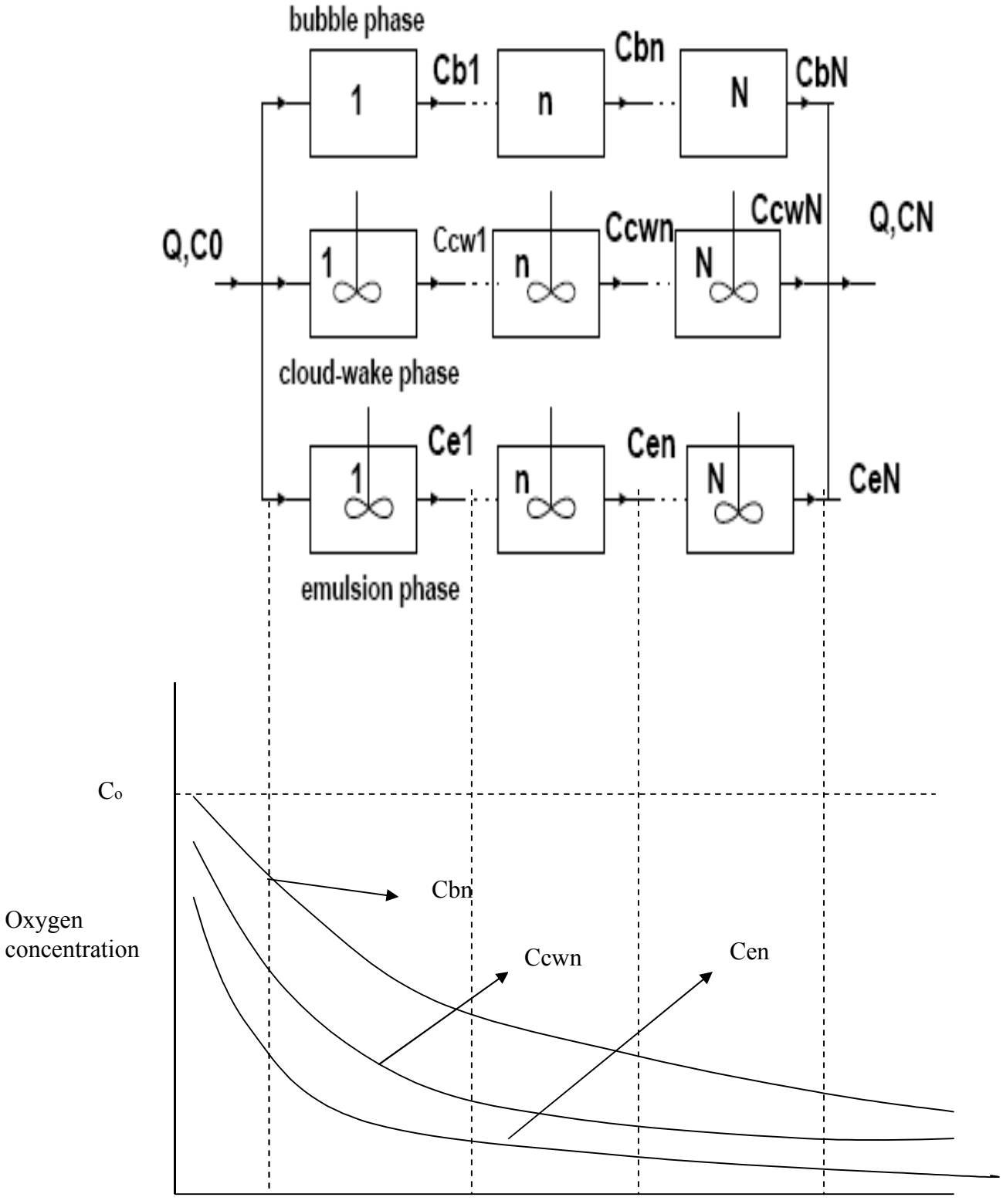


**Figure 5.3 – Multistage three-phase model**

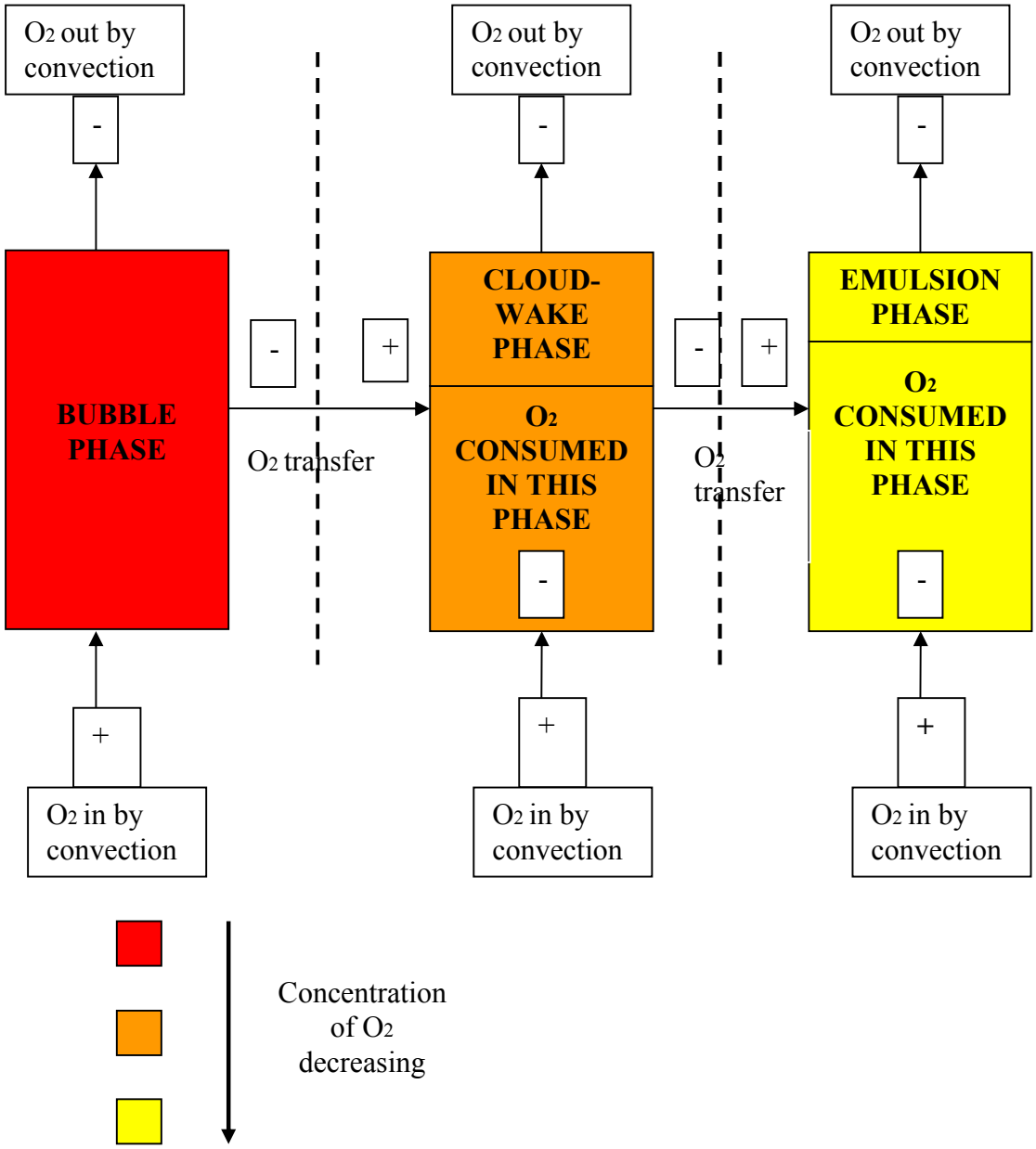


**Figure 5.4 – Oxygen mass balance in different phases**

Material balance of reactant gas (for the bubble phase) over the differential element of height dZ can be written as

$$U_b C_b - U_b (C_b + dC_b) - (K_{bc})_b \varepsilon_b (C_b - C_{cw_n}) dZ = 0 \qquad (5.92)$$

Expanding, we get

$$U_b C_b - U_b C_b - U_b dC_b - (K_{bc})_b \varepsilon_b (C_b - C_{cw_n}) dZ = 0 \qquad (5.93)$$

Which can be re-written as

$$- U_b dC_b = (K_{bc})_b \varepsilon_b (C_b - C_{cw_n}) dZ$$

$$\frac{dC_b}{(C_b - C_{cw_n})} = -\frac{(K_{bc})_b \varepsilon_b dZ}{U_b} \tag{5.94}$$

Integrating, we get

$$\int_{C_{b_{n-1}}}^{C_b} \frac{dC_b}{(C_b - C_{cw_n})} = -\frac{(K_{bc})_b \varepsilon_b}{U_b} \int_{Z_{n-1}}^{Z_n} dZ \tag{5.95}$$

Which can be written as

$$- U_b \left| \log(C_b - C_{cw_n}) \right|_{C_{bn-1}}^{C_{b_n}} = (K_{bc})_b \varepsilon_b (Z_n - Z_{n-1})$$

Expanding the limits, we get

$$- U_b \left\{ \left| \log(C_b - C_{cw_n}) \right| - \left| \log(C_{b_{n-1}} - C_{cw_n}) \right| \right\} = (K_{bc})_b \varepsilon_b (Z_n - Z_{n-1})$$

Which can be written as

$$- U_b \left| \log(C_b - C_{cw_n}) \right|_{C_{bn-1}}^{C_{b_n}} = (K_{bc})_b \varepsilon_b (Z_n - Z_{n-1})$$

$$\log \left[ \frac{C_{b_n} - C_{cw_n}}{C_{b_{n-1}} - C_{cwn}} \right] = -\frac{(K_{bc})_b \varepsilon_b (Z_n - Z_{n-1})}{U_b}$$

Which implies

$$\frac{C_{b_n} - C_{cw_n}}{(C_{b_{n-1}} - C_{cwn})} = \exp\left[ -\frac{(K_{bc})_b \varepsilon_b (Z_n - Z_{n-1})}{U_b} \right] \tag{5.96}$$

At the bottom of the bed (n=0) the concentration of gas fed to each phase is the same as that of the incoming feed gas. Hence, the appropriate boundary conditions are

At n=0

$$C_{b_n} = C_o \tag{5.97}$$

$$C_{cw_n} = C_o \tag{5.98}$$

$$C_{e_n} = C_o \tag{5.99}$$

Equations (5.82), (5.84), (5.89) and (5.96) may be solved, as below

Subtracting 1 from both sides of equation (5.96), we get

$$1-\frac{C_{b_n}-C_{cw_n}}{(C_{b_{n-1}}-C_{cw_n})}=1-\exp\left[-\frac{(K_{bc})_b\,\varepsilon_b(Z_n-Z_{n-1})}{U_b}\right]$$

Rearranging, we get

$$C_{b_{n-1}}-C_{cwn}-C_{b_n}+C_{cw_n}=\frac{C_{b_{n-1}}-C_{cw_n}}{R}$$

$$\text{Where}\quad R=\frac{1}{1-\exp\left[-\frac{(K_{bc})_b\,\varepsilon_b(Z_n-Z_{n-1})}{U_b}\right]} \tag{5.100}$$

$$C_{b_{n-1}}-C_{b_n}=\frac{C_{b_{n-1}}-C_{cw_n}}{R} \tag{5.101}$$

From equations (5.82), we have

$$(K_{bc})_b\,\varepsilon_b\int_{Z_{-1}}^{Z_n}(C_{b_n}-C_{cw_n})dZ=U_b\left[C_{b_{n-1}}-C_{b_n}\right] \tag{5.102}$$

From equations (5.101) and (5.102), we get

$$(K_{bc})_b\,\varepsilon_b\int_{Z_{-1}}^{Z_n}(C_{b_n}-C_{cw_n})dZ=\frac{U_b}{R}\left[C_{b_{n-1}}-C_{b_n}\right] \tag{5.103}$$

Again from equation (5.101), we get

$$RC_{b_{n-1}}-RC_{b_n}=C_{b_{n-1}}-C_{cw_n}$$

Which implies

$$C_{cw_n}=RC_{b_n}-(R-1)C_{b_{n-1}} \tag{5.104}$$

Similarly, we can write

$$C_{cw_{n-1}}=RC_{b_{n-1}}-(R-1)C_{b_{n-2}} \tag{5.105}$$

From equation (5.84) and above three, we get

$$U_{cw}\left[RC_{b_{n-1}} - (R-1)C_{b_{n-2}}\right] + \frac{U_b}{R}\left[C_{b_{n-1}} - C_{b_n}\right] + K_{ce}C_{e_n} - (U_{cw} + K_{cw} + K_{ce})RC_{b_n} - (R-1)C_{b_{n-1}} = 0$$

Which implies

$$U_{cw}RC_{b_{n-1}} - U_{cw}(R-1)C_{b_{n-2}} + U_bC_{b_{n-1}} - U_bC_{b_n} + K_{ce}C_{e_n} - (U_{cw} + K_{cw} + K_{ce})RC_{b_n}$$

$$+ (U_{cw} + K_{cw} + K_{ce})(R-1)C_{b_n} = 0$$

Rearranging the above equation, we get

$$-\left[(U_{cw} + K_{cw} + K_{ce})R + U_b\right]C_{b_n} + \left[(U_{cw} + K_{cw} + K_{ce})(R-1) + U_b + U_{cw}R\right]C_{b_{n-1}} -$$

$$U_{cw}(R-1)C_{b_{n-2}} = -K_{ce}C_{en}$$

This implies

$$C_{e_n} = \frac{\left\{\begin{array}{l} U_{cw}(R-1)C_{b_{n-2}} - \left[(U_{cw} + K_{cw} + K_{ce})(R-1) + U_b + U_{cw}R\right]C_{b_{n-1}} \\ + \left[(U_{cw} + K_{cw} + K_{ce})R + U_b\right]C_{b_n} \end{array}\right\}}{K_{ce}}$$

Thus, we can write

$$C_{e_n} = a_1C_{b_n} + b_1C_{b_{n-1}} + c_1C_{b_{n-2}} \qquad (5.106)$$

Where,

$$a_1 = \left[\frac{U_b + R(U_{cw} + K_{cw} + K_{ce})}{K_{ce}}\right] \qquad (5.107)$$

$$b_1 = \left[-\frac{\left[(U_{cw} + K_{cw} + K_{ce})(R-1) + (((R-1) \times U_b)/R) + (U_b/R) + (R \times U_{cw})\right]}{K_{ce}}\right] \qquad (5.108)$$

$$c_1 = \left[\frac{[(U_{cw})(R-1)]}{K_{ce}}\right] \qquad (5.109)$$

From equation (5.89) and (5.109), we get

$$U_{mf}\left[a_1 C_{b_{n-1}} + b_1 C_{b_{n-2}} + c_1 C_{b_{n-3}}\right] + K_{ce}\left[RC_{b_n} - (R-1)C_{b_{n-1}}\right] -$$

$$\left(U_{mf} + K_e + K_{ce}\right)\left(a_1 C_{b_n} + b_1 C_{b_{n-1}} + c_1 C_{b_{n-2}}\right) = 0 \tag{5.110}$$

Rearranging, we get

$$U_{mf} a_1 C_{b_{n-1}} + U_{mf} b_1 C_{b_{n-2}} + U_{mf} c_1 C_{b-3} + K_{ce} R C_{b_n} - K_{ce}(R-1)C_{b_{n-1}} - \left(U_{mf} + K_e + K_{ce}\right) a_1 C_{b_n}$$

$$+\left(U_{mf} + K_e + K_{ce}\right) b_1 C_{b_{n-1}} + \left(U_{mf} + K_e + K_{ce}\right) c_1 C_{b_{n-2}} = 0$$

Which implies

$$C_{b_n}\left[-\left(U_{mf} + K_e + K_{ce}\right) a_1 + K_{ce} R\right] + C_{b_{n-1}}\left[U_{mf} a_1 - K_{ce}(R-1) - \left(U_{mf} + K_e + K_{ce}\right) b_1\right]$$

$$+C_{b_{n-2}}\left[b_1 U_{mf} - \left(U_{mf} + K_e + K_{ce}\right) c_1\right] + c_1 U_{mf} C_{b_{n-3}} = 0$$

Thus, we can write the above equation as

$$C_{b_n} + C_{b_{n-1}} b + C_{b_{n-2}} c + C_{b_{n-3}} d = 0 \tag{5.111}$$

Where,

$$a = \left[-\left(U_{mf} + K_e + K_{ce}\right) a_1 + K_{ce} R\right] \tag{5.112}$$

$$b = \frac{\left[U_{mf} a_1 - K_{ce}(R-1) - \left(U_{mf} + K_e + K_{ce}\right) b_1\right]}{a} \tag{5.113}$$

$$c = \frac{\left[b_1 U_{mf} - \left(U_{mf} + K_e + K_{ce}\right) c_1\right]}{a} \tag{5.114}$$

$$d = \frac{\left[c_1 U_{mf}\right]}{a} \tag{5.115}$$

Equation (5.111) is a third order homogeneous linear finite difference equation with constant coefficients. The solution of this equation is obtained by trying a solution of the form

$$C_{b_n} = fG^n \tag{5.116}$$

Where f is an arbitrary constant and G is a constant whose value is to be determined without recourse to the boundary conditions. When this solution is substituted in equation (5.103), it leads to

$$fG^{n-3}(G^3 + bG^2 + cG + d) = 0 \tag{5.117}$$

Which implies

$$(G^3 + bG^2 + cG + d) = 0 \tag{5.118}$$

This is a cubic algebraic equation which may be solved as follows:

Let

$$p = \frac{1}{3(3c - b^2)} \tag{5.119}$$

$$q = \frac{1}{27(27d - 9bc + 2b^3)} \tag{5.120}$$

$$T = \frac{p^3}{27} + \frac{q^2}{4} \tag{5.121}$$

$$\phi = \cos^{-1}\left(-\frac{q^2/4}{p^3/27}\right) \tag{5.122}$$

For T<0, equation (5.118) has three real and unequal roots given by

$$G_m = \mp 2\left\{(-p/3)^{1/2}\cos\left[\phi/3 + 120(m-1)\right]\right\} - b/3 \tag{5.123}$$

Where (m=1,2,3)

where the upper sign applies if q>0, and the lower if q<0. Thus the general solution of equation (5.111) is

$$C_{b_n} = f_1 G_1^{\,n} + f_2 G_2^{\,n} + f_3 G_3^{\,n} \tag{5.124}$$

Therefore

$$C_{b_{n-1}} = f_1 G_1^{\,n-1} + f_2 G_2^{\,n-1} + f_3 G_3^{\,n-1} \tag{5.125}$$

and

$$C_{b_{n-2}} = f_1 G_1^{\,n-2} + f_2 G_2^{\,n-2} + f_3 G_3^{\,n-2} \tag{5.126}$$

Substitution of equation (5.124) and (5.125) into (5.104) leads to

$$C_{cw_n} = g_1 f_1 G_1^{\,n} + g_2 f_2 G_2^{\,n} + g_3 f_3 G_3^{\,n} \tag{5.127}$$

$$g_m = \frac{R-(R-1)}{G_m} \tag{5.128}$$

Where m=1,2,3

Substituting equations (5.124) to (5.126) into equation (5.106), we have

$$C_{e_n} = r_1 f_1 G_1^{\,n} + r_2 f_2 G_2^{\,n} + r_3 f_3 G_3^{\,n} \tag{5.129}$$

Where

$$r_m = a_1 + \frac{b_1}{G_m} + \frac{c_1}{G_m^{\,2}} \tag{5.130}$$

Where m=1,2,3

Inserting the boundary conditions given by equations (5.97), (5.98) and (5.99) respectively, one may write

$$C_0 = f_1 + f_2 + f_3 \tag{5.131}$$

$$C_0 = g_1 f_1 + g_2 f_2 + g_3 f_3 \tag{5.132}$$

$$C_0 = r_1 f_1 + r_2 f_2 + r_3 f_3 \tag{5.133}$$

Solving equations (5.131) to (5.133) Simultaneously for $f_1$-$f_3$, we obtain

$$f_1 = \frac{[r_2 - r_3 + g_2(r_3 - 1) + g_3(1 - r_2)]C_o}{D} \tag{5.134}$$

$$D = [g_1(r_2 - r_3) + g_2(r_3 - r_1) + g_3(r_1 - r_2)] \tag{5.135}$$

$$f_2 = \frac{[g_1(1 - r_3) + (r_3 - r_1) + g_3(r_1 - 1)]C_o}{D} \tag{5.136}$$

$$f_3 = \frac{[g_1(r_2 - 1) + g_2(1 - r_1) + (r_1 - r_2)]C_o}{D} \tag{5.137}$$

The average gas concentration of the reactant leaving the nth stage, $C_{avg_n}$ is defined as the concentration that one would measure by sampling the gas leaving stage n in proportion to the volumetric flow rates of the three phases, i.e.

$$C_{avgn} = \frac{U_b C_{b_n} + U_{cw} C_{cw_n} + U_{mf} C_{e_n}}{U_o} \qquad (5.138)$$

The gas concentration profiles for the three phases and for the average concentration may be obtained from equations (5.124), (5.125), (5.126) and (5.138) respectively, and the outlet gas concentration, $C_{avg}$ is calculated directly by substituting for n=N in equation (5.138)

The overall fractional conversion is given by

$$x=1-(C_{avg}/C_0) \qquad (5.139)$$

The exit gas compositions can be found out as follows

Oxygen:

$$O_2 = C_{avg} \qquad (5.140)$$

Carbon dioxide:

$$C0_2=C_0-C_{avg} \qquad (5.141)$$

Nitrogen:

$$N_2 = 1000\left[\left(\frac{0.79}{22400}\right)(273/T_b) + \frac{(XN(1-XW)\times W)}{28000\times U_o \times A}\right] \qquad (5.142)$$

$$H_2 = 1000\left[\frac{(XH(1-XW)W)}{4000\times U\times A} + \frac{(XW)(W)}{18000\times U\times A}\right] \qquad (5.143)$$

## 5.4 Flow chart for the model

Figure 5.5 shows the step-wise procedure for the development of a mathematical model.

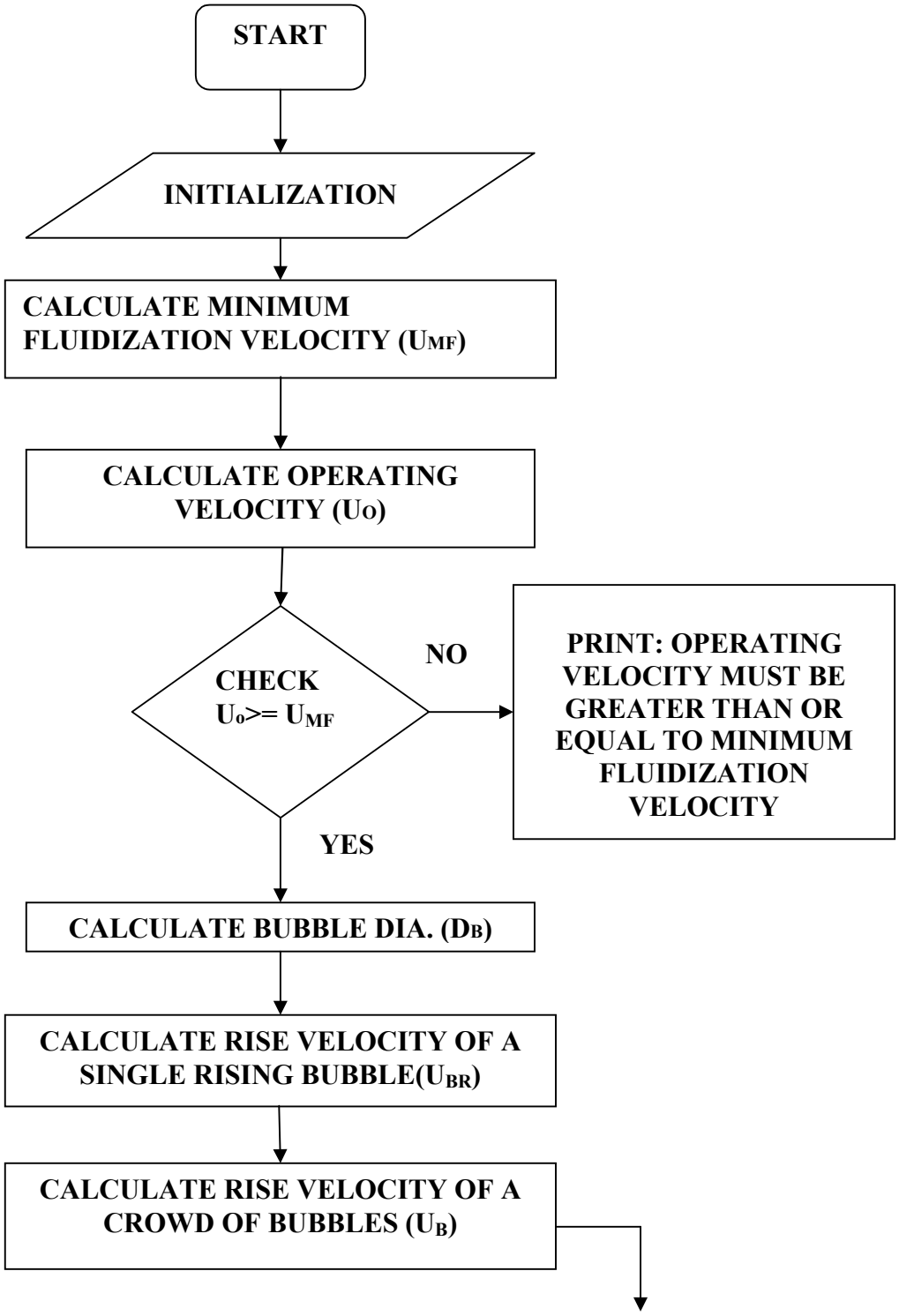

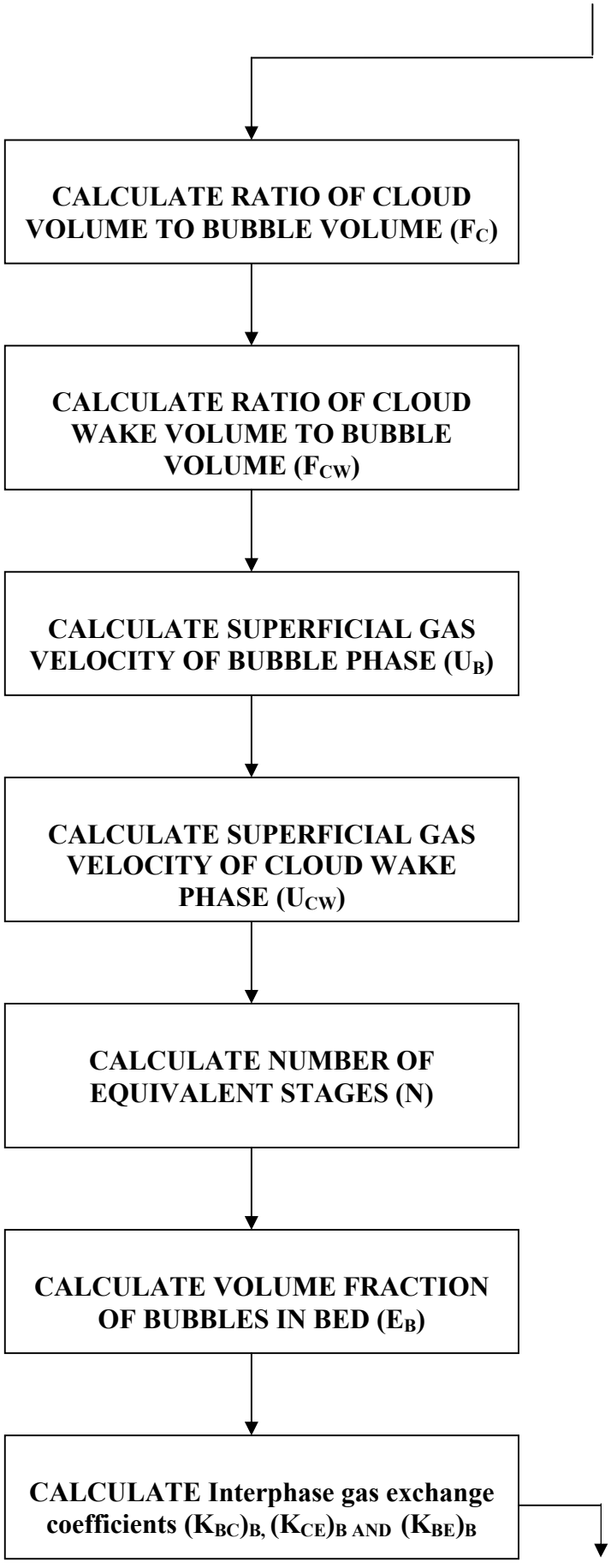

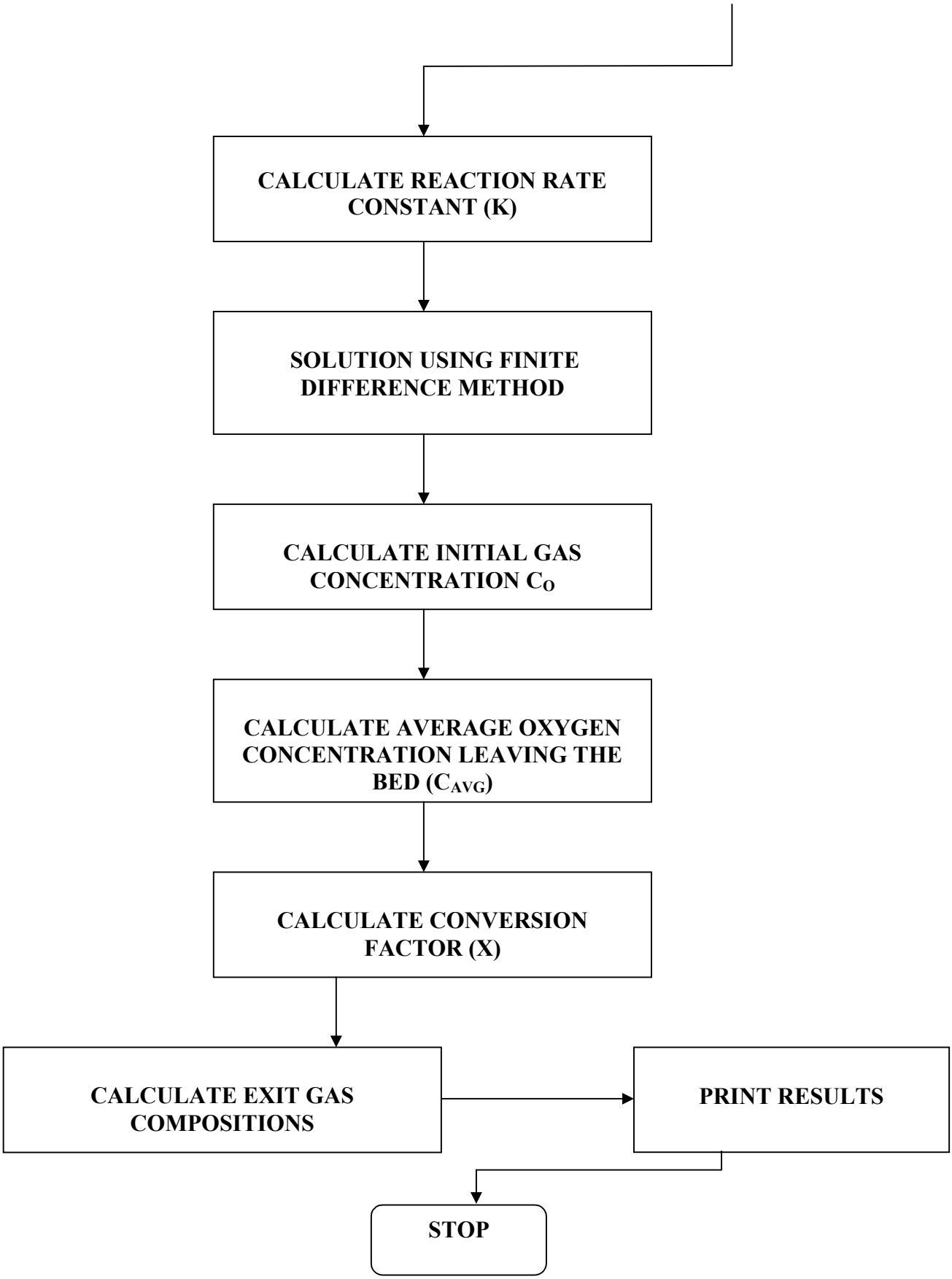


**Figure 5.5 – Flow chart for the mathematical model**

# CHAPTER – 6

# RESULTS AND DISCUSSION

## 6.1 Input parameters used in the model

The input data required for the proposed model has been taken from a Malwa power limited, Muktsar, details of which have been already explained. Various inputs required for the mathematical model were obtained from the plant and have been listed in Table 6.1 as follows.

**Table 6.1 – Various input parameters used in the model**

| Parameters | Symbols | Values | Units |
|---|---|---|---|
| Fuel feed rate | X | 2.778 | kg/s |
| Moisture content | XW | 0.1389 | - |
| Carbon content | XC | 0.4237 | - |
| Hydrogen content | XH | 0.0566 | - |
| Sulphur content | XS | 0.0 | - |
| Oxygen content | XO | 0.3658 | - |
| Nitrogen content | XN | 0.015 | - |
| Fractional excess air | $E_{xair}$ | 0.3 | - |
| Bed temperature | $T_b$ | 1023 | K |
| Pressure in the combustor | $P_{av}$ | 1.01 | atm |
| Cross-sectional area of the bed | A | 19.43 | $m^2$ |
| Bed height at minimum fluidization | $H_{mf}$ | 0.7 | m |
| Particle density | $\rho_s$ | 116.1 | $kg/m^3$ |
| Particle size | $d_p$ | 0.0118388 | m |
| Gas constant | $R_g$ | 0.08206 | atm-$m^3$/ (kg-mole K) |
| Bed diameter | $D_t$ | 4.972836 | m |
| Ratio of coud-wake volume to bubble volume | $f_{cw}$ | 0.3 | - |
| Mean voidage under minimum fluidization | $\varepsilon_{mf}$ | 0.41 | - |

Further, the effect of different input parameters on the results has been studied and presented in the form of graphs, and discussed in the following text.

## 6.2 Discussion of the results and comparison with plant data

The model has been used to predict the consumption of oxygen in a fluidized bed combustor that makes it possible to predict the outlet gas composition and variation of average oxygen concentration along the bed height, which has been divided into a number of stages. The height of each stage is equal to the average equivalent bubble diameter.

The fraction of cloud wake phase has been used as an adjustable parameter. The simulated results, using different values of $f_{cw}$ are compared with data obtained from the real plant and presented in Table 6.2. It can be seen that agreement between the real plant data and the simulated results is reasonably good and best results are obtained using $f_{cw}$=0.3.

**Table 6.2 Comparison of predicted and experimental results**

| Components | Real plant data | Simulated data | | |
|---|---|---|---|---|
| | | $f_{cw}$=0.5 | $f_{cw}$=0.4 | $f_{cw}$=0.3 |
| $CO_2$ | 14 to 16 % | 15.01 | 14.74 | 14.53 |
| $O_2$ | 6 to 7% | 5.95 | 6.21 | 6.42 |
| $N_2$ | 77 to 79% | 79.04 | 79.04 | 79.04 |

In figure 6.1, variation of minimum fluidization velocity with particle size, using Chiester et al., Wen and Yu's, Babu et al. etc, has been shown. It can be seen that minimum fluidization velocity tends to increase with an increase in particle size. The reason for this increase is that as particle size is increased, the resistance offered to the fluid flow is also increased and this will increase the bed weight. If rest of the input parameters are kept constant, we require more force and hence more value of fluidization velocity to overcome this increased weight.

Further, expressions given by Babu et al., Wen and Yu's, Zheng et al., Satyanarayna et al. etc were also checked but, all these expressions gave absurd values for minimum fluidization velocity, in the present case. Our particle size is large and for our model the expression given by Chiester et al. is used. It gives the best result from all other expressions.

In figure 6.2, the variation of minimum fluidization velocity with bed temperature is show. It is seen that as the bed temperature is increased the minimum fluidization velocity decreases. This is due to the fact that as the bed temperature is increased the resistance offered to the fluid flow is decreased because with increase in bed temperature the fluid particles get energised and they will break the inter-molecular attraction forces. If we keep the other parameters same then, lesser force is required to fluidize the bed and to over come the resistance offered to the fluid flow.

In figure 6.3, the variation of the operating velocity with bed temperature is shown. It is noticed that as the bed temperature is increased the operating velocity of gas increases because the operating velocity is directly proportional to the bed temperature and with increase in bed temperature the operating velocity also increases.

In figure 6.4, the change in superficial gas velocity of bubbles with bed temperature is shown. It is seen that as the bed temperature is increased the superficial velocity of bubbles is also increased because the superficial velocity of bubbles is directly proportional to $(U_o - U_{mf})$ and with increase in bed temperature, $U_o$ increases and $U_{mf}$ decreases.

In figure 6.5, the variation of operating velocity with moisture percentage is shown. It is seen that with increase in moisture percentage, operating velocity of gas decreases. This is due to the reason that with increase in moisture percentage the stiochiometric air feed rate decreases and this decreases the actual molar feed rate of fluidizing gas. Operating velocity of gas is directly proportional to the actual molar feed rate and decrease in molar feed rate will decrease the operating velocity of fluidizing gas.

In figure 6.6, the variation of diffusion coefficient of gas with bed temperature is shown and it is seen that diffusion coefficient of gas increases with increase in bed temperature because as the bed temperature increase, the molecular movement increases and due to this more molecules will diffuse through.

In figure 6.7, the variation of Sherwood number with particle size is shown. With increase in particle size, Sherwood number also increases because Sherwood number is directly proportional to the particle size and as the particle size increases the Sherwood number also increases.

In figure 6.8, the variation of reaction rate constant (K) with particle size is shown. It can be observed that as the particle size increases the reaction rate decreases. This is because the reaction rate is controlled by mass transfer which decreases with increase of particle size. And the reason for decrease in mass transfer is that as particle size increases, there is a decrease in the surface area available for mass transfer.

In figure 6.9, the variation of oxygen conversion(X) with carbon percentage is shown. It is seen that as the carbon percentage increases the oxygen conversion decreases because with increase in carbon percentage the operating gas velocity increases. Due to this the bubble diameter increases and gas interphase coefficients decreases and this will decrease the reaction of the particles and hence oxygen conversion decreases.

In figure 6.10, the change in oxygen conversion with moisture percentage is shown. It is seen that as the moisture percentage increases the oxygen conversion increases. As discussed earlier that the increase in moisture content will decrease the operating velocity. Due to this bubble diameter will decrease and thus less oxygen will go out un-reacted through the bubbles which means that more oxygen will take part in the combustion reaction. This will increase the oxygen conversion.

In figure 6.11, the variation of bubble diameter and oxygen conversion with bed temperature is shown. It is seen that, bubble diameter increases and oxygen conversion decreases with increase in bed temperature. This is due to the reason that as the bed temperature increases, operating velocity increases and this will increase the bubble diameter because it is directly proportional to the operating velocity and with increase in bubble diameter, more oxygen leave without taking part into the combustion and hence oxygen conversion decreases.

In figure 6.12, the variation of oxygen conversion with mean voidage at minimum fluidization is shown. There is a slight increase in oxygen conversion with increase in voidage at minimum fluidization because with the increase in voidage at minimum fluidization there is more chance for carbon particles to react with oxygen and due to increase combustion, the oxygen conversion also increases.

In figure 6.13, the variation of oxygen conversion with ratio of cloud-wake volume to bubble volume($f_{cw}$) is shown. It is noticed that with increase in $f_{cw}$, the oxygen conversion increases slightly. The reason for this is that with an increase in

volume of the cloud wake region, more oxygen is able to participate in combustion reaction as more carbon particles are available in the cloud wake region.

In figure 6.14, the variation of bubble diameter and oxygen conversion with excess air is shown. It is noticed that bubble diameter increases and oxygen conversion decreases with increase in excess air because with increase in excess air the operating velocity increases and due to this the bubble diameter increases and this increase in bubble diameter will decrease the gas-interphase coefficient and consequently decrease in oxygen conversion.

In figure 6.15, the variation of $CO_2$ and $O_2$ percentage with excess air is shown. As the excess air is increased the $CO_2$ percentage decreases and $O_2$ percentage increases. This happens because, with an increased value of excess air, the available oxygen increases beyond the value required for complete combustion of fuel, as the amount of fuel in the bed remains the same. In other words, for burning the same amount of fuel, extra amount of oxygen is available, which leaves the bed un-reacted, leading to an increase in oxygen percentage in exit gases. Further, because of an increase in excess air, exit gas volume increases but, amount of $CO_2$ formed remains the same, which leads to a decrease in $CO_2$ volume per unit exit gas volume and hence a decrease in percentage of $CO_2$.

In figure 6.16, the variation of oxygen conversion with fuel feed rate is shown. It is found that oxygen conversion decreases with increase in fuel feed rate. This is because operating velocity tends to increase with increase in fuel feed rate and due to increase in the superficial velocity the bubble diameter will increase, thus decrease in oxygen conversion.

In figure 6.17, the change in oxygen conversion with particle size is shown. It is seen that with increase in particle size the oxygen conversion decreases because with increase in particle size the reaction rate decreases due to increased surface area of the particle and due to decreased reaction rate less oxygen will be consumed for combustion which will increase the oxygen at the exit and thus oxygen conversion decreases.

In figure 6.18, the variation of bubble diameter with bed height is shown. It is found that with increase in bed height the bubble diameter will also increase. This is due to the reason that with

In figure 6.19, the variation of oxygen concentration with bed height in different phases is shown. . It can be observed that the oxygen concentration of each of the three phases and the average oxygen concentration go on decreasing with bed height. This can be attributed to the fact that along the bed height, oxygen present in reactant gas gets consumed in the combustion reaction. Further, it can be observed from the graph that fall of oxygen concentration in the bubble phase is gradual. Whereas it is steep in case of cloud-wake and emulsion phase.

The steepness of the curve is maximum in case of emulsion phase. Oxygen concentration in bubble phase is highest followed by cloud-wake and emulsion phase. This is because the main combustion reaction is taking place in emulsion phase, as a result of which the oxygen consumption in this phase is highest, therefore oxygen concentration is lowest.

In cloud-wake phase, oxygen concentration is in between that of bubble phase and emulsion phase. This is because in cloud-wake phase, oxygen consumption is due to combustion as well as transfer to emulsion phase, due to the presence of lesser particulate matter. Oxygen consumption in the emulsion phase is highest and hence, values of oxygen concentration are lowest in this phase. Further, it can be seen that the variation of average oxygen concentration with bed height is similar to the variation of bubble phase oxygen concentration with bed height, indicating that bubble phase, because of its higher oxygen levels has more influence on the average values.

In figure 6.20, variation of average oxygen concentration with bed height, using different values of excess air is shown. The model predicts a fall in the oxygen concentration with bed height and, as the value of excess air increases, keeping other parameters same, the average oxygen concentration tends to increase. This is because we are providing more air than that is required for burning the same amount of fuel, thus increases the average oxygen concentration.

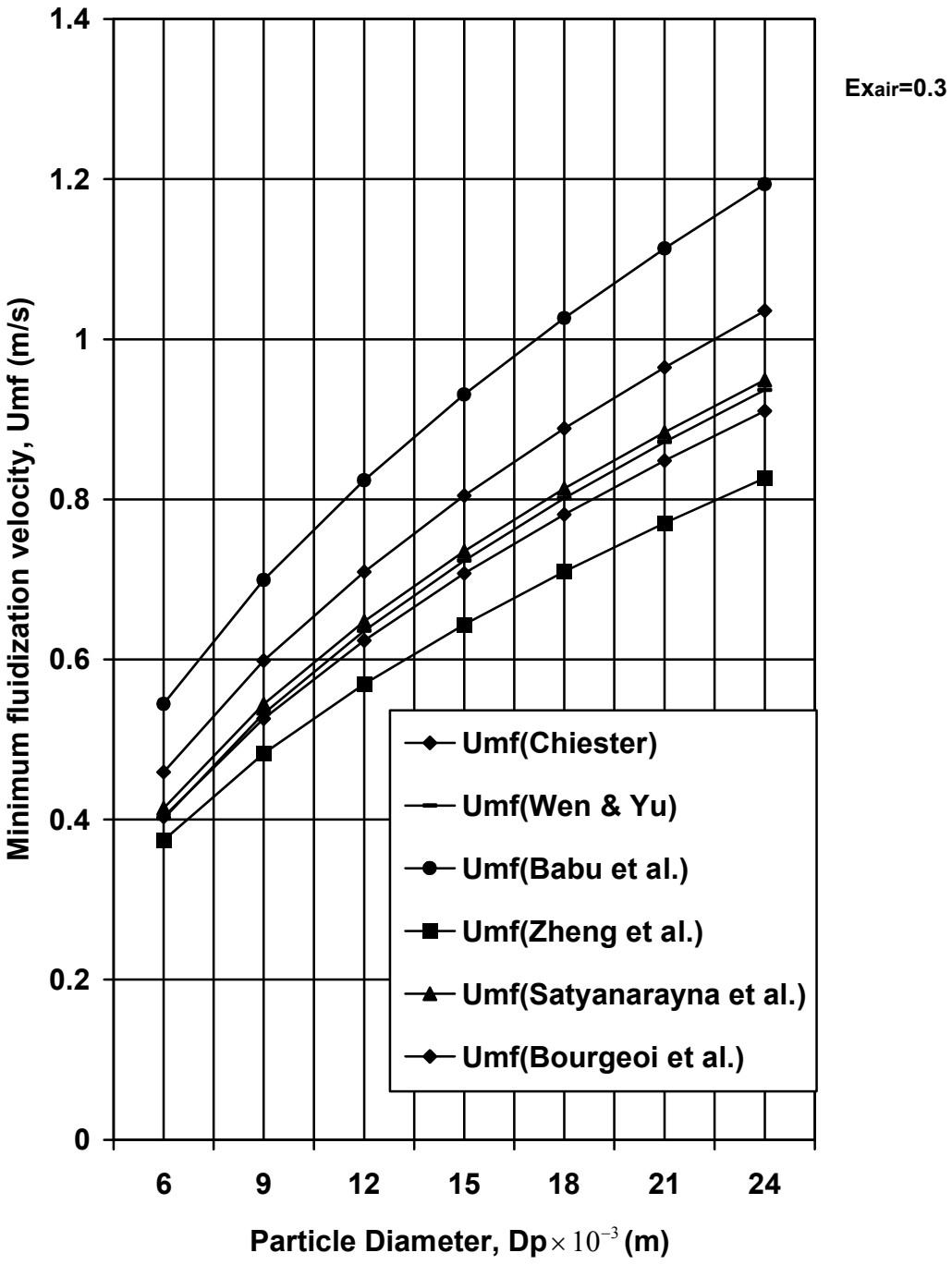


**Figure 6.1 - Variation of minimum fluidization velocity with particle diameter**

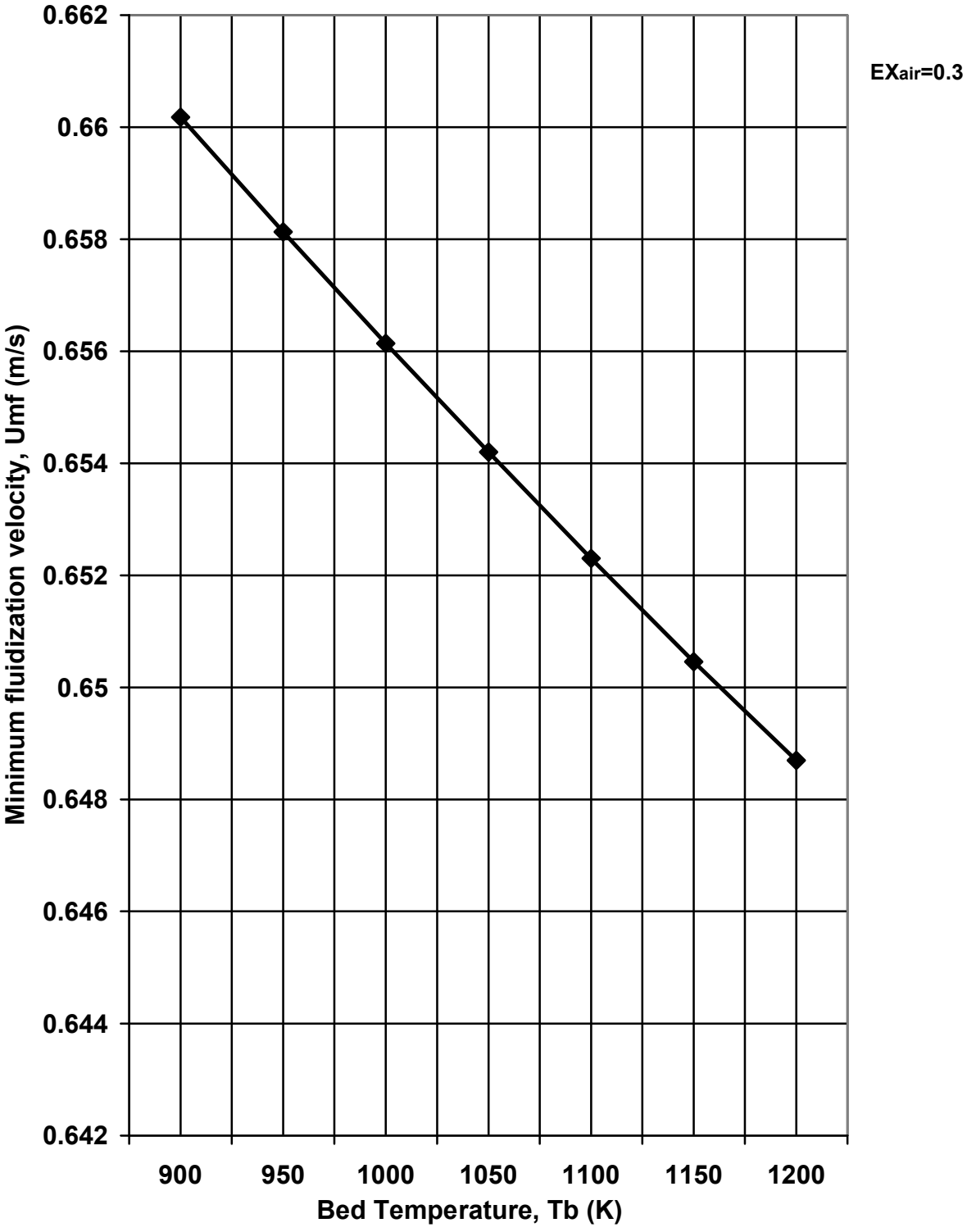


**Figure 6.2 - Variation of minimum fluidization velocity with Bed temperature**

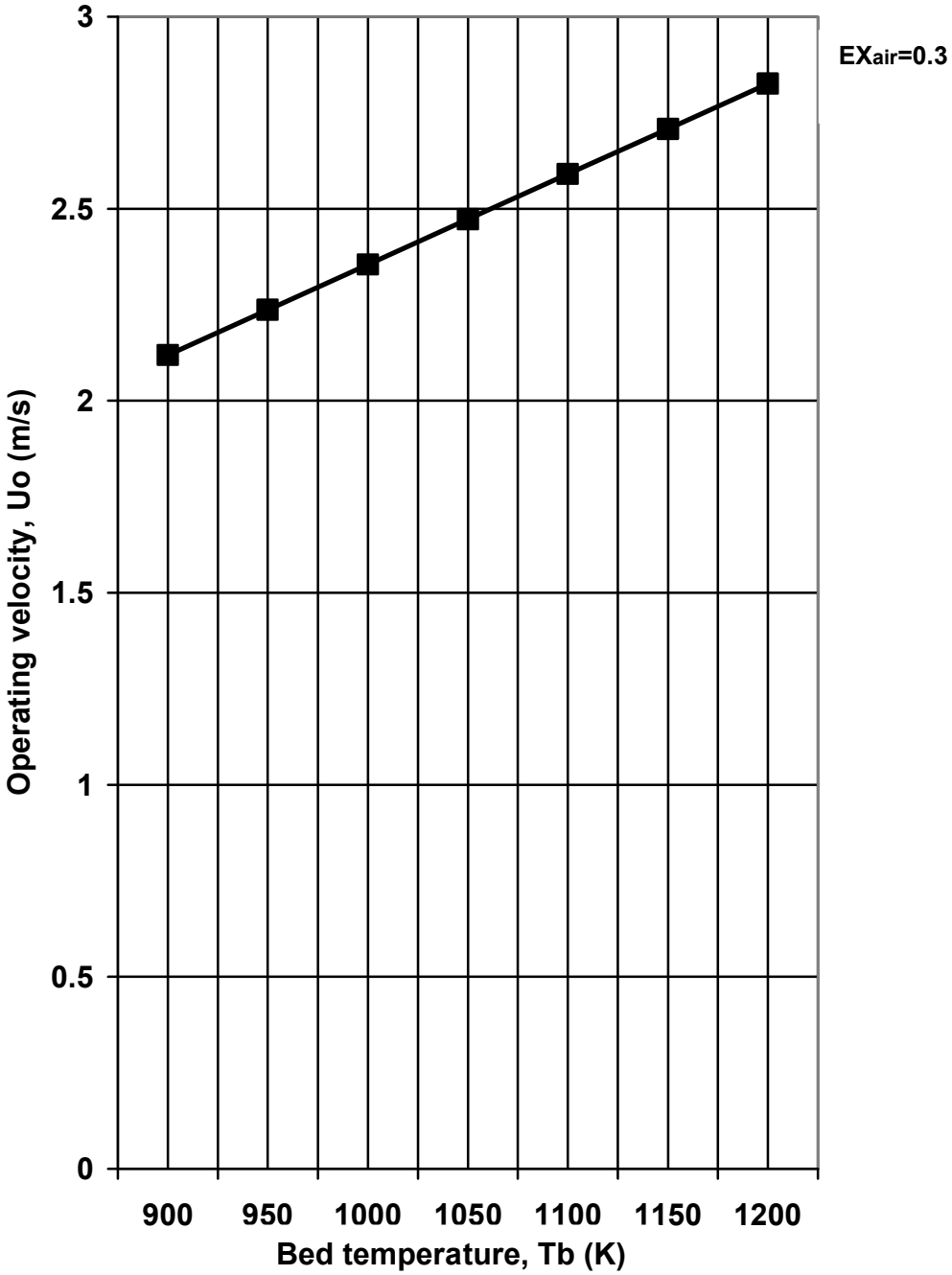


**Figure 6.3 - Variation of operating velocity with bed temperature**

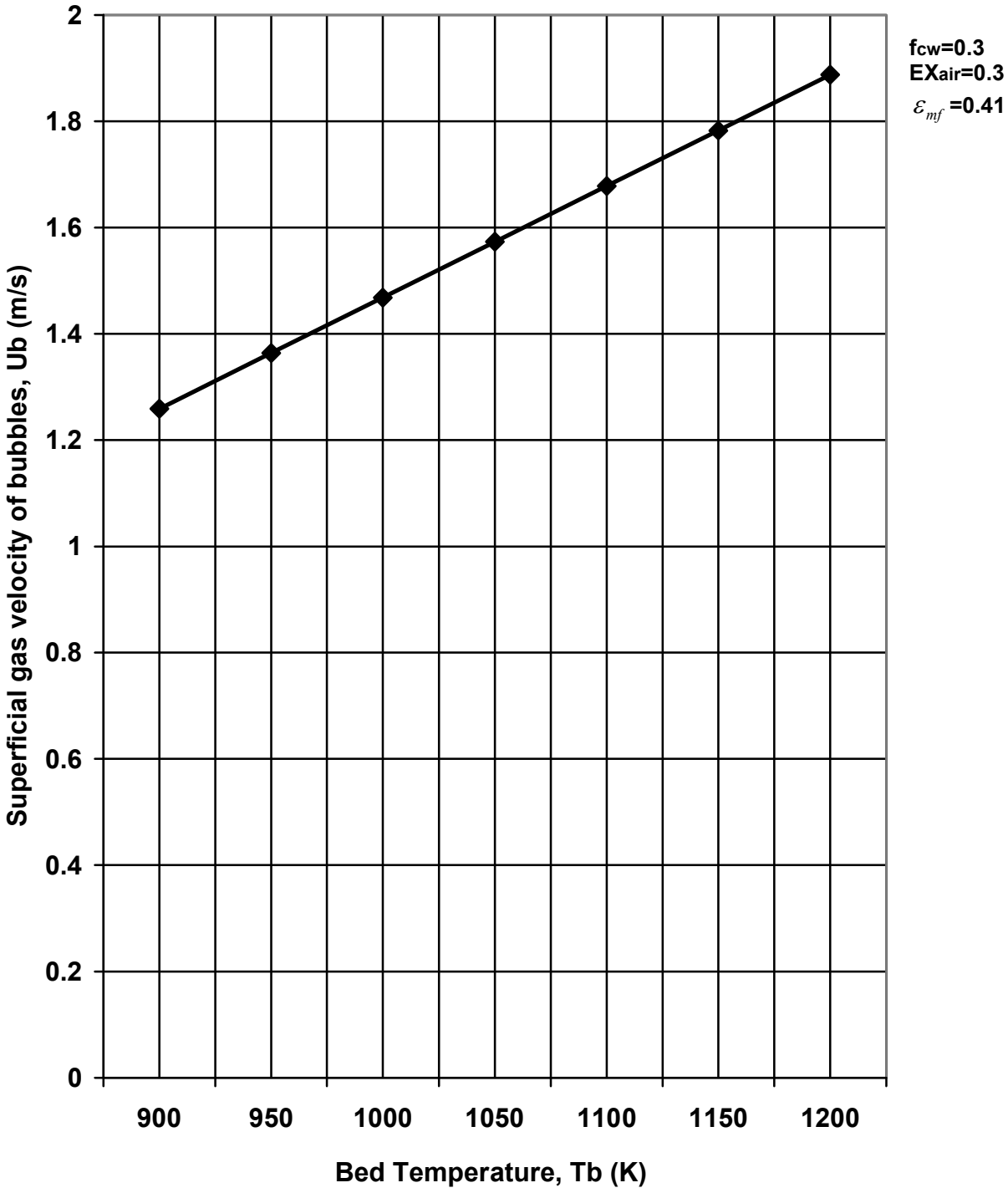


**Figure 6.4 - Variation of superficial gas velocity of bubbles with Bed temperature**

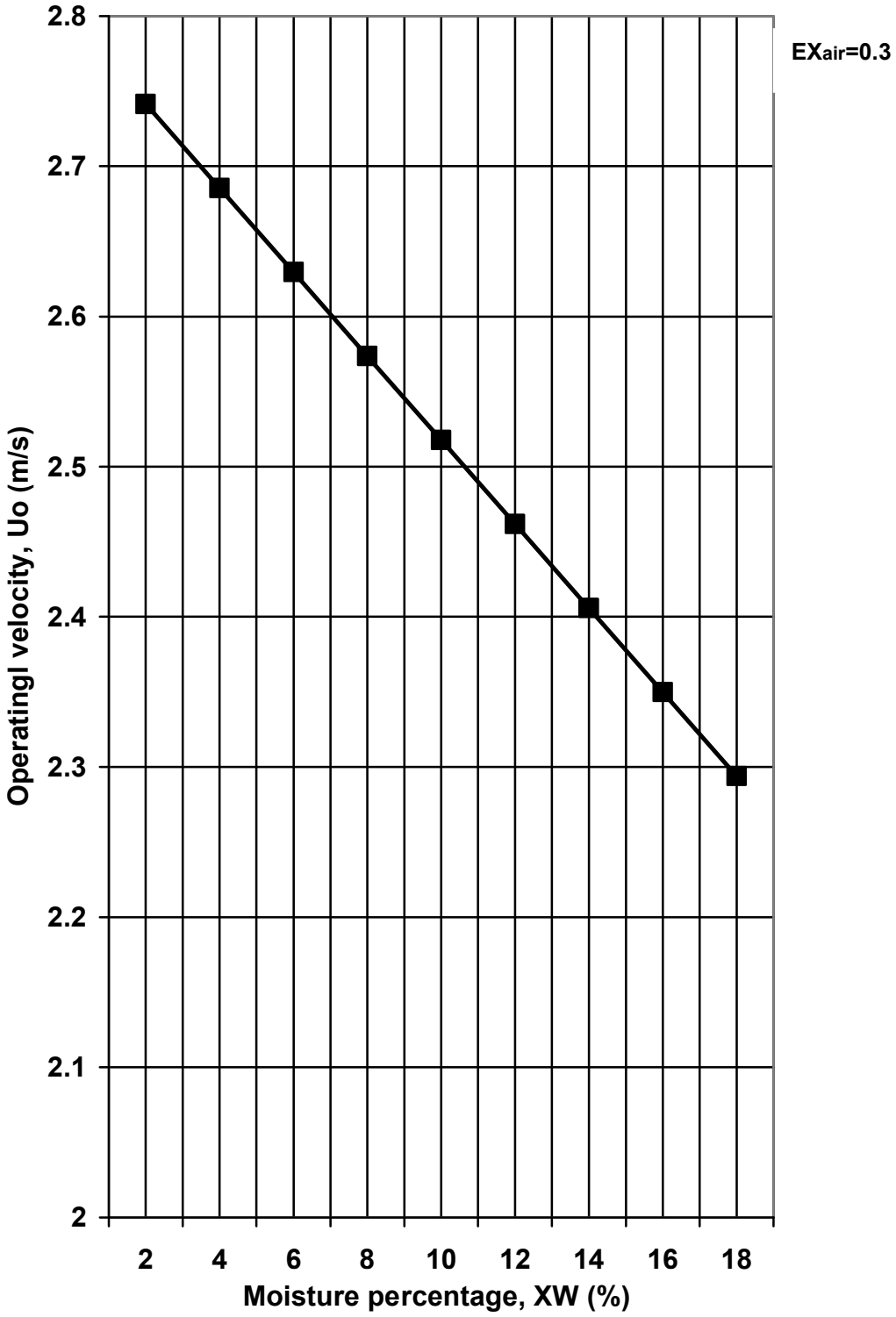


**Figure 6.5 - Variation of operating velocity with moisture percentage**

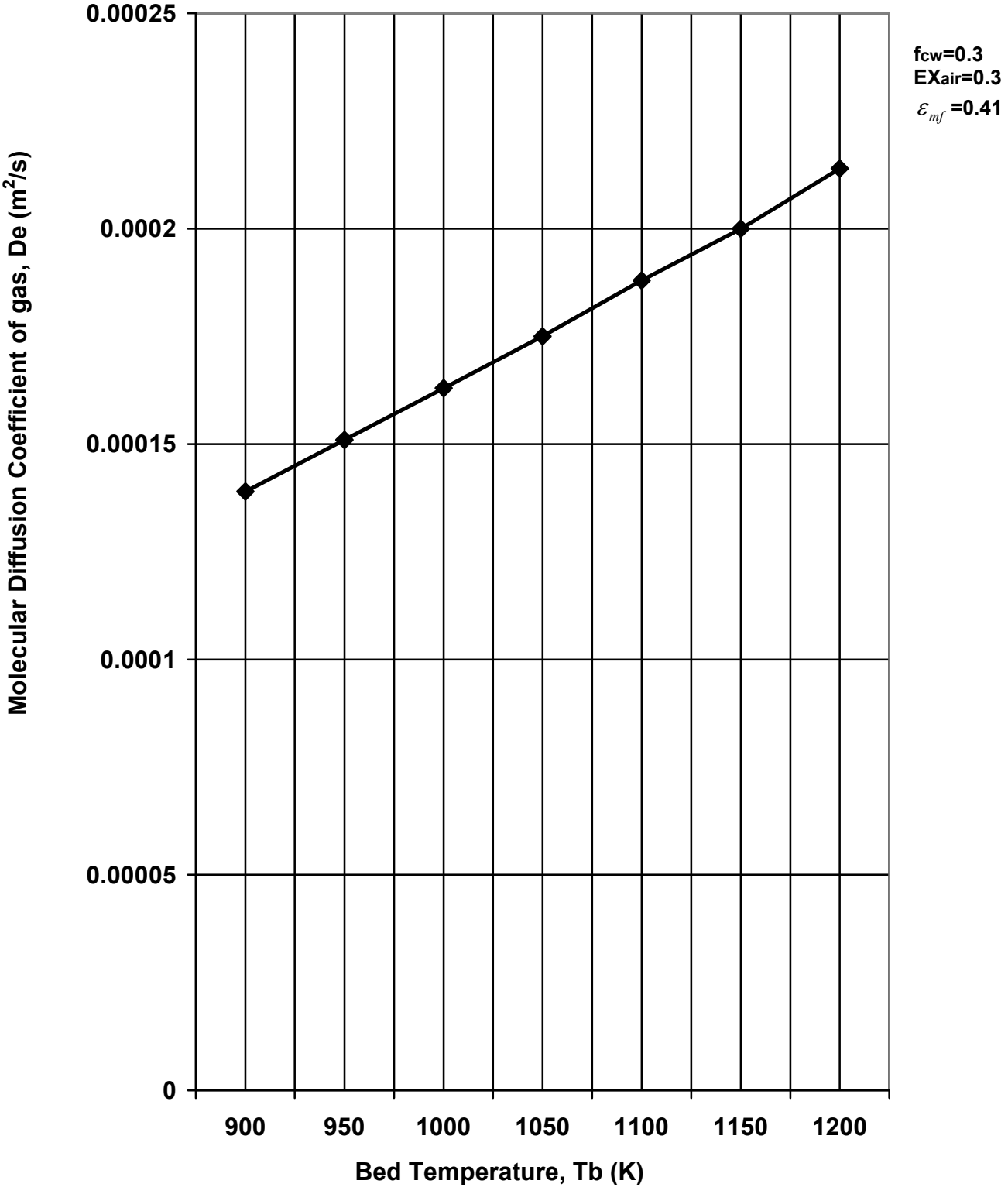


**Figure 6.6 - Variation of Molecular Diffusion Coefficient of gas with Bed temperature**

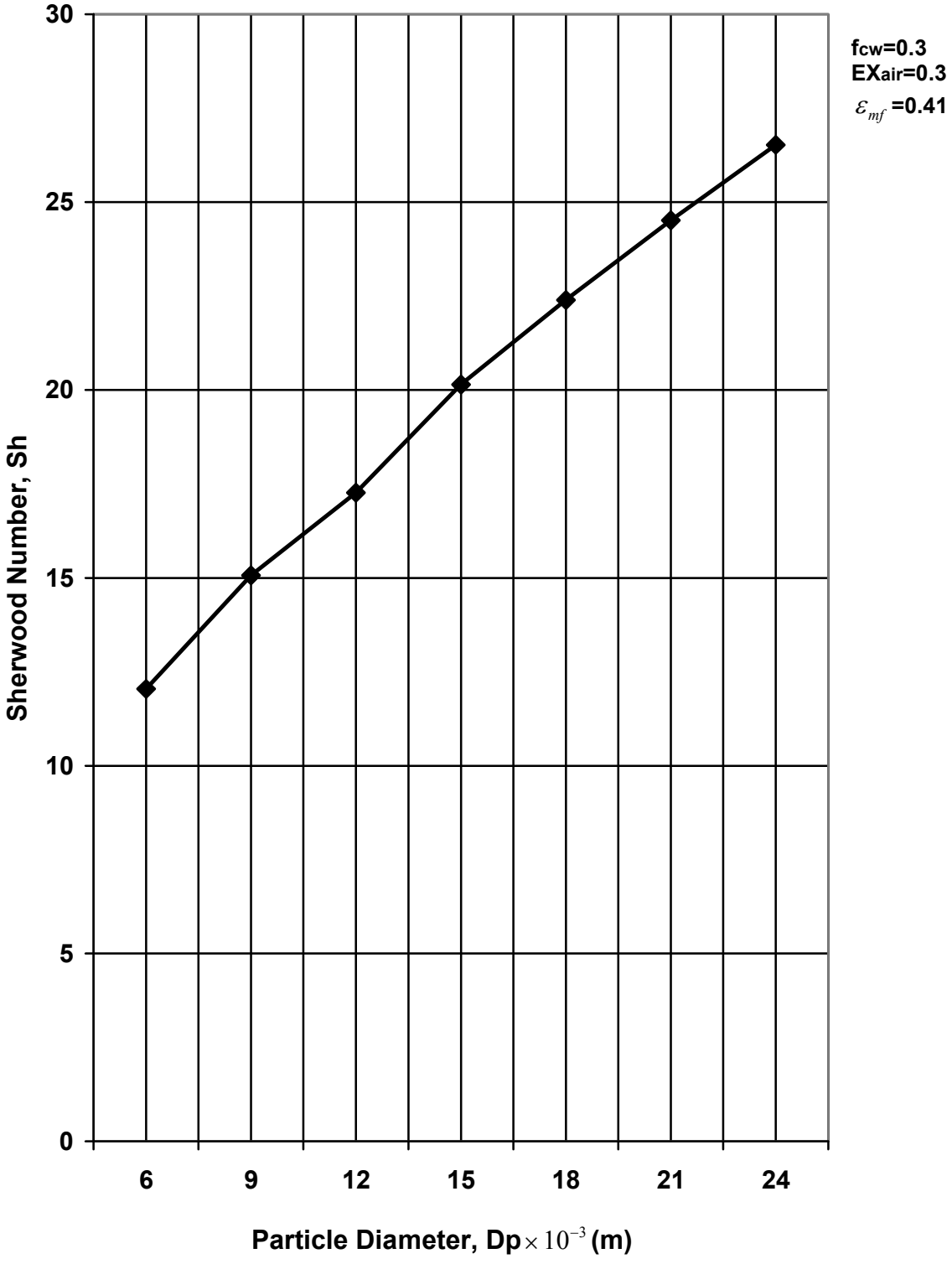


**Figure 6.7 - Variation of Sherwood Number with particle size**

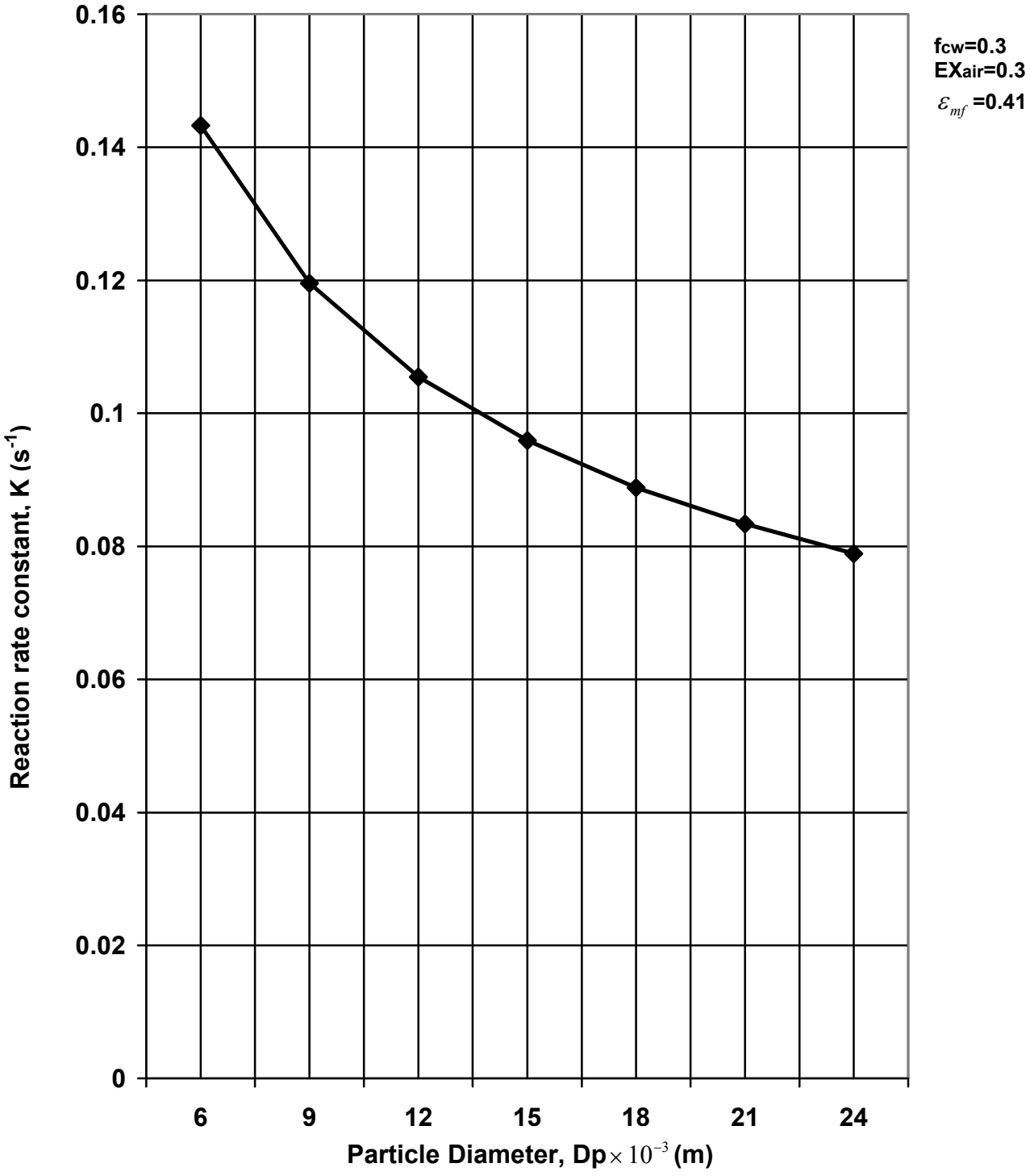


**Figure 6.8 - Variation of Reaction rate constant with particle size**

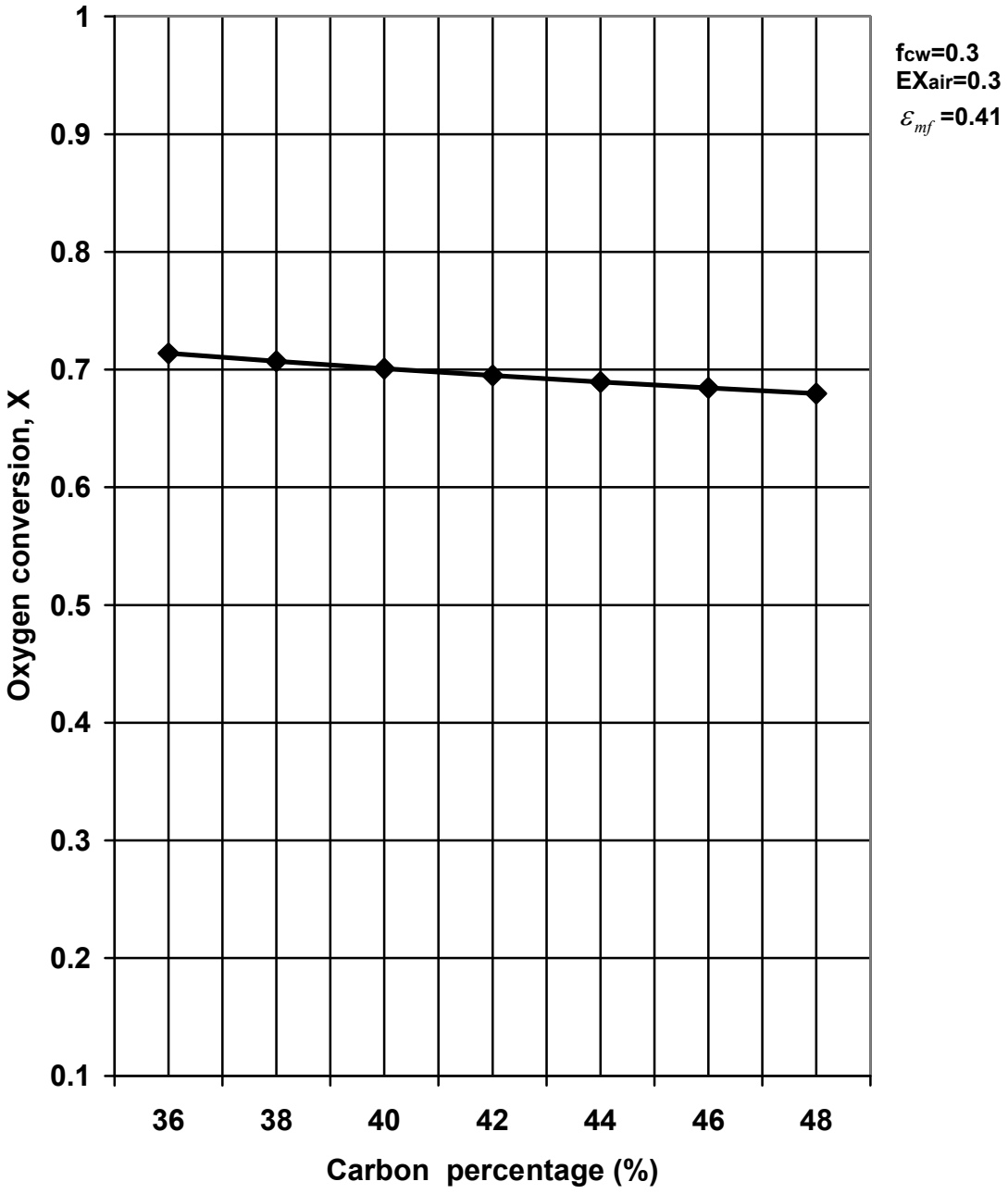


**Figure 6.9 - Variation of oxygen conversion with carbon percentage**

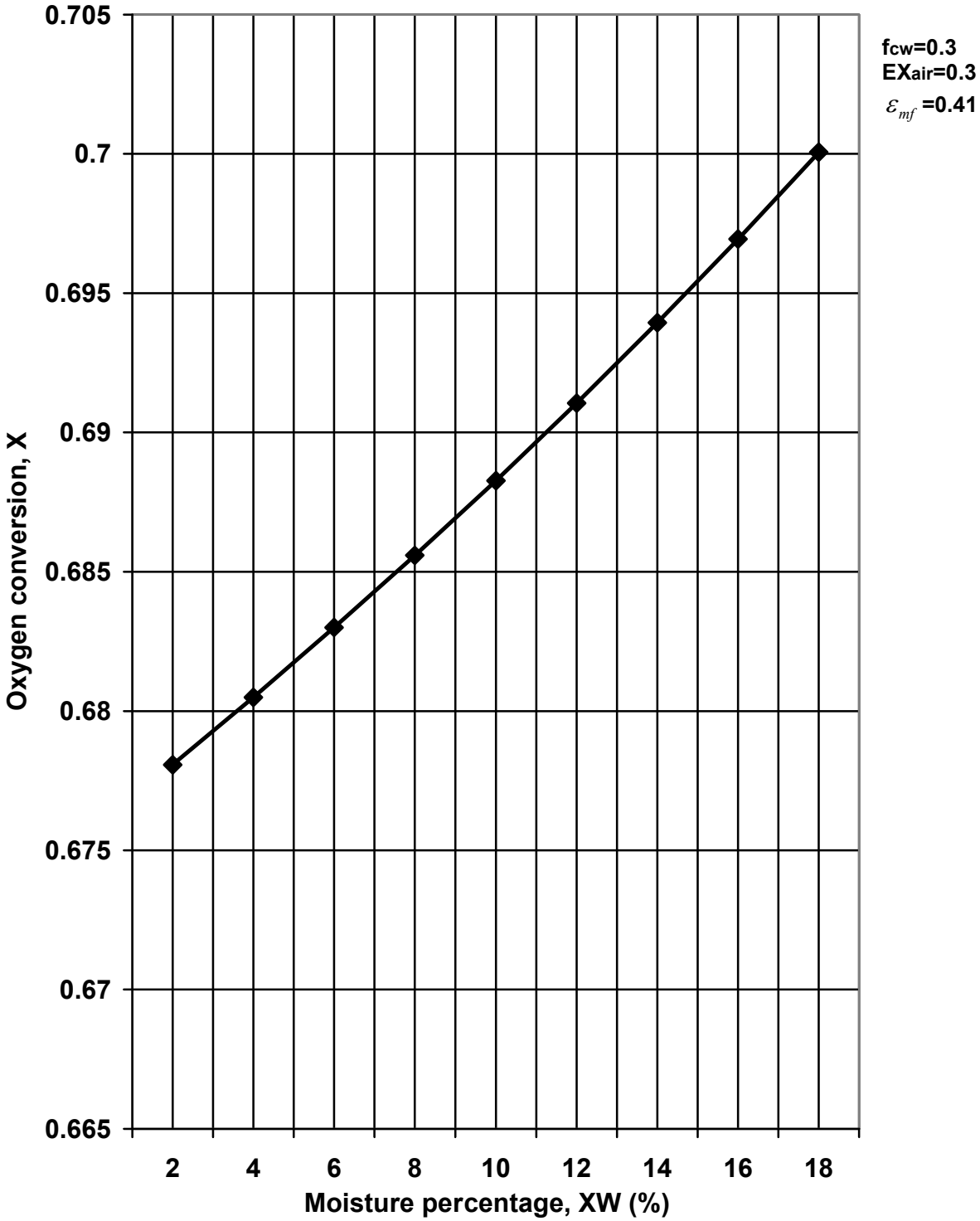


**Figure 6.10 - Variation of oxygen conversion with moisture percentage**

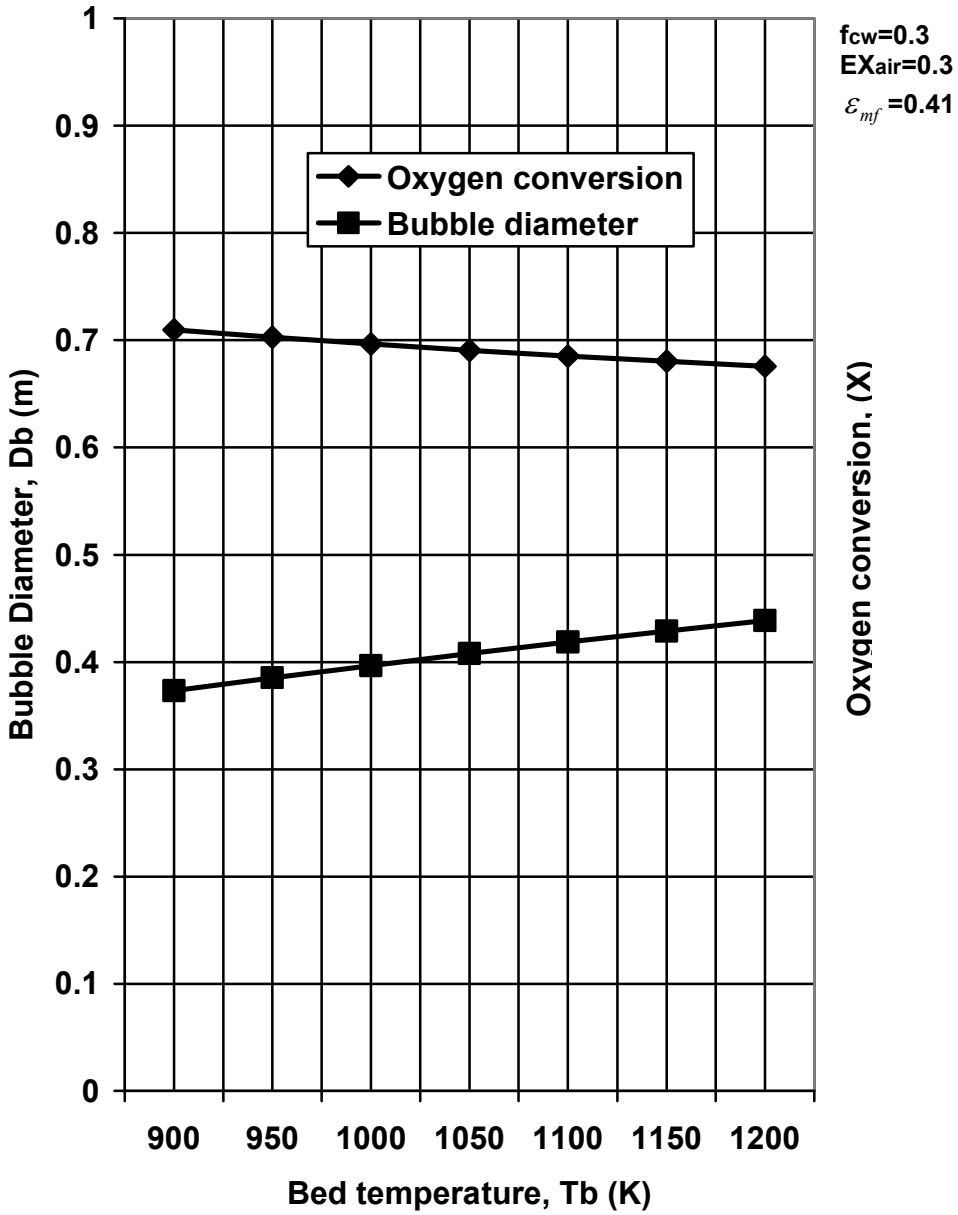


**Figure 6.11 - Variation of oxygen conversion and bubble diameter with bed temperature**

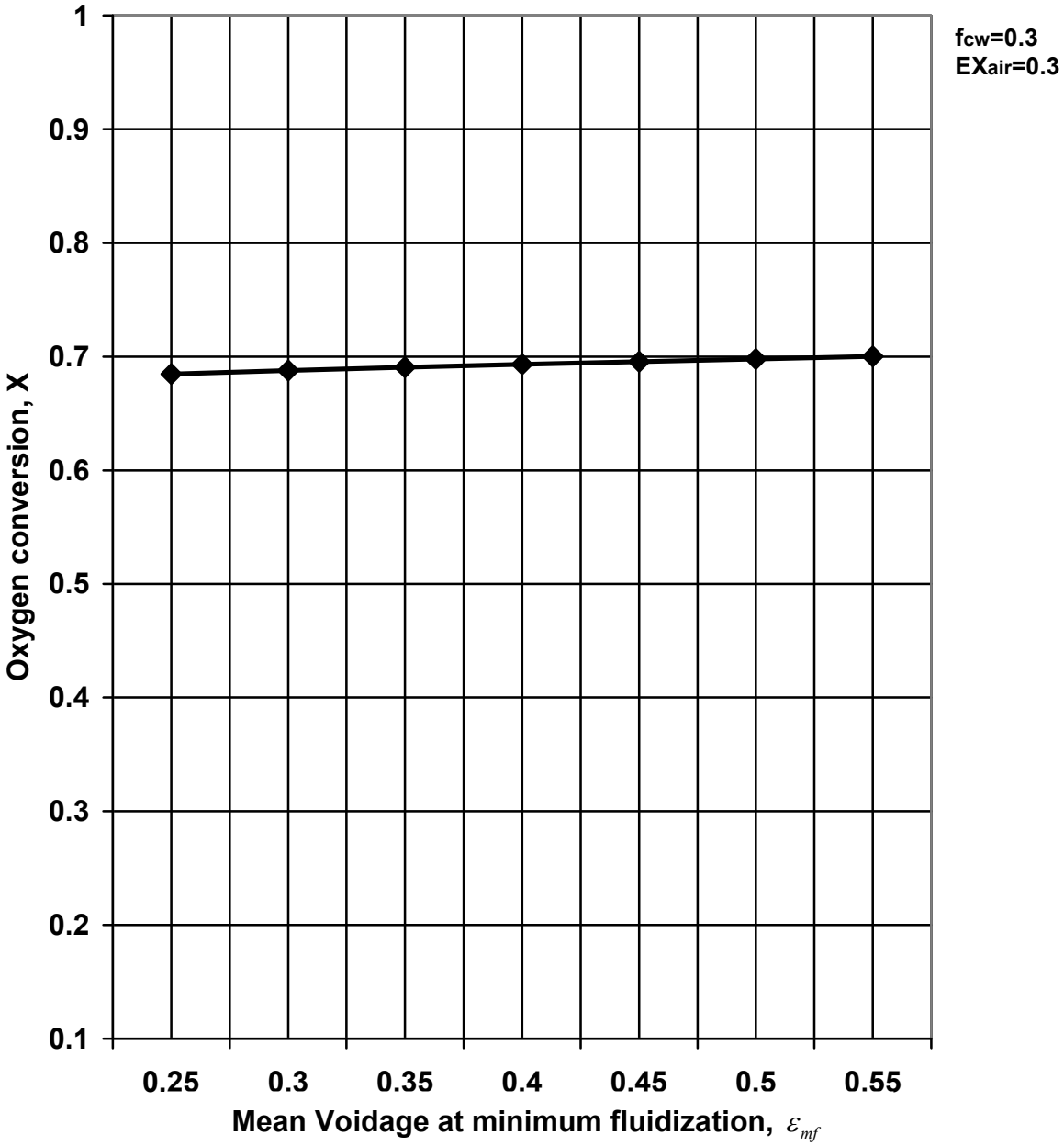


**Figure 6.12 - Variation of oxygen conversion with mean voidage at minimum fluidization**

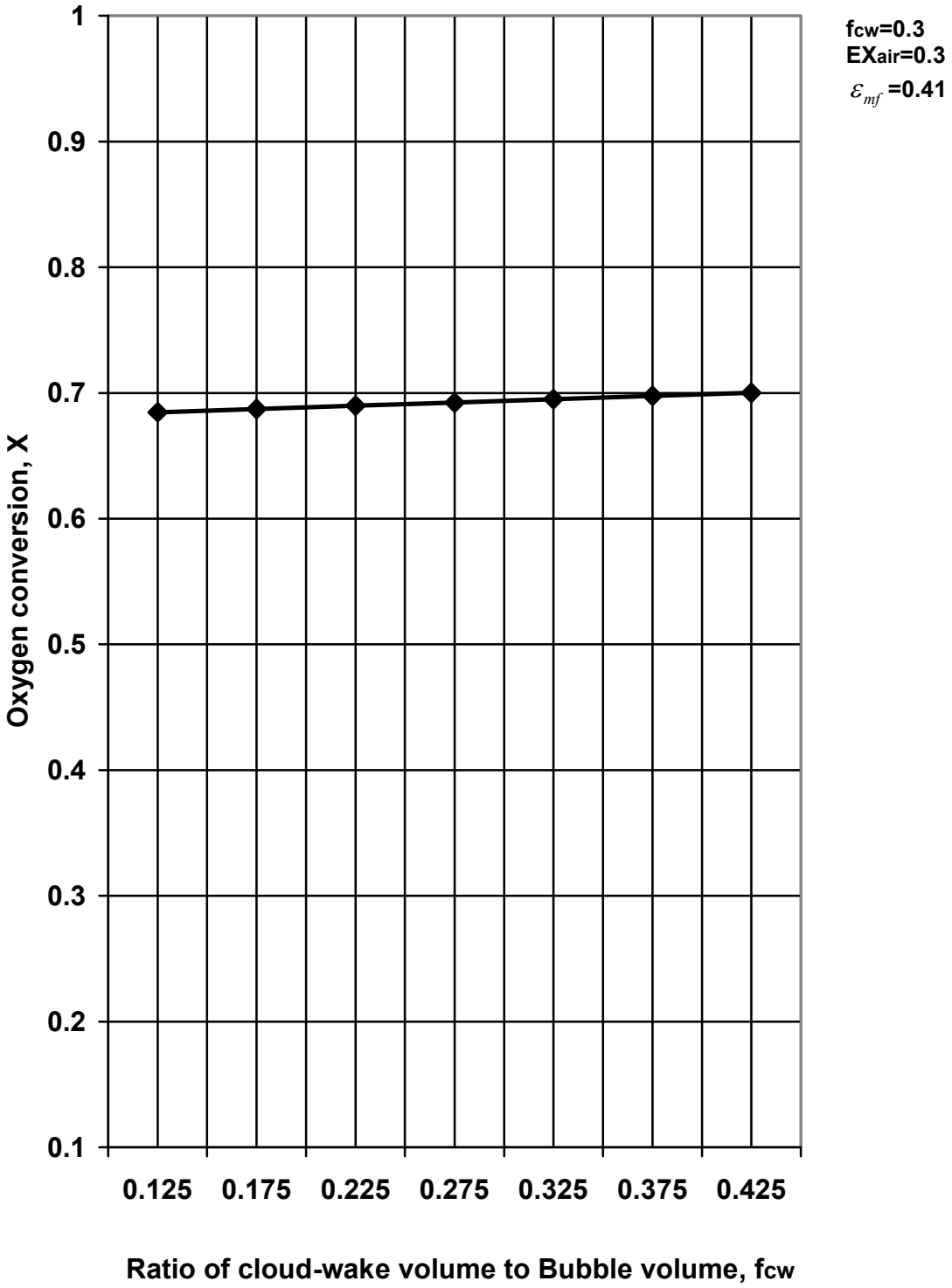


**Figure 6.13 - Variation of oxygen conversion with cloud-wake volume to bubble volume**

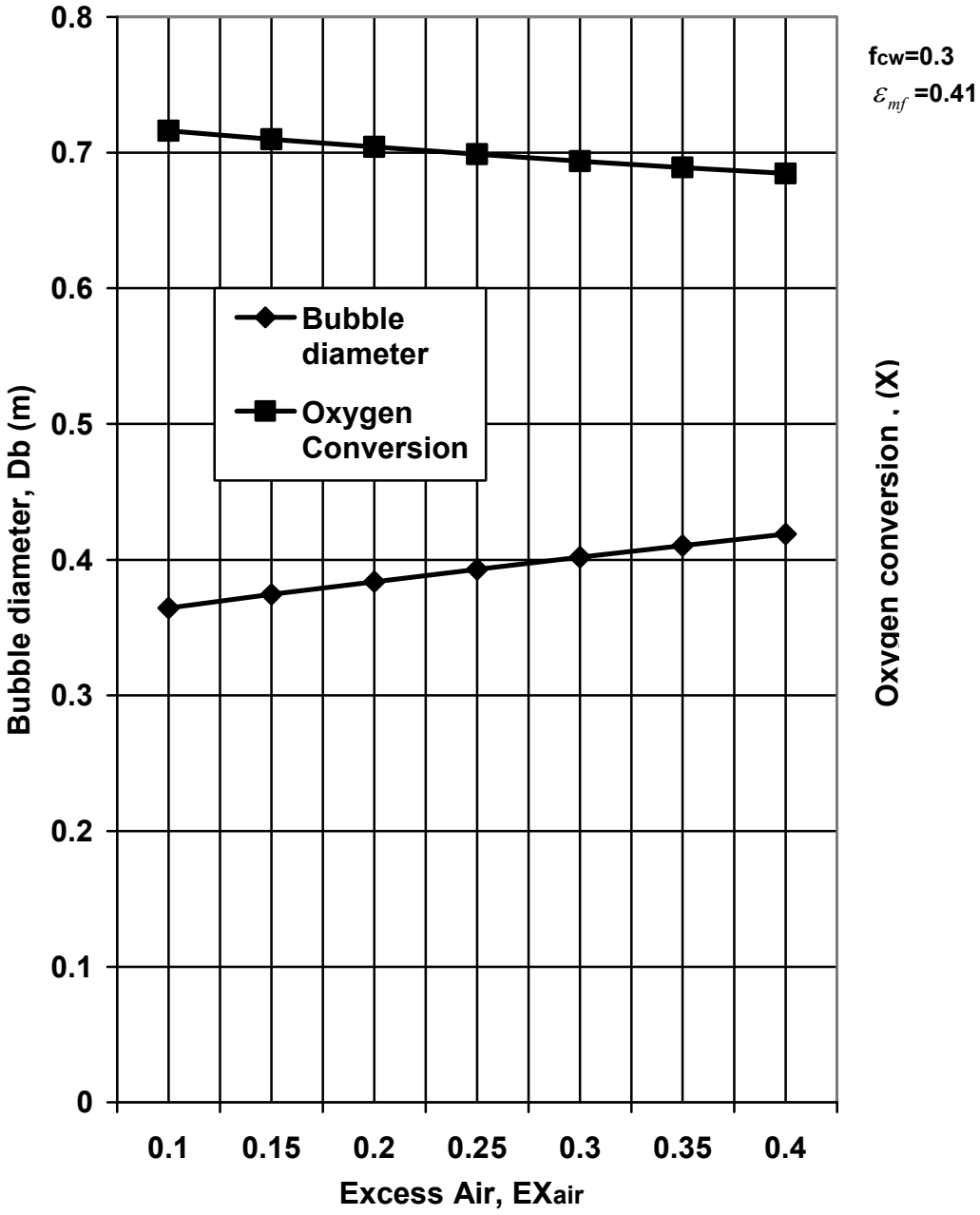


**Figure 6.14 - Variation of Bubble Diameter and Oxygen conversion with excess air**

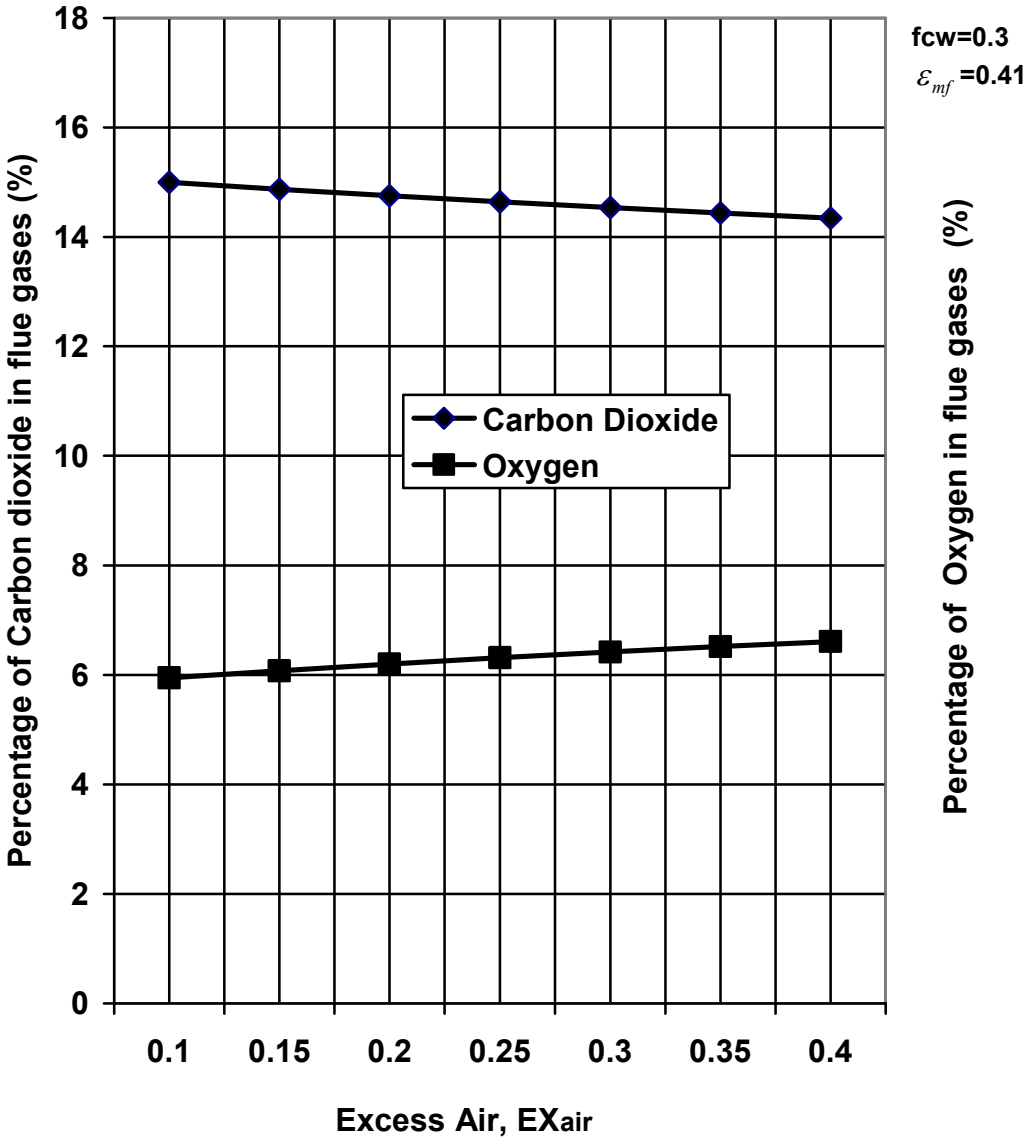


**Figure 6.15 - Variation of $CO_2$ and $O_2$ percentage with excess air**

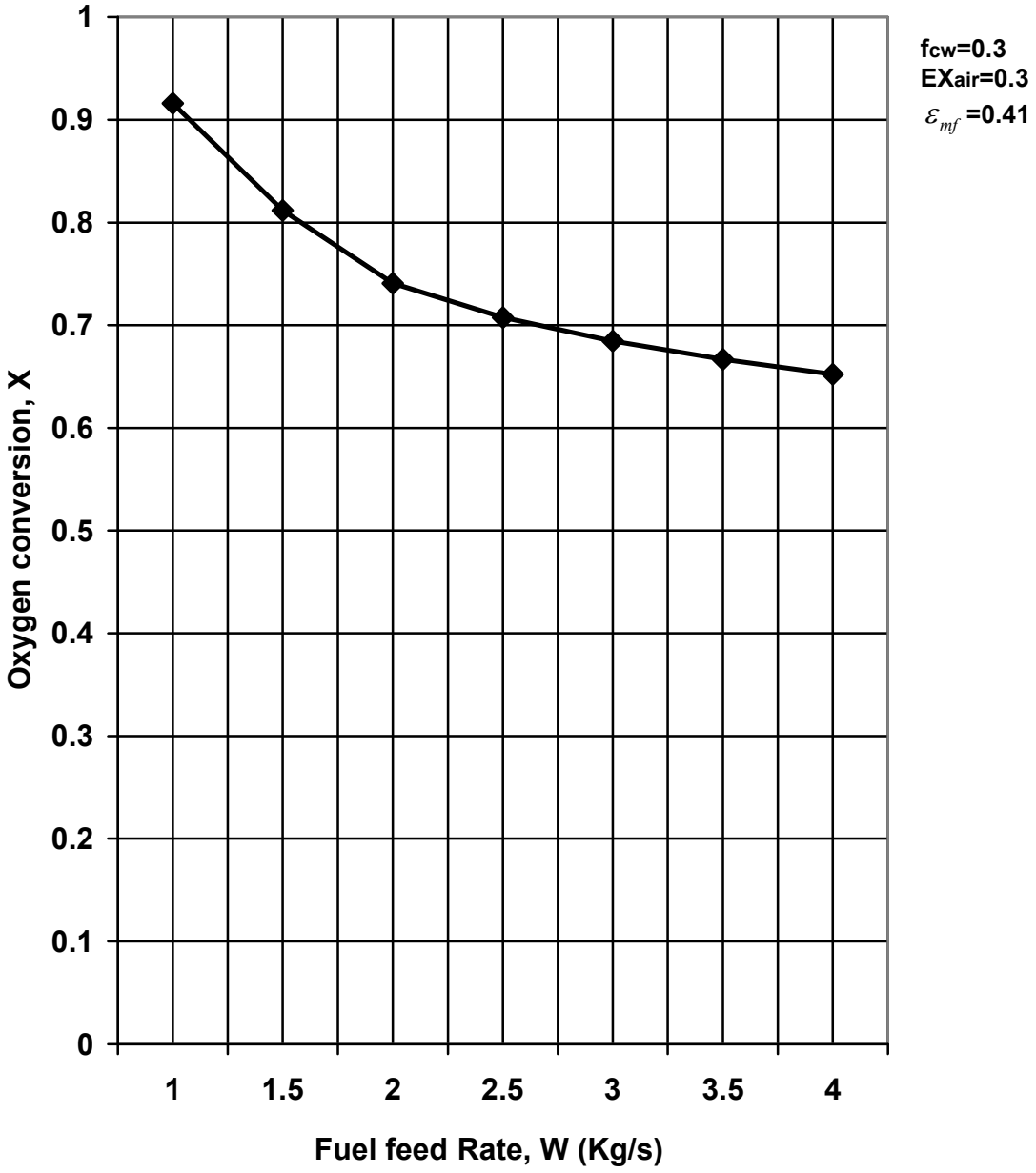


**Figure 6.16 - Variation of oxygen conversion with fuel feed rate**

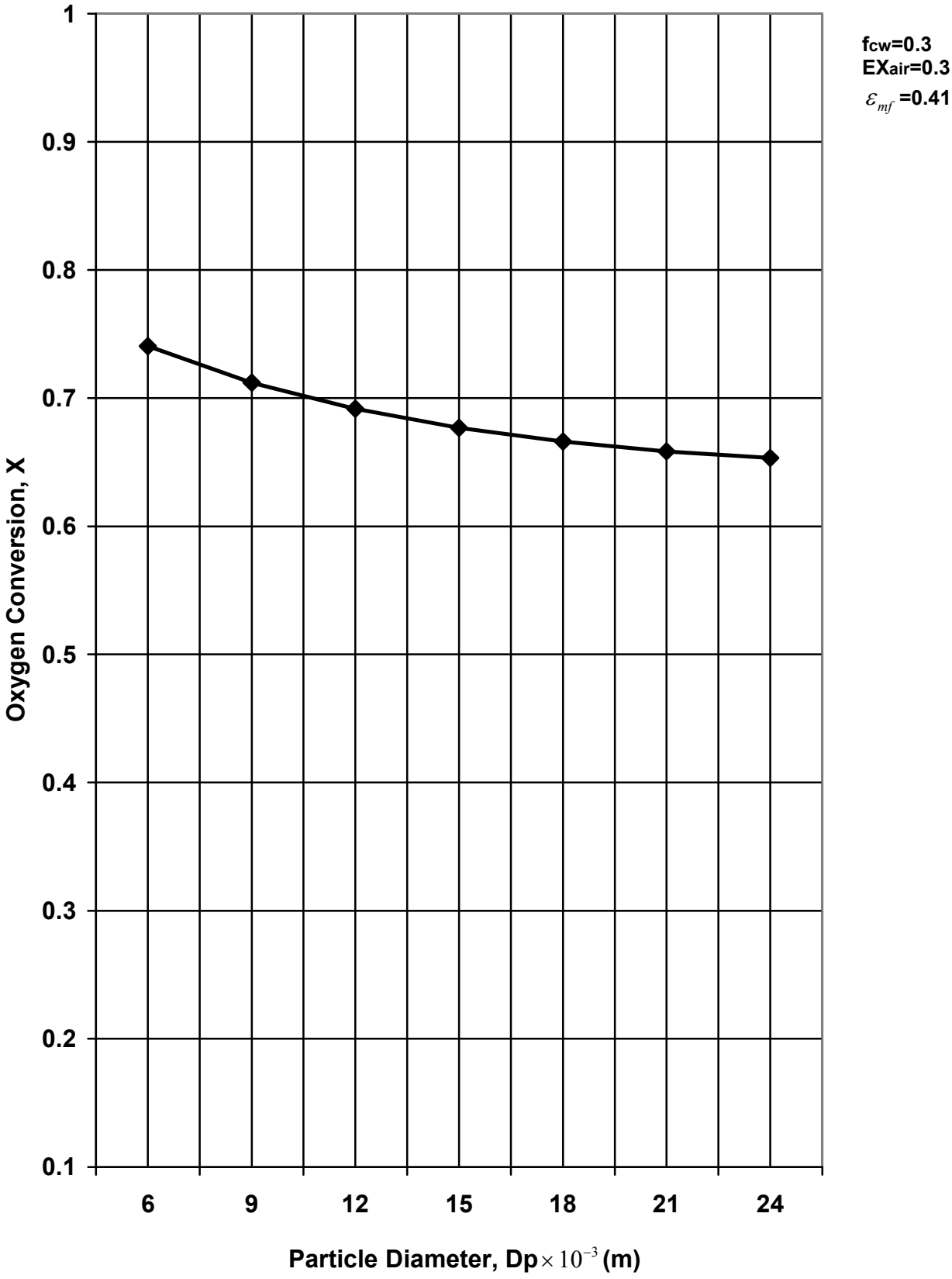


**Figure 6.17 - Variation of Oxygen Conversion with particle size**

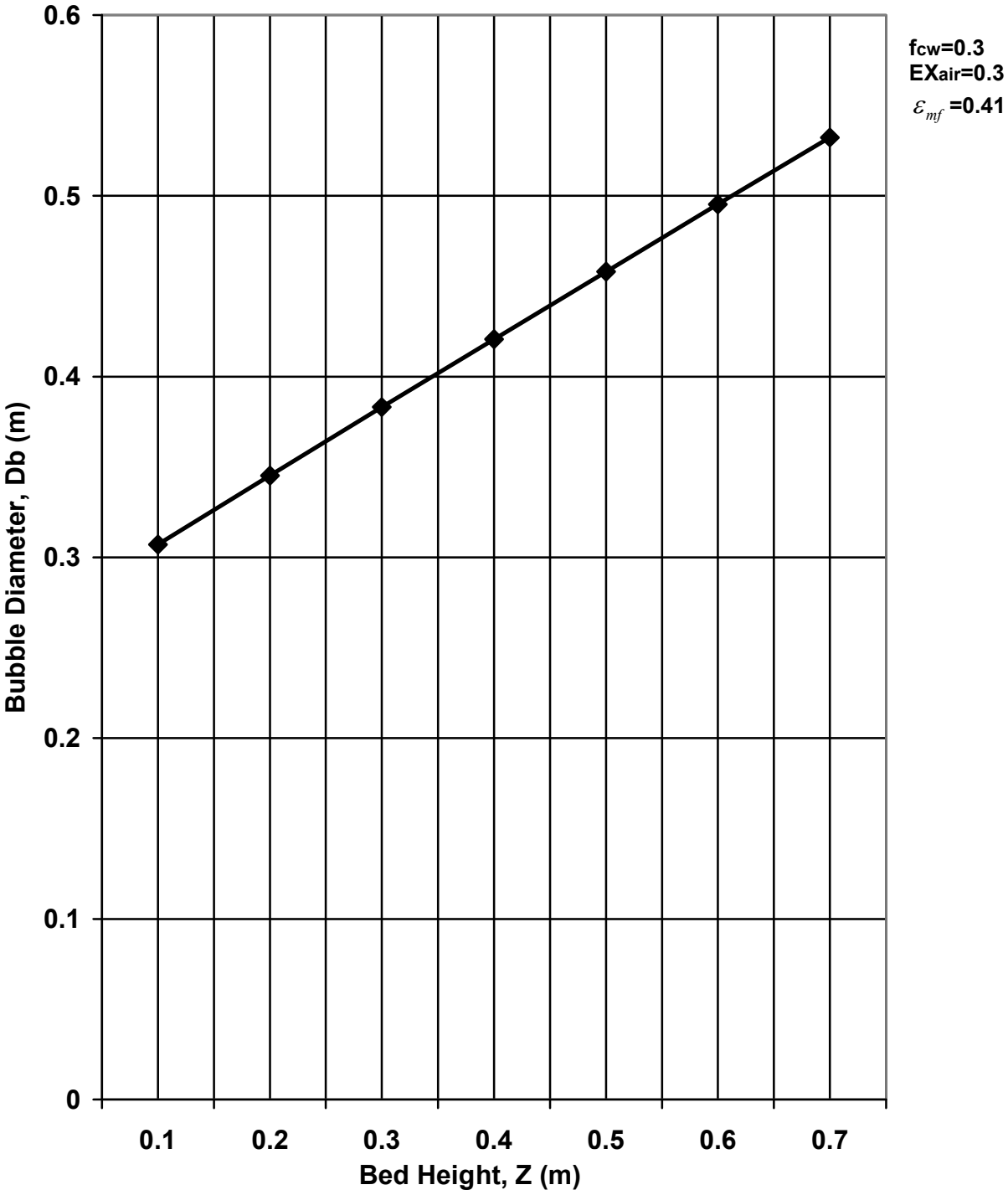


**Figure 6.18 - Variation of Bubble Diameter with Bed Height**

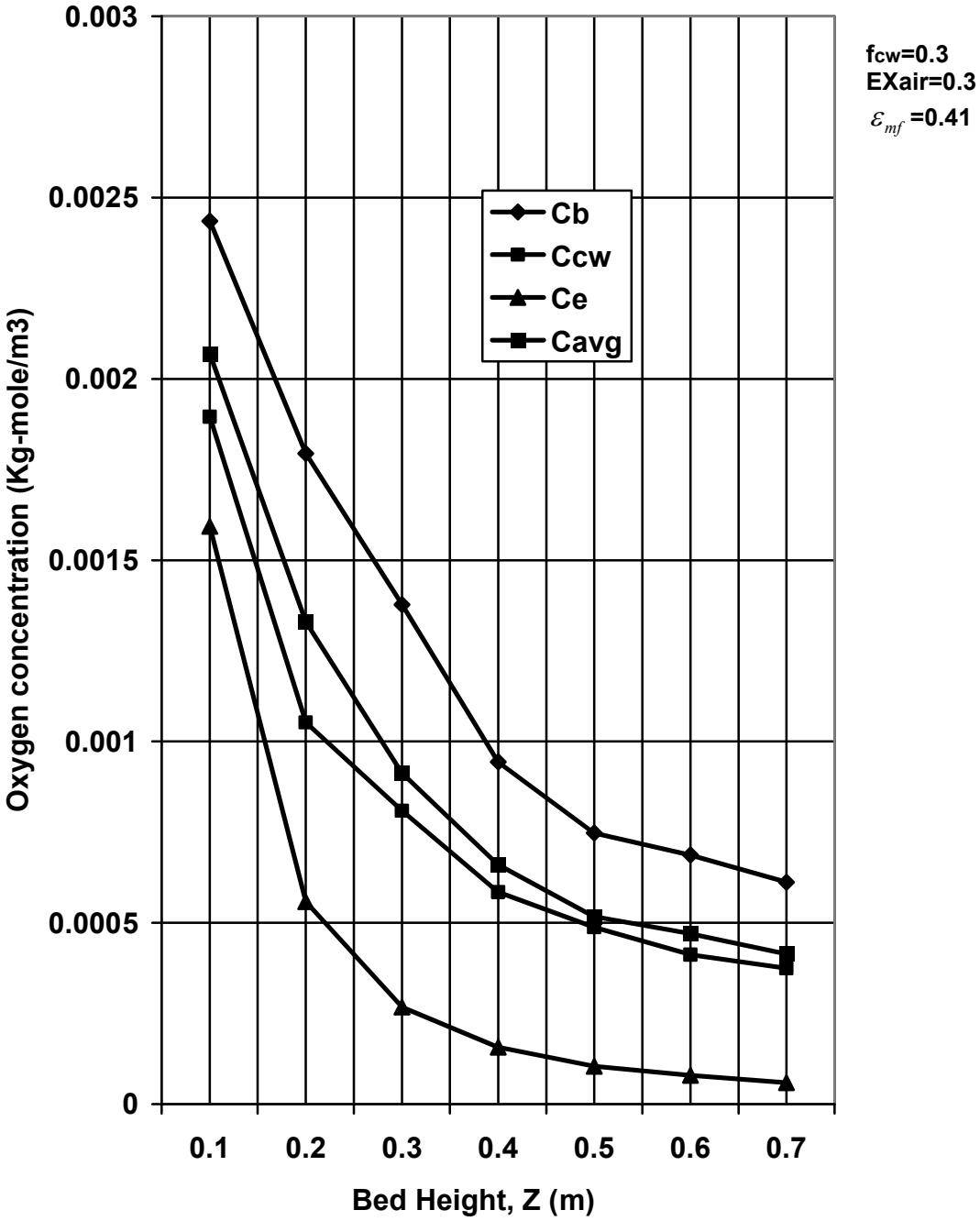


**Figure 6.19 - Variation of oxygen concentration with bed height in different phases**

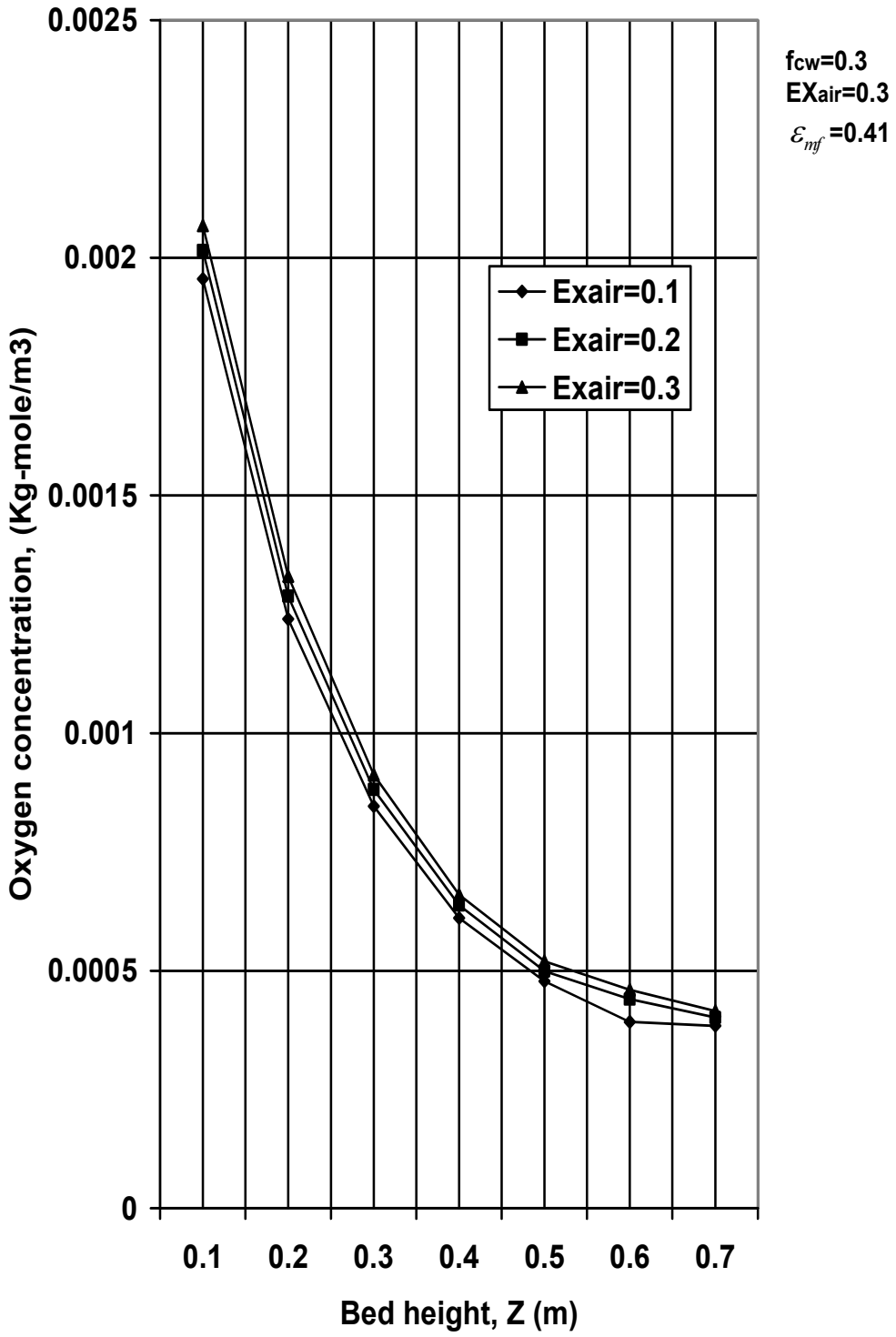


**Figure 6.20 - Variation of oxygen concentration with bed height at different values of excess air**

# CHAPTER – 7

# CONCLUSIONS AND SCOPE FOR FUTURE

## 7.1 Conclusions

1) Minimum fluidization velocity increases with increase in fuel particle size.
2) Minimum fluidization velocity decreases with increase in bed temperature.
3) Operating velocity of gas increases with increase in bed temperature.
4) Operating velocity of gas decreases with increase in moisture content.
5) Reaction rate decreases with increase in particle size.
6) Oxygen conversion decreases with increase in carbon percentage.
7) Oxygen conversion increases with increase in moisture percentage.
8) Bubble diameter increases and oxygen conversion decreases with increase in bed temperature.
9) Bubble diameter increases and oxygen conversion decreases with increase in excess air.
10) $CO_2$ percentage decreases and $O_2$ percentage increases with increase in excess air.
11) Oxygen conversion decreases with increase in fuel feed rate.
12) Oxygen conversion decreases with increase in particle size.
13) Bubble diameter increases with increase in bed height.
14) Oxygen concentration of each phase i.e bubble phase, cloud-wake phase and emulsion phase and average oxygen concentration decreases with increase in bed height.
15) Average oxygen concentration increases with increase in excess air.
16) Exit gas composition i.e percentage of oxygen, carbon dioxide and nitrogen predicted through this model matches with the real plant data.

## 7.2 Scope of future work

1) The model can be further extended in order to study the effect of bubble size variation on various parameters of the bubbling fluidized bed combustion.

# SELECTED REFERENCES


**[1]** Avedesian, M. M., and Davidson, J. F., Two phase theory of fluidization to the batch combustion of char and coke particles in a hot bed of inert material fluidized by air., *Trans. Inst. Chem. Engg.,* **51**,121, (1973).

**[2]** Bird, R. B., Stewart, W. E., and Lightfoot, F. N., *Transport phenomena*, Wiley, New York, (1960).

**[3]** Caram, H. S., and Amundson, N. R., Diffusion and reaction in a stagnant boundary layer about a carbon particle, *I. and E.C. Fundamentals*, **16**, 3, (1977).

**[4]** Chavarie, C., and Grace J. R., Performance of a fluidized bed reactor: Visible flow behaviour., *Department of Chemical Engg., McGill University,* Canada, **14**, 75-78, (1975).

**[5]** Chern, J. S., and Hayhurst A. N., Does large coal particles in a hot fluidized bed lose its volatile content according to the Shrinking core model., *University Of Cambridge, Department Of Chemical Engg.,* England, U.K., **139**, 208-221, (2004).

**[6]** Ciesielczyk, W., and Iwanowski, J., Analysis of fluidized bed drying kinetics on the basis of inter-phase mass transfer coefficient., *Institute of Chemical and Process Engg., Cracow University of Technology,* Poland, **24**, 1153-1157, (2006).

**[7]** Davidson, J. F., and Harrison, D., Two Phase Theory of Fluidization., *Cambridge University Press,* (1963).

**[8]** Degirmenci, E., Seluk, N., and Gogebakan, Y., Modeling of a bubbling fluidized bed combustor with volatiles release, *Journal of Energy Resources Technology*, **72**, 125, (2003).

**[9]** Delebarre, A., Does the minimum fluidization exist?, *Journal of Fluids Engineering*, ASME, **124**, 595-600, (2002).

**[10]** Dennis, J. S., Hayhurst, A. N., and Scott, S. A., The combustion of large particles of char in bubbling fluidized bed: The dependence of Sherwood number and rate of burning on particle diameter.**,** *University Of Cambridge, Department Of Chemical Engg.,* England, U.K., **147**, 185-194, (2006).

**[11]** Domkundwar., and Arora, S., A course in Power Plant Engineering, *Dhanpat Rai & Company (P) Ltd.*, Delhi, (1998).

**[12]** El-Halwagi, M. M., and El-Rifai, M. A., Mathematical modeling of a catalytic fluidized bed reactor: The multistage three model, *Chem. Engg. Sc.*, **43**, 2477-2486, (1988).

**[13]** Faravelli, T., Frassoldati, A., and Ranzi, E., Modeling homogeneous combustion in bubbling beds burning liquid fuels, *Journal of energy resources technology*, ASME, **129**, 33-41, (2007).

**[14]** Farshi, A, Naderi, F., and Sadeghzadeh, J., Approach to modeling of a gas solid fluidized bed reactor., *Development Engineering Department, Research Institute Of Petroleum Industry,* Tehran, Iran, **48(2),**53-62, (2006).

**[15]** Fu, Y., and Liu, D., Novel experimental phenomenon of fine-particle fluidized beds, Experimental Thermal and Fluid Science, **32**, 341-344, (2007).

**[16]** Galgano, A., Salatino, P., Scale F., and Maffettone, P. L., A model of the dynamics of a fluidized bed combustor burning bio-mass, (*Combustion and Flame*), (2005).

**[17]** Hayhurst, A. N., and Parmar M. S., Measurement of mass transfer coefficient and Sherwood number for carbon spheres burning in a bubbling fluidized bed., *University Of Cambridge, Department Of Chemical Engg.,* England, U.K., **130**, 361-375, (2002).

**[18]** Janvijitsakul, K., Kuprianov, V. I., and Premchart, W., Co-firing of rice-husk and bagasse in a conical fluidized bed combustor., *Sirindhorn International Institute of Technology, Thammasart University,* Thailand,**3-016(0)**, 232-237, (2004).

**[19]** Jiang, H., Zhu, X., Guo, Q. and Zhu, Q., Gasification of Rice Husk in a Fluidized-Bed Gasifier without Inert Additives, *Ind. Eng. Chem. Res.*, **42**, 5745-5750, (2003).

**[20]** Khan, A.A., Jong W. D., Gort D. R., and Spliethoff, H., A fluidized bed biomass combustion model with discretized population balance**.,** *Department Of Process And Energy*, Netherland., **21**, 2346-2356, (2007).

**[21]** Kunni, D., Levenspiel, O., *Fluidization Engineering*, Wiley, NY, (1969).

**[22]** Kunni, D. and Levenspiel, O., Bubbling bed model for kinetic processes in fluidized bed, *Ind. Engg. Chem. Process Des. Dev.*, **7,** 481-492, (1968).

**[23]** Mihalyko, C., Lakatos, B., Matejdesz, A. and Blickle, T., Population balance model for particle-to-particle heat transfer in gas-solid systems, *International Journal of Heat and Mass Transfer*, **47**, 1325-1334, (2004).

**[24]** Mohapatra, S. K., Modeling of a fluidized bed combustor, Ph.D. Thesis, ISM Dhanbad, India., (1997).

**[25]** Mori, S., and Wen, C. Y., Simulation of Fluidized bed reactor performance by modified bubble assemblage model, *Fluidization Technology* (Ed. D.L. Keirns), 1, Hemisphere, Washington, 179–203, (1975).

**[26]** Nag, P., Power Plant Engineering, *Tata Mcgraw-Hill Publishing Company Limited*, New Delhi, (1998).

**[27]** Natrajan, E., Nordin, A., and Rao, A. N., Overview of combustion and gasification of rice husk in fluidized bed reactors, *Biomass and Bio Energy,* **14**, 533-546, (1998).

**[28]** Okasha, F., Staged combustion of Rice Straw in a fluidized bed., *Department of Mechanical Engg., Mansoura University,* Egypt*,* **32**, 52-59, (2007).

**[29]** Premchart, W., and Koupranov, V. I., Emission performance and combustion efficiency of a conical fluidized combustor firing various biomass fuels, *Bio Resources technology,* 83-91, (2004).

**[30]** Tsutsumi, A., Chen, W., and Kim, Y. H., Classification and Characterization of hydrodynamic and transport behaviour of three-phase reactors., *Department of Chemical Engg., University of Tokyo,* Japan*,***16(6)**, 709-720, (1999).

**[31]** Wang, A. L., Clough, S. J., and Stubington, J. F., Gas flow regimes in fluidized bed combustor., *School of Chemical Engg. and Industrial Chemistry, University of New South Wales,* Australia*,* **29**, 819-826, (2002).

**[32]** Wang, A. L. T., Xu, J., and Stubington, J. F., "Hydrodynamic Performance of the novel design of pressurized fluidized bed combustor.", *Journal of Energy Resources Technology*, **128**, 111-117, (2006).

**[33]** Yagi and Kunii D., Studies on combustion of carbon particles in flames and fluidized bed, *5th Int. Symp. on combustion, Reinhold,* NY, (1955).

# APPENDIX

The final results are obtained as follow from C++ program using the input parameters given in Table 6.1.

Turbo C++ IDE

```
Enter the value of density of fuel=Rohs= 116.1 Kg/m3
Enter the value of average particle diameter=Dp= 0.0118388 m
Enter the temp. of bed=Tb= 1023 K
Stiochimertic Air feed rate=FMTH=  0.433171 Kg-mole/sec
Actual molar feed rate of fluidizing gas=FME= 0.563123 Kg-mole/sec
Value of superficial velocity=Uo= 2.408884 m/sec
Archimedes number=Ar= 6797993
Minimum fluidization velocity acc. to chitester=Umf= 0.704192 m/sec
Terminal velocity=Ut= 5.862228 m/sec
Reynold's number=Re= 4591.192383
Reynold's number at minimum fluidization=Remf= 551.510803
Voidage at minimum fluidization=Emf= 0.413374
Bed Diameter=Dt= 4.973836 m
Effective bubble diameter=Db= 0.401911 m
Rise velocity of the bubble w.r.t emulsion phase=Ubr=1.411788 m/sec
Rise velocity of the crowd of bubbles=ub= 3.116479 m/sec
Ratio of cloud-wake to the volume of bubbles=fcw= 0.3
Interphase exchange coeff. b/w bubble & cl-wk=Kbc=8.304049 sec-1
Interphase exchange coeff. b/w cl-wk & emulsion=Kce=0.391675 sec-1
Interphase exchange coeff. b/w bubble & emulsion=Kbe=0.374033 sec-1
Superficial velocity of bubbles=Ub= 1.516613 m/sec
The Sherwood number=Sh= 17.590399
Mass Transfer coeff.=Kg= 0.106088 m/sec
```

Surface reaction rate constant=Ks= 1.330877e+10 m/sec

Overall Reaction rate constant=K= 0.106088 sec-1

Volume fraction of bubbles in the bed=Eb= 0.446176

Cross-sectional area of the bed occupied by bubbles=Ab=8.669199 m2

Cross-sectional area of the bed occupied by cl-wk =Acw=1.075087 m2

Superficial velocity of the cl-wk =Ucw= 0.083916 m/sec

Volumetric flow rate through bubbles=Qb= 29.467794 m3/sec

Volumetric flow rate through cl-wk region=Qcw= 1.630491 m3/sec

Volumetric flow rate emulsion region=Qmf= 13.682455 m3/sec

Total volumetric flow rate=Q= 44.780743 m3/sec

Number of equivalent stages=N= 3

Shrinkage rate due to attrition=SHRTatt= 1.056909e-07 m/sec

Shrinkage rate due to combustion=SHRTcom= 0.752055 m/sec

Overall Shrinkage rate=SHRTover= 0.752055 m/sec

Inlet Oxygen conc.=Co= 0.002502 Kg-mole/m3

O2 conc. at stage-n in bubble phase=Cbn= 0.001086 Kg-mole/m3

O2 conc. at stage-n in cl-wk phase=Ccwn= 0.00068 Kg-mole/m3

O2 conc. at stage-n in emulsion phase=Cen= 0.000201Kg-mole/m3

Average O2 conc.=Cavgn= 0.000766Kg-mole/m3

oxygen conversion=x= 0.693776

O2 conc. leaving top of the bed= 0.000766Kg-mole/m3

CO2 conc. leaving top of the bed= 0.001736Kg-mole/m3

N2 conc. leaving top of the bed= 0.009439Kg-mole/m3

Percentage of O2 in exit gas= 6.415969

Percentage of CO2 in exit gas= 14.53588

Percentage of N2 in exit gas= 79.048157